University of Alberta
Department of Civil &
Environmental Engineering

Structural Engineering Report No. 210

FATIGUE TESTS OF RIVETED BRIDGE GIRDERS

by

Daniel E. J. Adamson

and

Geoffrey L. Kulak

August 1995

FATIGUE TESTS OF RIVETED BRIDGE GIRDERS

by

Daniel Edward Joseph Adamson

and

Geoffrey L. Kulak

Structural Engineering Report No. 210

Department of Civil Engineering

University of Alberta

Edmonton, Canada T6G 2G7

August 1995

Abstract

The remaining fatigue life evaluation of riveted bridges is becoming more important as the number of bridges that have reached the limit of their theoretical life increases each year. Often, the evaluations are overly conservative because of the limited amount of information concerning the actual structural behaviour of bridges, the fatigue resistance of riveted details, and conservative fatigue damage calculation techniques.

Strains due to live loads were measured on a bridge on the CN Rail mainline. The bridge was then dismantled and six stringers were tested in fatigue. These tests showed that the fatigue resistance of riveted members exceeds the AREA Category D curve. The results of a subsequent remaining fatigue life calculation showed that predictions of fatigue life can be significantly improved by use of accurate influence lines, a modified fatigue resistance curve, and a new method of damage accumulation.

Acknowledgments

This study was funded by CN North America and their generous support is acknowledged with thanks. The authors wish particularly to thank Dr. R.A.P. Sweeney and Mr. J. Lowe of CN North America for their assistance during the development of this report. The contributions of Dr. S. Alexander, Mr. L. Burden, Mr. R. Helfrich, and Mr. D. Lathe during the field measurements and experimental portions of this work and the assistance of Dr. M.L. Wayman of the Department of Metallurgical Engineering with the crack surface examinations are greatly appreciated. Dr. P.M. Kunz, a Post-Doctoral Fellow at the University of Alberta during a portion of the time the work was being done, provided significant technical assistance to the authors that otherwise would not have been available.

Table of Contents

List of Symbols

n_i	=	number of cycles at stress range level i
N_i	=	number of cycles to cause failure at stress range level i
N	=	total number of applied variable amplitude stress cycles; number of cycles to a given point on fatigue resistance curve
M	=	fatigue life constant
$\Delta\sigma_i$	=	stress range at level i
m	=	slope of the fatigue resistance curve
$\Delta\sigma_e$	=	effective stress range
α	=	effective stress range factor to reflect the beneficial load resistance effect of secondary members and the fact that impact does not occur with every cycle
ΔK	=	stress intensity factor range
Y(a)	=	geometric factor used in Equation 2.5
$\Delta\sigma$	=	applied stress range
a	=	crack size
ΔK_{th}	=	threshold stress intensity factor range
$\Delta\sigma_{th}$	=	threshold stress range
$\Delta\sigma_d$	=	damage limit stress range
$\Delta\sigma_c$	=	constant amplitude fatigue limit stress range

1. INTRODUCTION

1.1 General

Fatigue occurs in structures that carry moving loads, for example, bridges. Under the application of repeated stresses, microscopic cracks in structural members can propagate into large cracks [1]. The presence of large cracks will reduce the load-carrying capacity of a structural member, and, in extreme circumstances, can cause total failure of the part. Three major factors affect fatigue crack growth. These are: 1) the magnitude of the applied stress range, 2) the number of stress cycles, and 3) the magnitude and shape of the initial flaw [2]. In civil engineering practice, the latter is usually represented by the structural detail present, e.g., a welded cover plate, a bolted connection detail, etc.

Many of the bridges on Canadian railway systems were built during the late nineteenth to early twentieth centuries. At this time, riveted construction was the method used for building up members and for connection of one member to another. Of course, the intention of the designers of these bridges was that they have a long useful life. However, since their construction, changes in rail traffic and general deterioration has continually required the re-evaluation of these bridges. For example, the recent introduction of double stacked container cars in Canadian railroads means that the previous maximum axle load of 30 tonnes has been increased to 35.7 tonnes [3]. When changes of this nature occur, railway bridges must be re-evaluated in terms of strength, serviceability, and fatigue. Even under constant loading, the fact that many of these structures are now over 100 years old means that the question of their remaining fatigue life must be addressed.

Remaining fatigue life of these bridges is directly influenced by the changing bridge traffic. The age of the bridges and the increasing axle loads directly affect two of the three major factors that govern fatigue life. First, the increasing axle loads applied to the bridge increase the stress range at a given structural detail. The effect of this on fatigue life is an acceleration of any pre-existing fatigue crack growth and an increase in the number of structural details where fatigue cracks could initiate [3]. Second, the age of the bridges means that millions of load cycles have now been imposed on them since their

construction. Any structural details that have had fatigue crack growth, even at low stress ranges, may now be reaching the end of their fatigue life.

A fatigue evaluation of a bridge generally involves obtaining information about the three major factors that cause fatigue. Structural details that are thought to be susceptible to fatigue are evaluated in terms of the stress range they experience and the number of cycles for which the stress range is applied. Structural details are selected either on the basis of previous experience with a certain type of detail, or by some sort of analytical justification. The stress range at a detail can be calculated analytically using the appropriate influence lines and railcar weights, or by direct measurement of strains while the bridge is in service. The number of cycles can be estimated using traffic histories of the particular railway line. These are usually kept by the railway companies. Once all this information is obtained, it is compared with the allowable limits of the fatigue resistance [2,4].

This report discusses the partial fatigue evaluation of a bridge located on the Canadian National Railway mainline. Strains due to live loads were measured in members of the bridge while it was still in service. The bridge was then removed from service, and some of the members were fatigue tested in a laboratory. The resulting information from the strain measurements and fatigue tests was used to calculate the remaining fatigue life of the bridge members.

1.2 Statement of the Problem

In an effort to minimize expenditure, railroad companies are continually trying to improve the accuracy of their remaining fatigue life calculations [3]. Accurate evaluations can help to ensure that bridges are not retrofitted or replaced before necessary. One part of the evaluation process where there can be significant differences between calculations and actual conditions is the determination of the stress range at structural details. The ideal way would be to directly measure the strains while the bridge is still in service. However, this is not often possible and an analytical approach is required. This is usually in the form of a static analysis using the influence line of the detail.

The problem that arises is that in a real structure there may be partial restraint at end connections or secondary load paths that are not taken into account by the usual structural analysis. These realities can have large effects on the fatigue evaluation

calculations, either on the amount of fatigue life available or in determining if a detail is critical. Information is needed to improve the use of analytical modeling of bridges. The first part of this report is concerned with the development of suitable influence lines for stresses in members of the bridge. Strain measurements done on the bridge while it was still in service are compared with corresponding strains from a static analysis.

The remaining fatigue life of a particular detail is determined by comparing its stress range and corresponding number of stress cycles with the standard fatigue resistance for the type of detail. Current standards are based upon empirical data from laboratory tests, which have been developed by subjecting different types of details to fatigue loading. For modern details, such as bolted and welded connections, the fatigue resistance has been well established. However, for riveted details less work has been done. Also, most of the work that has been done on fatigue resistance of riveted details has been in the high stress range region. In reality, most railway bridges are subjected to low stress ranges. More information is needed in this region of fatigue resistance. In the second part of this report, six riveted built-up stringers taken from the bridge recently removed from service are fatigue-tested in a laboratory. Focus is on the low stress range region.

Calculation of remaining fatigue life requires that the previous damage to the bridge be determined. This can be very difficult. Not only do the stress range history and number of cycles of loading at the detail since the inception of traffic have to be estimated, but the comparison basis, laboratory testing of standard details, is usually conducted using constant amplitude loading. In constant amplitude loading, the stress range remains the same for all stress cycles. Actual loading is more often variable amplitude loading.

The problem here is to apply the real life variable amplitude cycles to the constant amplitude standards. This is done in the third part of the report, using computer software that internally generates variable amplitude stress range loadings based upon load histories and influence lines and calculates damage accumulation using a fracture mechanics approach.

1.3 Objectives

The objectives of this investigation are:

1. To evaluate bridge strain measurements taken in the field with a theoretical analysis.

2. To supplement the data base of fatigue resistance for riveted details in the low stress range region.
3. To calculate the remaining fatigue life of the bridge under examination using theoretical methods.

2. LITERATURE REVIEW

2.1 Field Strain Measurement

In 1976 Fisher and Daniels reported on an investigation of the fatigue life of a riveted railway bridge [5]. Part of the investigation involved measuring strains in some of the hangers and stringers. The purpose of the strain measurements was to determine an appropriate analytical model of the bridge so that past, present, and future traffic loads could be applied to calculate stress ranges for the fatigue evaluation. Two analytical models were evaluated. The first was a plane simple truss that modeled one truss span and assumed that all connections were pinned. An equation based on frame action between the floorbeam and hanger was developed to convert the load applied to the floorbeam by the rails into a combined moment and axial stress in the hanger. The plane model was assumed to closely represent the upper bound solution for the load on the hanger.

The second model was a three-dimensional model of the bridge that included all major load carrying members. Because of symmetry, only one-quarter of the bridge needed to be modeled. The influence of longitudinal and transverse members that were cut off in this quarter-model was considered by specifying displacements conditions at the boundaries, obtained from a separate plane-frame analysis. In the model, the stringer-to-floorbeam and the gusset plate connections were modeled as continuous and pin connections were modeled as pinned. The loads applied to the model were the same as those applied statically to the bridge by a special work train.

The results of the analysis were expressed as the ratio between the measured and calculated strains. No specific numbers were given for the plane model, but, reading from plotted results, the calculated strains were higher than the measured strains. For the three-dimensional model, the ratio of measured to calculated axial stress in the hangers ranged from 0.96 to 1.02.

Szeliski and Elkholy reported on a fatigue investigation of a railway truss bridge that had geometry very similar to the one in this report [6]. Strain gages were attached to the top and bottom chords, end posts, hangers, stringers, floorbeams, and bracing. Gages were also attached on the rails to measure the wheel loads. Measurements were made for several days under normal traffic conditions, and a special work train was used for more

controlled tests. All strain measurements were converted to a single equivalent stress range (root mean square). It was found that for this bridge the impact loads due to flat wheels did not significantly affect the equivalent stress ranges. The impact measured on the stringer for trains traveling at 65 km/h (40 mph) ranged from 5.0% to 9.0%, and at 80 km/h (50 mph) it ranged from 4.2% to 7.4%. It was noted that these values are much less than the 51.5% recommended in the 1980 AREA manual (current at the time of the paper) [7].

Four analytical models were developed to compare the measured strains to the calculated strains. The four analytical models were: (1) a simple beam, (2) a plane model of one truss span with all connections pinned, (3) a plane model of one truss span with all connections continuous, and (4) a space frame of the entire bridge with all connections continuous. All the models except the simple beam were used to compare the measured and calculated strains in the hangers. The ratio of measured to calculated strains varied from 0.913 to 1.013. The stringer and floorbeam measurements were compared with the results obtained from the simple beam model and the space frame model. For the stringers, the ratio of measured-to-calculated strains for the simple beam model ranged from 0.994 to 1.091, and for the space frame model the ratio ranged from 1.233 to 1.261. The measured-to-calculated ratios for the floorbeams were 1.074 to 1.041 and 1.006 to 1.089 for the same two models, respectively. It was concluded that stringers and floorbeams generally behave as simple beams.

In 1991 Pietraszek and Oommen reported on the static and dynamic behavior of a four-span riveted plate girder railway bridge [8]. Strain gages were attached to the top and bottom flanges of one of the girders, on the lateral bracing and cross bracing between the girders, and on the rails in order to measure the lateral and vertical wheel loads. Displacement transducers were attached to the span center and to the abutments in order to measure vertical and horizontal displacements. Measurements were made under controlled static and dynamic loads, using both a special work train and regular traffic. The measurement of the vertical shear in the rails showed there was a difference of about four percent between the yard scale and the wheel loads. The maximum impact was measured as a factor of 1.154 for the top flange strains and 1.160 for the bottom flange when traffic passed over at 96.5 km/h (60 mph). A simple beam model was used to

compare the measured stresses to the calculated stresses. The ratio of measured-to-calculated strains for the top flange ranged from 1.25 to 1.32, and for the bottom flange it ranged from 1.00 to 1.05. Large top flange strains were measured, and these were attributed to local bending effects caused by the rail ties, which lay directly on the flange.

The measured deflections were compared to a two-dimensional model and a three-dimensional model. The two-dimensional model included elements for the girders and single elements for the cross-bracing. The plane of the two-dimensional model was a plan view of the bridge. The three-dimensional model consisted of beam and plate elements used to model girder flanges, webs, stiffeners, and bracing. Both models used simple supports as boundary conditions, and influence lines were calculated for the points at which deflection measurements were taken. The ratio of measured-to-calculated deflections for the two-dimensional model ranged from 0.92 to 1.08, and for the three-dimensional model the ratio ranged from 0.97 to 1.03.

2.2 Fatigue Resistance of Riveted Connections and Members

2.2.1 Fatigue of Small Scale Riveted Connections

Much of the fatigue test data of riveted connections that are available today began from the work of Wilson and Thomas done in 1938 [9]. They reported on the results of extensive static and fatigue tests on rivets and riveted lap and butt joints. Some of the variables examined were stress range, rivet bearing, and effect of hole preparation. The behavior of the riveted connections was also compared to high-strength pretensioned bolted connections. It was found that, although the bolts were not pretensioned as much as they could have been [10], the bolted joints provided a fatigue resistance as great as joints with well-driven hot rivets. This showed the importance of clamping force on fatigue resistance of a connection.

The clamping force that is developed in a fastener squeezes the connected parts together. Bolts develop their clamping force in a different manner than do hot-driven rivets. In bolts, the clamping force, or pretension, is developed as nut is turned on, and the level of clamping force is controlled by the amount the nut is turned (i.e. by the bolt elongation). For hot-driven rivets, the clamping force is developed as the rivet cools and shrinks. The base of the rivet heads tend to shrink away from the plate, but the shrinkage of the shank is greater. Therefore, the net change in deformation of the rivet is a reduction

of the rivet length, and the connected parts are squeezed together. The level of clamping force in a rivet varies substantially because it is influenced by the initial and final rivet temperatures, the length of the rivet, and the driving pressure [11].

The effect of clamping force on fatigue resistance of riveted connections was confirmed by Lenzen when he compared the fatigue strength of connections made using high-strength bolts, hot-driven rivets, and cold-driven rivets [12]. In summary, these fasteners have less clamping force and lower fatigue resistance in the order listed. The study showed that the large clamping force developed with the high-strength bolt enabled large forces to be transferred by friction between joint plates rather than by bearing. Because less load was transferred by bearing, the fatigue resistance of the connection increased. The effect of bearing ratio on fatigue resistance was specifically examined by Parola, Chesson, and Munse, who came to the same conclusion, that is, that increased bearing of the fasteners decreases the fatigue resistance of the connection [13].

Munse, Wright, and Newmark performed static and fatigue tests on riveted and bolted connections [14]. The fatigue tests again showed that fatigue resistance is lower in riveted connections than bolted ones. In the static tests, they observed that the riveted connection slipped less than did the pretensioned bolted connection. The reason for this was that the hot-driven rivets filled the holes more completely than did the bolts. Therefore, as load is applied to a connection, one fastened with rivets would more likely act in bearing than a bolted one because there is more chance of the rivet touching the sides of the holes. Similarly, if a connection is subjected to fatigue loads, rivets would more likely be in bearing than bolts, and thus it would likely have a lower fatigue resistance.

The effect of rivet grip upon fatigue strength was reported by Baron and Larson in 1954 [15]. They reported that the fatigue resistance of a connected plate increased with increasing grip. The reason for this is that in a longer rivet, the shrinkage of the rivet head is a smaller proportion of the shrinkage of the shank, and thus there is a larger reduction of rivet length and consequently a higher clamping force. As was seen in the previously reviewed reports, high clamping force in a riveted connection generally produces fatigue resistance that is superior to a case in which the clamping force is low. Elsewhere, it has been reported that rivets with short grip almost completely fill the holes, while rivets with

longer grip have greater clearances between the rivet and plate [11]. This suggests that, for longer grip rivets, the load is less likely to be transferred by bearing because there is more space for the rivet to move, and, hence, the connection will have a higher fatigue resistance.

Based upon previous research, Carter, Lenzen, and Wyly developed and verified a working hypothesis on fatigue failure in structural joints [16]. They assumed that fatigue crack growth occurred in regions of tensile stress concentrations, and that in a structural connection the highest stress concentrations occurred at the holes where rivets were bearing against the edge of the hole. In their words, "these concentrations occur most frequently with rivets that have lost—or never had—high clamping force." Fatigue failure is more likely to occur when rivets are bearing, and bearing is more likely to occur under reduced clamping. Clamping force has a two-fold benefit. It enables the joint to transfer load by friction, and it creates favorable compressive stresses in the vicinity of the hole.

This review of the literature indicates that fatigue failure of a riveted connection is precipitated by the high stresses around a rivet hole, and that these result from both the stress concentration of the hole itself and from the bearing stresses produced by the rivet acting against the side of the hole. The higher the stresses around a rivet hole, the lower the fatigue resistance. Since high stresses are more likely to occur when the fastener is in bearing, riveted connections tend to have lower fatigue resistances than do equivalent bolted ones because rivets fill more of the hole, leading to bearing. Moreover, they do not always develop high enough clamping forces to transfer load by friction.

Fatigue crack propagation can also occur in the gross cross-section of riveted and bolted connections [11]. When fatigue loads are transferred by friction in a joint, the strain in adjacent connected components can be very different. The result of this is microslip between the faying surfaces. The fretting that results can damage the faying surfaces and thereby create stress concentrations that could initiate fatigue cracks. Because in friction-type connections the fasteners develop high clamping stresses between the connected parts, the critical section for the fretting fatigue is moved away from the fastener region and into the gross cross-section. Hence, cracking is most likely to occur in the gross cross-section in such cases.

An extensive database of the available fatigue test data on riveted shear splices was prepared by Fisher et al. [17]. All of the reported tests were carried out above 97 MPa (14 ksi), and most of the results exceeded the Category D fatigue resistance curve. Fatigue resistance curves are discussed below.

2.2.2 Fatigue Tests of Full-Scale Riveted Members

It has been shown that the most important variables that govern fatigue resistance of fabricated steel members are stress range, number of cycles, and type of detail [18]. Both physical tests and a fracture mechanics analysis show that a linear relationship exists between the logarithm of the stress range ($\Delta\sigma$) and the logarithm of the number of cycles (N) [1]. It is convenient to group the results of physical testing according to "detail categories." These appear in standards or codes for design. They represent the mean of test results less two standard deviations (of cycle life) for a given set of data, and they can be presented graphically (log $\Delta\sigma$ vs. log N), in tabular form, or simply as the equation of the line. The standard categories referred to in this report are the AASHTO detail categories, and they represent the 95% confidence limit for 95% survival [19, 20]. The particular detail categories of interest in this report are Categories C and D. They are shown in Figure 2.1. Also in this figure are test results from the literature reviewed in this section; those test results are presented and discussed below.

In 1975, Reemsnyder reported the results of fatigue tests on full-size truss tension chords and gusset plate connections [21]. Sixteen newly constructed full-size models, and two specimens taken from service were tested in axial tension and compression (i.e., a load reversal stress range). All specimens except two were tested under constant amplitude loads: the two exceptions were tested under variable amplitude loads. The critical detail was the connection between the tension chord and gusset plate. The connection resembled a lap splice that transferred load by shear. The primary purpose of the test program was to examine a method of rehabilitating fatigue cracked members by replacing rivets with high-strength bolts. Of interest here are the test results for new constant amplitude test specimens that did not have the rivets replaced, and these are shown in Figure 2.1. The plotted points correspond to the condition wherein there was partial fracture of one component of the built-up truss chord.

Baker and Kulak examined riveted hangers taken from a 70-year-old highway bridge [22]. The hangers consisted of two back-to-back angles for each flange and lattice bars as a web. Each lattice bar was connected to the angle by a single rivet at each end. The hangers taken from the bridge were divided into two specimens by flame-cutting the lattice bars in half. Specimens were loaded in constant amplitude axial tension in such a way that the rivets did not take any load. Analytical modeling of the traffic concluded that previous fatigue damage was negligible. Failure was defined as the time at which one component of the hanger fractured. After each failure, the remaining uncracked portion of the specimen was reinserted into the test setup so cracking could be developed at another rivet hole. These results are also shown in Figure 2.1.

In 1984, Out, Fisher, and Yen reported the results of fatigue tests on six stringers taken from an existing railway bridge [23]. The purpose of the investigation was to gain information on built-up sections, particularly because the majority of previous testing had been done on small butt splices. The stringers consisted of a web plate and two angles each for the top and bottom flanges. There was significant local corrosion at lateral bracing connections to the flanges. Constant amplitude four-point bending was used to test the stringers, and, apart from cracks originating from corrosion notches, the critical detail was the continuous riveted connection between the web and the flange. Measurements made while the bridge was in service indicated that only about 1% of the loads exceeded the Category D endurance limit. The effect of previous loading was therefore neglected.

The data given in Figure 2.1 represent the fracture of one component due to a crack initiating in the critical detail. Failures due to cracks initiating in corrosion are not included. Net section calculations took into account any area lost by corrosion, and therefore the stress range at each crack generally was different. Most cracking began at the lower rivet hole of the continuous connection. Crack initiation was best described by Category D, but fracture of one component did not significantly impair the load-carrying capability of the stringer. Usually between one-half and one million additional stress cycles after component fracture were required to eliminate the load-carrying capacity of the member. According to this study, corrosion did not affect fatigue resistance unless the flange thickness had been reduced by at least one-half.

In 1987, Fisher, Yen, and Wang published a report on fatigue evaluation of riveted bridges [17]. They did an extensive review of previous fatigue data on riveted shear splices and tests on full-scale members. Based on this review, it was concluded that differing riveted details were not significantly different in fatigue resistance, that Category D provided a lower bound for crack detection, and that failure of the cross-section and loss of load-carrying capacity did not happen until Category C was reached.

As well as reviewing the work of others, Fisher et al. reported on a new set of full-scale fatigue tests that they carried out on riveted members that had been removed from service. All of the stringers had coverplates riveted to the top and bottom flanges and were tested under constant amplitude four-point bending. One of the goals of the test program was to examine the behavior of coverplate terminations. Accordingly, simulated terminations were created by grind-cutting out a gap in the plate. The results of the fatigue tests showed that most cracks began in the web-to-flange continuous connection, and that only a few cracks began at rivet holes at a coverplate termination. The fatigue lives of these tests supported the conclusions from the previous data review, that is, that cracks could be detected by the time the Category D life was reached and that the fatigue life could actually extend to the Category C life, because of the inherent cross-section redundancy of riveted members. Cracks in one component of a riveted member do not immediately propagate into another component, which is different than in, say, welded members. Hence there can be a relatively long load-carrying capacity after first detection of cracks. All data from the fatigue tests are plotted in Figure 2.1.

Brühwiler, Smith, and Hirt reported the results of fatigue tests on rolled, mild steel girders with coverplates riveted to the bottom flange [24]. All specimens were tested in constant amplitude four-point bending. Failure was defined as the time at which the deflection of the girder had increased by 0.2 mm. This criterion was chosen because at this deflection crack propagation was rapid enough that it was assumed failure was imminent and further cycles would be unnecessary. When this point was reached, the cracks were repaired and the test was continued so as to develop cracking elsewhere in the specimen. These test results are also plotted in Figure 2.1.

In 1990, Fisher, Yen, and Wang published a paper that reviewed results of the previous 1987 Fisher et al. report, and the Brühwiler et al. report [25]. Again, the

conclusions were that Category D provides a lower bound to crack detection and Category C characterizes the fatigue strength of riveted members. These conclusions were based upon the following observations. Initial cracking occurred only when stress ranges exceeded Category D. All tested members were able to retain their load-carrying capacity by redistribution after one or two components had cracked, even under reduced temperature conditions. Another conclusion reached was that, from observations of field measurements, stress ranges rarely exceeded the applicable fatigue limit, hence, most fatigue cracking in riveted bridge members would be the result of secondary stresses or out-of-plane distortions.

In a discussion to the Fisher et al. paper, it was pointed out that the use of the term "lower bound" departs from the standard convention used for fatigue curves, which are generally defined by two standard deviations of cycle life from the mean of the test data [26]. It was also pointed out that the amount of internal load redistribution will depend on which component is cracked, and would vary in different girder configurations. Concern was also expressed about applying some of the conclusions to long life fatigue conditions. Although actual stresses may presently be less than calculated stresses, new demands from higher axle loads and section loss due to corrosion can be expected to increase actual stress levels. The discusser concluded that Category D should still be used for fatigue strength assessment.

The Fisher et al. reply to the lower bound issue was that because there was not enough fatigue data to calculate the two standard deviation offset, Category C and D curves were used to describe the behaviour of riveted member crack growth. Thus, for the "lower bound," the lowest strength observed in the test data was used (initial crack development), and the actual fatigue strength was described as being best estimated by Category C. It is unclear whether a "best estimate" means Category C is the mean of the data, or some portion of a standard deviation less. Concerning the amount of redundancy, it was replied that no significant failure by fracture has been reported in actual riveted bridge members, and that the aim of the conclusion in the paper was to say that immediate fracture does not occur when a crack is observed in one component. As to the question of long life fatigue behaviour of riveted members, Fisher et al. agreed that much work needs to be done for both constant and variable amplitude stress ranges. However, since

information is required now, it was restated that the dual category approach should be used for guidance.

A research project sponsored by CN Rail was underway at Lehigh University at the time this literature review was being done [27]. Full-scale riveted bridge girders were being tested under constant and variable amplitude loads. In order to eliminate the influence of previous loadings, the stringers were tested in the inverted position relative to their original orientation, thereby testing the top flange detail. The top flange has the same continuous riveted web-to-flange connection as the bottom flange. The constant amplitude test results from this program are included in Figure 2.1.

The test results plotted in Figure 2.1 show that the fatigue resistance of riveted members appears to have Category D as a lower bound. Failure was defined as loss of the load carrying capability of the specimen, and generally did not occur until more than one component of the specimen had begun cracking. For riveted beams, most cracks began at a rivet hole in the continuous web flange connection within the constant moment region. In this region there is no shear, and therefore no shear forces are applied to the rivets. Thus, the stress concentration that started crack growth probably was caused by the presence of the hole only, and not by any bearing of the rivet on the edge of the hole, even under reduced clamping.

In the tests of tension members by Baker et al., cracks also only developed at the rivet holes. Under ideal conditions, rivets in tension members only hold the connected parts together: no shear forces are applied to the rivet. Therefore, the stress concentration needed for fatigue crack growth was probably caused by the presence of the hole only. These fatigue tests appear to have been carried out on details that are different than the small-scale shear specimens referred to earlier. Except for the testing by Reemsnyder, in all the full-scale tests the rivets are under little, if any, bearing, while in the small-scale shear tests, the rivets are more likely to have been in bearing.

2.3 Remaining Fatigue Life

Various committees that write standards in North America and Europe provide guidelines for evaluating the remaining fatigue life of existing bridges. The basic procedures for this evaluation are the same for all the codes reviewed in this report. The standards reviewed were those of the American Association of State Highway and

Transportation Officials (AASHTO) [4], the American Railway Engineering Association (AREA) [2], the European Convention for Constructional Steelwork (ECCS) [28], and the Ontario Highway Bridge Design Code (OHBDC) [29]. In this section, a brief overview of the common evaluation procedure recommended by these codes will be described, followed by the specific recommendations of each.

2.3.1 Common Method of Fatigue Evaluation

There are three basic steps that are used in all the evaluation procedures: (1) an assessment of the magnitude of variable stress ranges and the corresponding number of cycles at critical details, (2) damage accumulation of these variable stress range cycles and conversion into an effective stress range, and (3) calculation of the remaining fatigue life.

The variable stress range and the number of cycles can be determined either from traffic surveys and field measurements of bridges under normal traffic conditions or from an analytical analysis of the bridge using influence lines and vehicle loads. The individual variable stress ranges are converted into a constant amplitude effective stress range by a method of damage accumulation. The constant amplitude effective stress range is that stress range which would cause the same fatigue damage as the variable stress ranges it represents.

The damage accumulation method to convert variable stress ranges into the effective stress range is based on the simple and widely-used Palmgren-Miner cumulative damage rule [1]:

$$\sum \frac{n_i}{N_i} = 1 \qquad (2.1)$$

where: n_i = number of cycles at stress range level i

N_i = number of cycles to cause failure at stress range level i.

This equation can be combined with the theoretical relationship between stress range and number of cycles:

$$N = M\ \Delta\sigma_i^{-m} \qquad (2.2a)$$

or:

$$\log N = \log M - m \log \Delta\sigma_i \qquad (2.2b)$$

where: N = total number of applied stress cycles

M = a constant obtained from the test data

$\Delta\sigma_i$ = stress range level i

m = slope of the fatigue resistance curve

to produce the damage accumulation equation in terms of an effective stress range. This takes the form [28]:

$$\Delta\sigma_e = \left[\sum_{i=1}^{k} \frac{\Delta\sigma_i^m n_i}{N}\right]^{\frac{1}{m}} \qquad (2.3)$$

where $\Delta\sigma_e$ = the effective stress range.

Equation 2.3 was examined in detail by Schilling et al. [30]. Two forms of the equation may be used. If m is taken as two, Eq. 2.3 is known as the root mean square (RMS) of the stress spectrum. If m is taken as three, then the equation is known as the Miner summation, because it is equivalent to Eq. 2.1. The results of this study showed that both forms of the equation represent the variable amplitude stress spectra, but that the RMS form fits the data slightly better. The difference between the two is usually less than 10%, with the Miner summation the more conservative.

All of the standards reviewed recommend use of Eq. 2.3, with slightly different notation, for the calculation of the effective stress range. The value m is given as three because that is the conservative choice. The remaining fatigue life can be seen visually by plotting the effective stress range $\Delta\sigma_e$ and the number of stress cycles N on the constant amplitude fatigue resistance curves provided in the standards. The number of cycles between the plotted point and the detail Category line is the remaining fatigue life for the detail. For reasonable accuracy, the projection should be made by calculation. If desired, the number of remaining cycles can then be converted to time on the basis of an assumption as to future traffic conditions.

2.3.2 Review of Current Standards

In 1990, AASHTO produced a guide for fatigue evaluation of existing steel bridges based upon an extensive report by Moses et al. [31]. It was intended that the guide eventually be included in the AASHTO Manual for Maintenance Inspection of Bridges [20]. The guide focuses on highway bridges and traffic loadings, and it provides guidelines for calculating remaining fatigue life as either the remaining mean fatigue life or as the

remaining safe fatigue life. The remaining mean life has a 50% probability of being exceeded, and it is considered the best estimate of the remaining fatigue life. It is generally used for cost comparisons and estimates. The remaining safe fatigue life has a 97.7% or a 99.9% probability of being exceeded for redundant or non-redundant members, respectively, and is used in specific evaluations that require a higher degree of safety.

In the AASHTO guide, the fatigue evaluation is divided into three sections; calculation of stress range, calculation of remaining life, and options to be considered if remaining life is inadequate. A number of different calculation procedures are given in each category, and these attempt to account for varying levels of initial information and the final precision desired. In the stress range section, it is advised that variable stress ranges should be determined from field measurements. If this is not possible, then alternative methods using standard fatigue trucks, weigh scale measurements, and traffic surveys are described, along with procedures for calculating superposition of truck traffic, impact, and load distribution. After the variable stress ranges have been calculated, they are converted to the effective stress range using an equation similar to Eq. 2.3 and with $m = 3$.

In the AASHTO guide, the remaining fatigue life section compares the calculated effective stress range to a set of fatigue resistance curves. The fatigue resistance curves are the standard AASHTO curves except that the constant amplitude fatigue limits have been removed and replaced with lower limits called the variable amplitude fatigue limits. These are shown in Figure 2.2 [19]. The new variable amplitude fatigue limits are 0.367 times the original constant amplitude fatigue limits. These new limits come from the concept that if the effective stress range is below the variable amplitude fatigue limit, then virtually all the cycles in the spectrum will be below the respective constant amplitude fatigue limit. If the effective stress range is less than this limit, then the fatigue life is assumed to be infinite for the detail under examination. This limit is also considered a cut-off limit, which means that any stresses below this limit are not considered to contribute to fatigue damage during the calculation of the effective stress range.

The final section of the AASHTO guide provides options if the calculated remaining fatigue life is inadequate. These options are to recalculate the remaining fatigue life using one of the alternative methods, to restrict the traffic that uses the bridge, to

modify the bridge to eliminate or extend the life of the critical detail, or to institute inspections of the critical details so as to enable timely discovery of any crack growth.

AASHTO recommends use of fatigue resistance Category D for the base metal at the net section of a riveted connection. The Fisher et al. 1987 report on fatigue of riveted bridges recommended changes to the AASHTO Manual for Maintenance Inspection of Bridges to the effect that riveted steel members that resist net section tensile stress by three or more components (e.g., one web and two flange angles) can be checked according to Category C for fatigue resistance. This is based upon their conclusions that Category D identifies fatigue crack development and Category C characterizes fatigue resistance, defined as the ability of a member to carry load with one or two cracked components.

Fatigue evaluation of existing railway bridges is covered in the AREA standard [2]. As in the AASHTO standard, an effective stress range is calculated using a formula similar to Eq. 2.3 with $m = 3$. The equation is modified by a factor to account for contribution to load resistance from the lateral bracing, floor systems, or other three-dimensional effects, and, the fact that impact is not present for every stress cycle. For the bridge under consideration in this report, the factor, α, is equal to 0.85. The Standard allows for substitution of another value if an analysis provides a more accurate estimate.

The effective stress range is compared to the AREA fatigue resistance detail categories, shown in Figure 2.3, which are the same as the AASHTO categories. For variable amplitude loading, the constant amplitude fatigue limit is to be removed and extended at the same slope if more than 0.1 % of the stress ranges have exceeded it. The curves are extended to 100 million cycles and there is no mention of a variable amplitude fatigue limit or a cut-off limit.

AREA recommends use of Category D for members with riveted or bolted connections with low slip resistance. However, this may be increased to category C if the effective stress range is less than 83 MPa (12 ksi), and the engineer can verify that the rivets have developed normal clamping force. Under such circumstances the constant amplitude fatigue limit for Category D must still be used. No guidance is provided as to how to verify the clamping force. The reasoning behind this benefit is that Category D was defined with riveted connections that had low clamping force, and that rivets with high

clamping force are better defined by Category C. Hence, a higher fatigue resistance is permissible for rivets with normal clamping force.

More stringent fatigue category requirements are specified for fracture critical members, i.e., members whose failure would make the bridge unable to fulfill its intended service. However, riveted members are not considered to be this type of member because of their internal cross-sectional redundancy. If the riveted members do not satisfy the fatigue category requirements, the requirements may be waived if it can be deemed that the members have adequate structural redundancy to redistribute the load when one of the components cracks. Inspections must be frequent enough to discover the local failure and to complete repairs.

The ECCS standard recommends use of the rainflow counting method with the Miner summation (Eq. 2.3) to determine the effective stress range and then comparison with the fatigue resistance curves shown in Figure 2.4 [28]. In this standard, the slope of the curves (m) is three and detail categories are defined by the value of the curve at two million cycles, rather than by letter designation as used in the North American standards. For all details, constant amplitude fatigue limits are at five million cycles. If all of the variable amplitude stress ranges are below this limit for the particular detail, then the fatigue life is assumed to be infinite. However, if one cycle has a stress range higher than the constant amplitude fatigue limit, then all stresses are expected to contribute to fatigue damage and the constant amplitude fatigue limit is replaced. In its place, the Engineer has the option of either continuing the slope downward at three (conservative), or changing the slope to five. In both cases, the sloping straight line is cut off at 100 million cycles. If the slope is changed to five, then the Miner summation for effective stress range takes the form

$$\Delta\sigma_e = \left[\sum_{i=1}^{k} \frac{\Delta\sigma_i^3 n_i}{N}\right]^{\frac{1}{3}} + \left[\sum_{i=1}^{k} \frac{\Delta\sigma_i^5 n_i}{N}\right]^{\frac{1}{5}} \qquad (2.4)$$

where the first term is for stress ranges above the constant amplitude fatigue limit and the second is for the stress ranges below that value.

No detail categories are specified for riveted members and connections because the ECCS standard is intended to be used for new work. However, the standard indicates that

it may be used for fatigue assessment of existing structures following a suitable adaptation of the standard. However, no guidance is given for the adaptation. In the Eurocode, a standard for the European Community, the recommendations of the ECCS are repeated [32]. Further provision is made for using test data to determine detail categories. A detail category is specified as the 75% confidence limit of 95% probability of survival, in cycle life, of the test data. A minimum of 10 data points are required. If the North American Category D is plotted on the ECCS graph, it would be equivalent to a Detail Category 69.

In Canada, the OHBDC can be used to evaluate existing bridges [29]. This standard uses the same fatigue resistance curves as those given by AASHTO. No specific recommendations are made in the code regarding variable amplitude stress ranges, but the commentary provides detailed information regarding the use of Eq. 2.3, with m = 3.

2.3.3 Alternative Method of Fatigue Evaluation

In addition to the fatigue evaluation methods recommended in the standards reviewed, some alternatives have been developed. One that is used in this report consists of a new damage accumulation technique and a modified form of the AREA fatigue resistance curve, both based on fracture mechanics. The purpose of the new damage accumulation method is to more accurately reproduce the effect of variable amplitude stress ranges that straddle the constant amplitude fatigue limit. This evaluation method has been developed elsewhere and information about the concepts and calculation procedures has been published [33, 34]. It will be referred to hereafter as the Kunz evaluation method. For purposes of discussion, a general description will be given as to how fracture mechanics was used to develop the new damage accumulation technique and the modified fatigue resistance curve. The discussion will begin by describing how fracture mechanics can be related to the conventional fatigue resistance curves given in contemporary standards.

Fatigue resistance curves represent the number of constant amplitude stress cycles to which a structural detail can be subjected before a fatigue crack will propagate enough to cause failure. Between the first and last applied stress cycles there exists stable crack propagation. Fracture mechanics can describe stable crack propagation by the following equation [34]:

$$\Delta K = Y(a)\Delta\sigma\sqrt{\pi a} \qquad (2.5)$$

where: ΔK = stress intensity factor range

$Y(a)$ = correction factor based on specimen and crack geometry

$\Delta\sigma$ = applied stress range

a = crack size

The stress intensity factor range describes the range of stress intensity at the crack tip. The larger the stress intensity factor range, the more a crack will propagate under a stress cycle. This can be seen in Figure 2.5, where experimental data is used to plot the stress intensity factor range against the rate of crack propagation. In the nearly linear sloping portion of the graph, it is seen that as the stress intensity factor range is increased, so does the rate of crack propagation. This portion of the graph has been described by the Paris Law [1].

The graph also shows a threshold stress intensity factor range. When the applied stress range causes a stress intensity factor range less than this threshold, no crack propagation will occur. Conversely, if the stress intensity factor range is greater than the threshold, crack propagation will occur. Observed between the threshold region and the linear portion is a transition region, which will be discussed later in this report.

A typical fatigue resistance curve is shown in Figure 2.6. This curve can be derived from Eq. 2.5 and the Paris Law, and has been done elsewhere [1]. However, for purposes of discussion in this report, it can be seen by inspection that if Figure 2.5 is rotated 90 degrees counter-clockwise, it is very similar to Figure 2.6, notwithstanding dimensions. The Paris Law portion of the fracture mechanics curve is analogous to the sloping detail category, and the threshold stress intensity factor range is analogous to the constant amplitude fatigue limit.

We will now discuss the development of the new damage accumulation method based on fracture mechanics. When Eq. 2.5 is modified to represent the threshold stress intensity factor range it takes the form:

$$\Delta K_{th} = Y(a)\Delta\sigma_{th}\sqrt{\pi a} \qquad (2.6)$$

where: ΔK_{th} = threshold stress intensity factor range

$\Delta\sigma_{th}$ = threshold stress range.

For materials such as steel, the threshold stress intensity factor range is essentially a constant. This means that for crack propagation to occur, either the applied stress range

must be higher than the threshold stress range, or there must be a large crack size. Both of these cases can cause the applied stress intensity factor range to be higher than the threshold stress intensity factor range.

When a detail is subjected to variable amplitude loading and all of the applied stress ranges produce stress intensity factor ranges below the threshold stress intensity factor range, no crack propagation will occur. However if one stress intensity factor range is above the threshold stress intensity factor range, then crack propagation will occur. The result of this crack propagation is that both the crack size and the geometric factor will become larger. Referring to Eq. 2.6, if both the term Y(a) and the crack size "a" become larger, $\Delta\sigma_{th}$ must be decreased in order to balance the equation, since ΔK_{th} is a constant. Decreasing the threshold stress range means that a lower stress range is required to produce further crack propagation. When this concept is applied to the fatigue resistance curve, the constant amplitude fatigue limit is removed and is replaced with a new lower limit, called the damage limit. Each subsequent stress cycle that exceeds this damage limit will cause another new, reduced damage limit.

This concept is used in the Kunz evaluation method. Evaluation is begun using the constant amplitude fatigue limit but, as soon as it is exceed by one stress cycle, a new damage limit is calculated. The new damage limit is used until it is exceeded by another stress range, and then another damage limit is calculated, and so on. The formula used to calculate the damage limit is:

$$\Delta\sigma_d = \Delta\sigma_c\,(1 - D) \qquad (2.7)$$

where: $\Delta\sigma_d$ = damage limit

$\Delta\sigma_c$ = constant amplitude fatigue limit

D = existing damage

The existing damage is calculated using the Miner summation, and the damage limit is a fraction of the constant amplitude fatigue limit based on the amount of existing damage. Fatigue resistances for the Miner summation are obtained from the conventional fatigue resistance curves provided in the governing standard. Note that specific fracture mechanic parameters, such as initial crack size and stress concentration factors, are not used in the calculation.

The second part of the Kunz evaluation method is referred to as the modified fatigue resistance curve. From the crack propagation rate curve shown in Figure 2.5, there exists a transition region between the threshold stress intensity factor range and the Paris Law region. This transition region is observed from the experimental data. In conventional fatigue resistance curves, this region is ignored. However, in the Kunz evaluation method, it is incorporated in a manner similar to that shown in Figure 2.6.

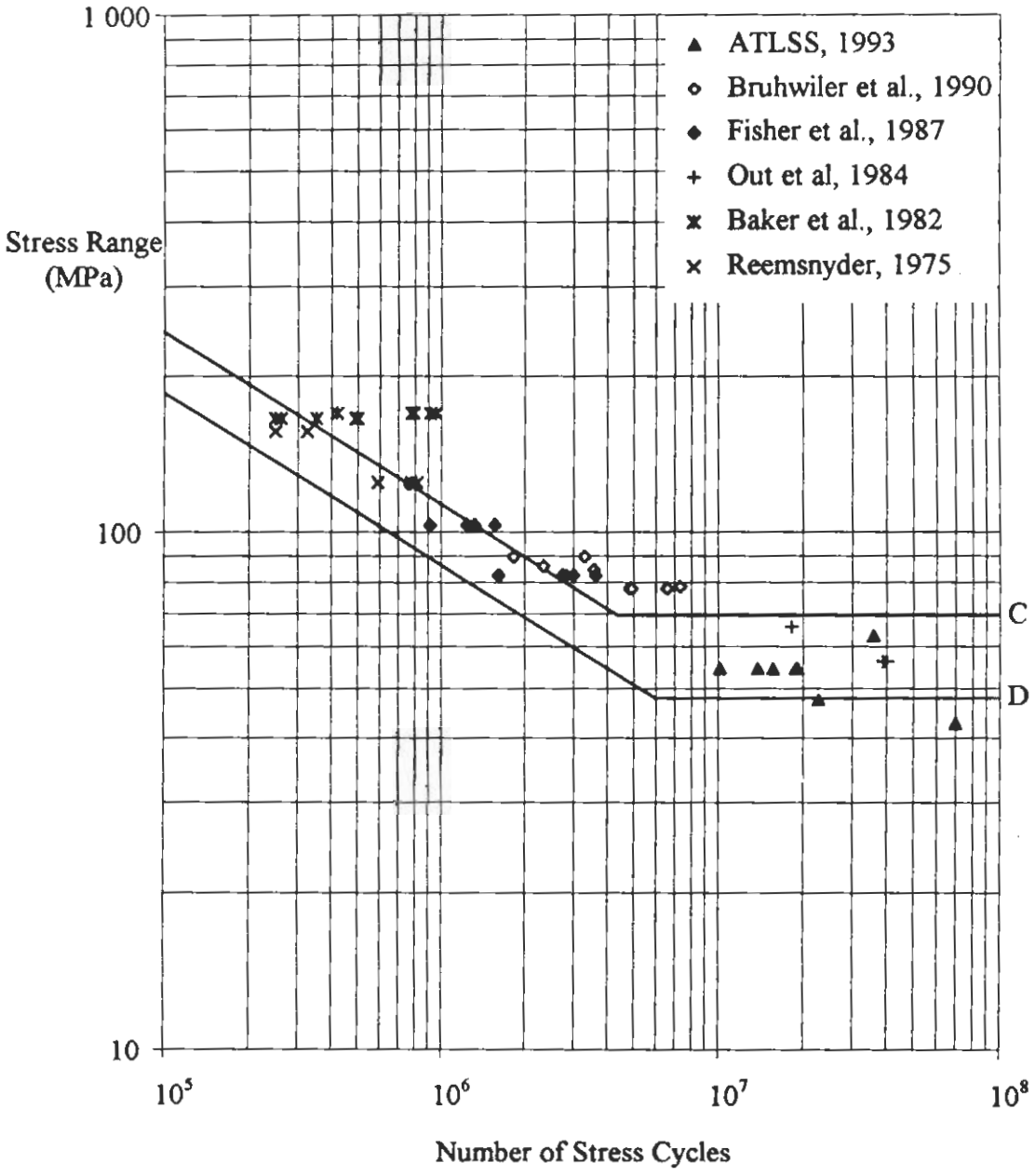

Figure 2.1 Fatigue tests of riveted members from literature

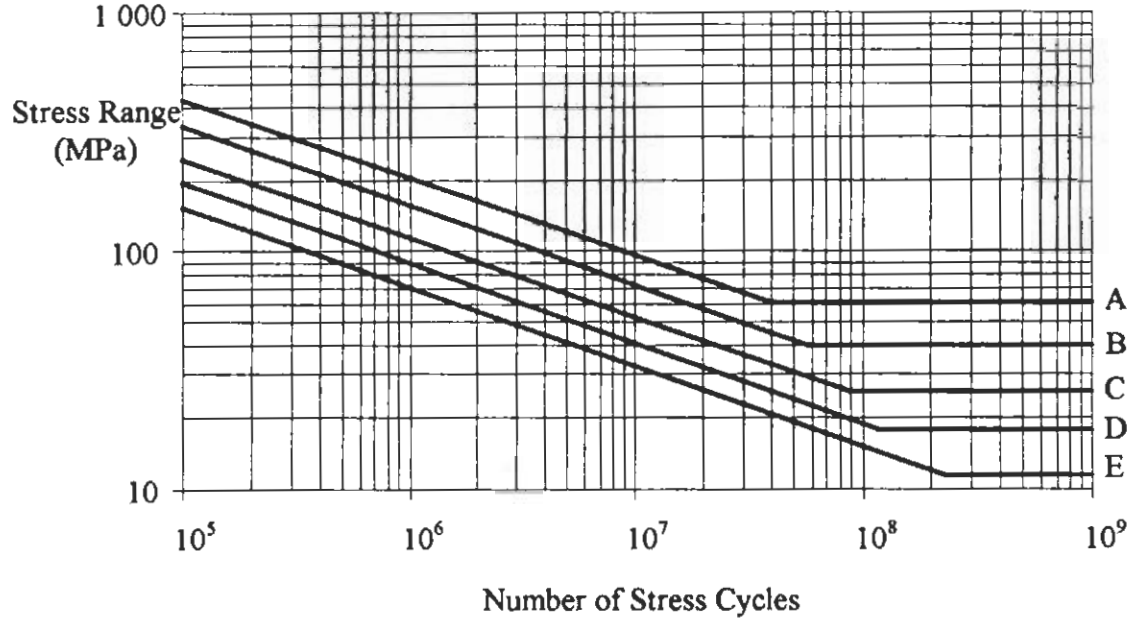

Figure 2.2 AASHTO variable amplitude fatigue rules

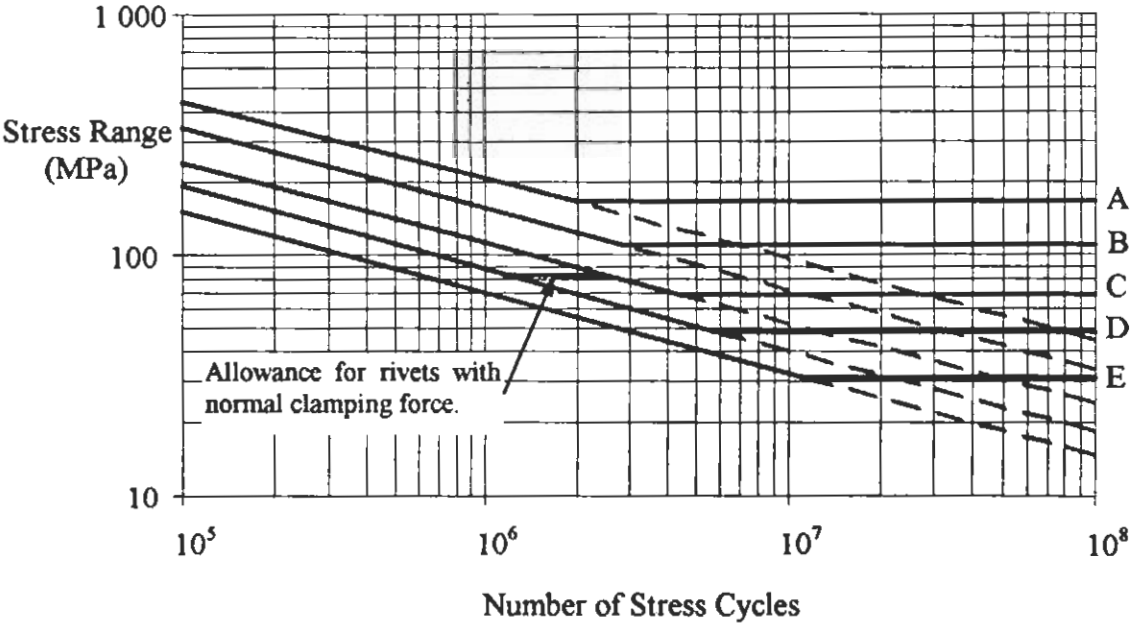

Figure 2.3 AREA constant and variable amplitude fatigue rules

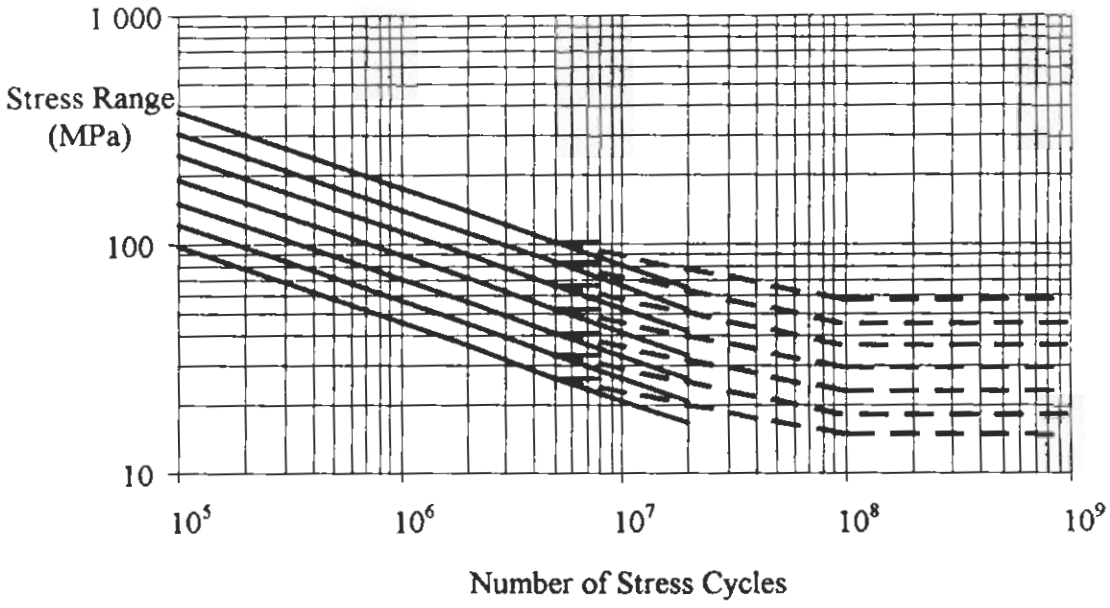

Figure 2.4 ECCS constant and variable amplitude fatigue rules

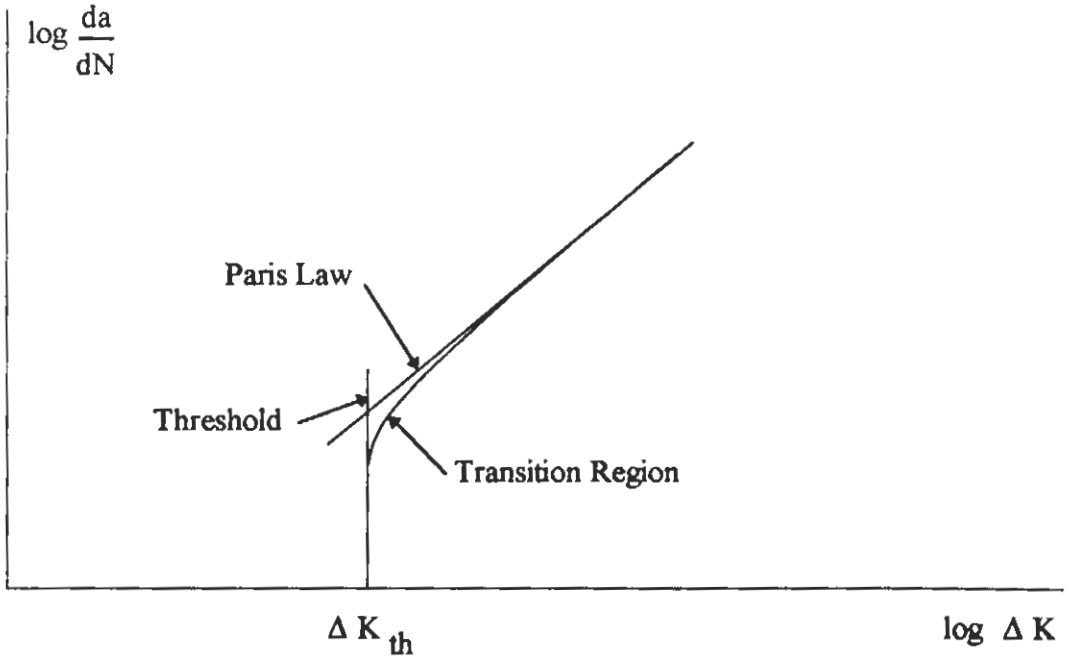

Figure 2.5 Crack propagation rate vs. stress intensity factor range

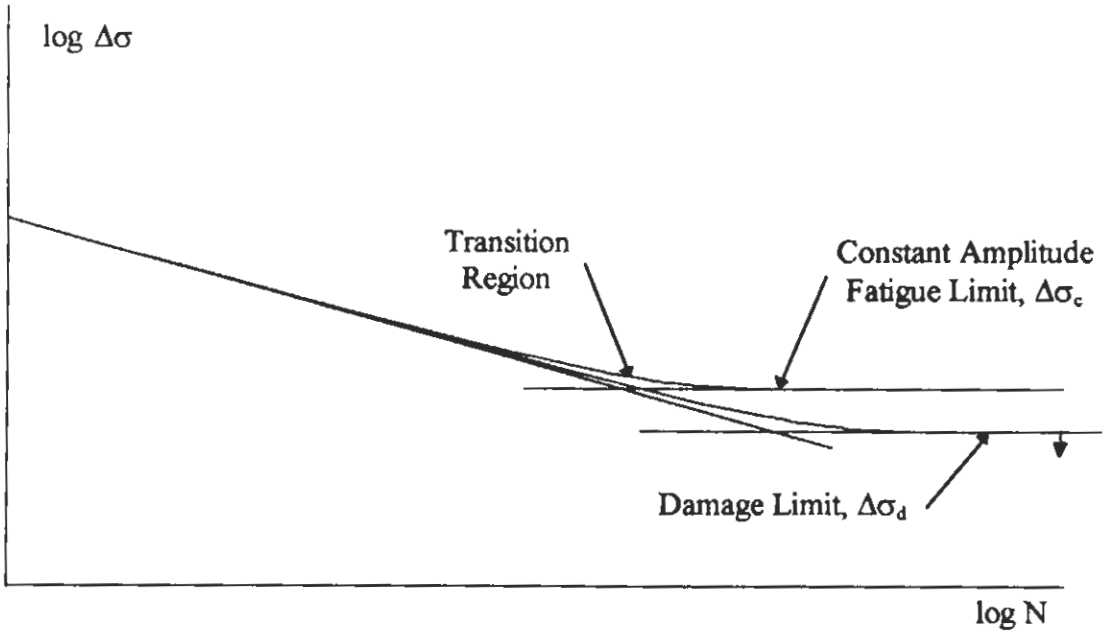

Figure 2.6 Typical fatigue resistance curve

3. FIELD STRAIN MEASUREMENTS

3.1 General

Evaluation of a bridge for its remaining fatigue life requires that the stresses in various members be determined, and that the number of cycles to which the bridge has been subjected in the past be established. If the stresses cannot be measured directly, for instance by measuring the strains on the bridge while it is still in service, then they must be determined analytically. However, analytical analysis usually cannot easily account for irregularities such as unintended restraint at connections or secondary load paths that exist in the real structure. For example, often connections were originally designed as pinned, but, because of realities of fabrication and conditions of corrosion, actually transfer some moment. In this Section, live load strains that were measured on the bridge while it was still in service will be compared with a corresponding static analysis. The purpose is to examine varying levels of analysis effort and to develop accurate influence lines that can be used for a subsequent remaining fatigue life analysis.

3.2 Bridge Description

The bridge under investigation was located across the Miette River on the Canadian National Railway (hereinafter referred to as CN Rail) mainline west of Jasper, Alberta (specifically, Mile 7.8 of the Albreda subdivision). It was originally constructed for the Grand Trunk Pacific Railway Company in 1911 by the Canadian Bridge Company Limited, of Walkerville, Ontario, and it was designed in accordance with the 1908 Dominion Government Specifications. In 1981, the railway was double-tracked at this location, and a composite beam girder bridge was constructed next to the existing bridge. In 1991, the bridge was replaced, primarily because of clearance restrictions for double-stacked container cars. A few days prior to removal, strain gages were attached to the structure to measure the live load stresses.

The bridge, shown in Figures 3.1 and 3.2, was a single track, 5 500 mm (18 ft) wide and 38 100 mm (125 ft) long straight through riveted truss structure with an inner stringer and floorbeam structural system, referred to as the floor system. One tension

diagonal and one stringer were instrumented in order that measured strains could be compared with calculated strains. These members were selected in order to separately examine the behaviour of the truss and the floor system. After the field measurements were completed, the bridge was removed from service. Ten stringers and four diagonals were taken to the I.F. Morrison Structural Laboratory at the University of Alberta for fatigue testing. The fatigue testing is discussed in Section 4.0.

Details of the strain-gaged diagonal and stringer are provided in Figure 3.3. The diagonal is a built-up section consisting of a 355 mm deep by 9.5 mm thick web plate (14 inch x 3/8 inch), and two 152 mm x 89 mm x 11 mm angles (6 inch x 3-1/2 inch x 11/16 inch) at each flange. The top and bottom flange angles were fastened by their short legs to the web plate by means of a single line of 22 mm diameter (7/8 inch) rivets. The rivets were spaced at 152 mm (6 inch) on centers, except near the ends of the diagonal, where the spacing was gradually reduced to 76 mm (3 inch). Rivet holes were punched to 21 mm diameter (13/16 inch) and then reamed to 24 mm (15/16 inch). Two 13 mm thick gusset plates (1/2 inch) were used to connect the flanges of the diagonal to the top and bottom chords of the truss. The diagonal was oriented in the bridge such that the web was perpendicular to the direction of the longitudinal axis of the structure.

The stringer was a built-up section consisting of a 1 220 mm deep by 9.5 mm thick web plate (48 inch x 3/8 inch) and two 152 mm x 152 mm x 17.5 mm angles (6 inch x 6 inch x 11/16 inch) for each flange. The flanges were fastened to the web by two lines of rivets placed in a staggered fashion. The transverse spacing (gauge) of the rivets was 57 mm (2-1/4 inch), and the stagger, or pitch, varied from a maximum of 108 mm (4-1/4 inch) at the centerline of the stringer to 38 mm (1-1/2 inch) near the ends. Along both sides of the web, 76 mm x 76 mm by 9.5 mm angles (3 inch x 3 inch x 3/8 inch) were attached as transverse stiffeners. A single line of rivets fastened the stiffener angles to one another though the web, and the ends of the angles were crimped to fit over the leg of the flange angles. The shop drawings indicate that the rivet holes were to be punched to 17.5 mm diameter (11/16 inch) and then reamed to 24 mm (15/16 inch) diameter. All rivets were 22 mm (7/8 inch). There was no indication on the drawings as to the grade of

the rivets. Standards from that time indicate that rivet steel should have a tensile strength between 317 to 386 MPa (46 to 56 ksi), and a yield point equal to one-half the tensile strength [35].

The stringer-to-floorbeam connection consisted of two angles between the respective webs of the members. Two 152 mm x 152 mm x 15 mm connecting angles (6 inch x 6 inch x 5/8 inch) were fastened on opposite sides of the stringer web. For interior floorbeams, two stringers framed into each side of the floorbeam web. Rivets fastened the outstanding legs of the stringer connecting angles through the web of the floorbeam. The floorbeam was a built-up section that used a 1 575 mm deep by 9.5 mm thick web plate (62 inch x 3/8 inch), and 152 mm x 152 mm x 14 mm flange angles (6 inch x 6 inch x 9/16 inch). The floorbeam was connected to the lower chord of the truss by means of two 152 mm x 152 mm x 15 mm (6 inch x 6 inch x 5/8 inch) angles attached to the floorbeam web. The outstanding legs of these angles were fastened to the truss panel point gusset plate.

3.3 Strain Measurement

Figure 3.3 also shows the arrangement of the strain gages on the diagonal and stringer. Strain gages were arranged into Wheatstone Bridge circuits in order to increase the sensitivity and accuracy of the measurements. The diagonal had one circuit on the web and one on each flange. These circuits had two strain gages measuring the maximum principle strain in the longitudinal direction of the diagonal and two transverse gages. The latter gages made the circuit insensitive to the transverse (Poisson) strains. Each circuit measured the axial strain in the particular component. On the stringer, there was one circuit on the web. The strain gages were arranged to measure the strong axis bending strain in the gross cross-section.

All four strain gage circuits were connected to a Validyne Carrier Demodulator. This device provided the excitation voltage to the circuits and also measured the output voltage. The output voltage was amplified with the same device and then sent to a datalogger. The datalogger sampled the amplified output voltage in all four circuits 40 times a second, meaning that each circuit was sampled 10 times a second. The sampled

output voltages were stored on diskette and, subsequently, converted to strain. The accuracy of the strain readings was judged to be about plus or minus one microstrain, based on the random fluctuations in the strain measurements when no load was on the bridge.

Live load strains were measured for six revenue trains as they passed over the structure. Revenue trains are the most common type of trains that use the line and they generally carry commercial products and natural resource materials. During the strain measurements, notes were made of the time, estimated speed, and a brief description of the train. The local freight speed limit at the location of the bridge is 48 km/h (30 mph), and for passenger trains it is 56 km/h (35 mph). Train speeds were estimated to vary between 26 and 56 km/h (16 to 35 mph). After the strain measurements were complete, train listings for the measured trains were provided by CN Rail. Train listings give details about the weight and length of each railcar and locomotive in a train. These listings are based on the train journals that are kept for all revenue traffic. The train listing information for this line is compiled at the CN yard in Edmonton, approximately 400 kilometers (250 miles) east of the bridge. CN Rail also provided detailed dimension information of the railcars and locomotives, so that axles could be located to establish the load points needed for the structural analysis of the system.

3.4 Bridge Analysis

3.4.1 General

A brief description of the analysis procedure is outlined following. Linear elastic structural models of the bridge were constructed using standard computer software. Using these models, influence lines were calculated for the internal forces at the strain-gaged locations on the real bridge. These forces were converted to strains using Young's modulus and the cross-section properties of the original (non-corroded) member listed on the drawings. Loading derived from the train listing information provided by CN Rail was then applied to the influence line in a manner consistent with that of a train moving across the bridge. The resulting calculated strains were then compared with the measured strains.

3.4.2 Structural Models

Construction of the structural models and calculation of the influence lines was done using the SAP90 series of programs [36, 37]. The models of the bridge were assembled using nodes and frame elements that were based upon the original dimensions of the bridge. These dimensions were obtained from a copy of the original blueprints. Only the main load-carrying members of the bridge were included in the models. Lateral, sway, and portal bracing were not included.

The section properties used in the models for the stringers were the gross area, the moment of inertia about the major bending plane, and the shear area in the major bending plane. Out-of-plane section properties were considered to have a minimal influence on the results and were therefore set to a very small value. For the floorbeams, moment of inertia values and shear areas in both planes were included, together with the gross area and the torsional constant. The effect of shear deformations on load transfer was considered by the program for both the stringer and the floorbeam. For the rest of the bridge, namely the truss members, cross-sectional area and moment of inertia about the strong axis were specified.

Three analytical models were developed for the bridge and are described herein as *Pinned*, *Continuous*, and *Continuous-with-Springs*. All models were three-dimensional representations of the bridge. The Pinned model used pinned connections between all truss and floor members. However, pins were only used in the major bending plane of the floor and in the vertical plane of the truss so that stability could be maintained since the lateral, sway, and portal bracing were not included in the model. Connections in the minor bending plane were continuous. The Pinned model was considered to provide an upper bound strain limit for the stringer since it was pinned at both ends, thus acting as simply-supported beam. This model was also considered to be that which would be used by an engineer for a conservative first estimate of the strains in the bridge. Often the model is constructed in two-dimensional space, and in many cases, it would likely be the only model used.

The Continuous model was developed mainly to be able to reflect the continuity between the members in the floor system. The stringers were connected to the floorbeams by two angles that fastened the full depth of the stringer web to the floorbeam web. The flanges of the two stringers were not connected. The usual assumption for this type of connection is that it is pinned; however, it is likely that the web angles can still transfer significant moment from one stringer to another because of the depth of the connection.

In the Continuous model, all member connections in both the truss and the floor system are specified as continuous. Theoretically, in this model each connection can transfer infinite moment, However, the actual amount of moment transferred depends on the stiffness of the members framing into the connection. For example, in the floor system, the amount of moment transferred between successive stringers depends on the bending stiffness of the stringers and the torsional stiffness of the floorbeam. Deformation of the connection angles is not represented in this model.

There is potential for transfer of moment between the truss members because all connections were made with gusset plates connecting the flanges. In the plane of the truss, such moments would not be very large, and it is reasonable to assume that the forces in the truss members are primarily axial. However, perpendicular to this plane, there could be moments due to the connection between the floorbeam and panel point gusset, which was connected in a manner similar to the stringer to floorbeam connection.

The Continuous-with-Springs model was developed to try to represent the behaviour of the bridge in the most accurate way possible. This model, and its resulting influence lines, will be used to represent the behaviour of the bridge in the subsequent calculation of remaining fatigue life. The model was developed after the strains predicted by the Pinned and Continuous models were compared with the measured strains, and where it was found that the Pinned and Continuous models predicted strains that were too high. In other words, the floor system in these models was not stiff enough.

Higher than expected floor stiffnesses may be attributed to several factors. Additional resistance may be provided by the lateral bracing that was attached directly to the bottom flange of the stringer. The presence of the rails may also have contributed to

the stiffness by taking loads directly or by increasing the bending resistance of the stringer. However, this resistance would likely be limited by the frictional resistance of the ties on the stringer and the use of expansion joints.

Another reason that the measured strains were lower than predicted is the way the models were loaded. In the model, the concentrated axle loads from the railcars were applied directly to the stringer flanges. In reality, the concentrated load would first be distributed among a number of rail ties, and the rail ties would then apply a distributed load to the stringer. A distributed load produces a lower midspan bending moment compared with a point load, hence lower strains in the stringer. It should be pointed out that there may also be decreases in the stiffness of the floor system caused, for example, by deformation of the stringer-to-floorbeam connecting angles.

It is difficult to judge the contribution of the variables affecting the floor stiffness, especially since strains were measured only in one location on the stringer. However, the purpose of the strain measurements is to develop an accurate influence line for the remaining fatigue life calculations, rather than to carry out an intensive analysis of the bridge. Therefore, the effects of all the components that are not directly included in the model are combined, and are represented by a rotational spring in the major bending plane at the stringer-to-floorbeam connection. The stiffness of the floor system is adjusted by modifying the spring constant until the calculated strains matched the measured strains.

The amount of spring stiffness was adjusted with two objectives in mind. The first was that the analytical model produce strains that are as close as possible to the measured strains. Obviously, this leads to a more accurate remaining fatigue life calculation. The second objective was that the model produce strains that are more conservative than unconservative, so as to reduce the chances that the calculated strains underestimate the real strains and thereby underestimate the amount of previous damage. To meet these objectives, the amount of spring stiffness was determined by an iterative process. Different stiffnesses were tried in the model and the strains were calculated from the applied loads. The calculated strains were compared to the measured strains, and, based on this comparison, the spring stiffness was adjusted. This process was continued until the ratio of

measured to calculated strains for one of the trains approached unity. The final rotational spring stiffness that was used was 271 160 kN·m per radian (2,400,000 in.-kips per radian).

Because the Continuous-with-Springs model is based on the measured strains, any effects of impact might be considered as already included, although this is not certain. It is unknown whether the train that this model is based upon is a true representative of normal impact conditions. The Pinned and Continuous models were developed using a static analysis, and therefore it is known that impact is not included. For these latter two models, not considering impact loads would produce slightly unconservative results.

3.4.3 Influence Lines

Influence lines were calculated by one of the SAP90 program modules. The location of the rails on the bridge was identified and the program used this information to calculate the influence line for any element. Figure 3.4 shows the influence lines developed by the various models for the stringer bending moment at the strain gaged location. The bending moment was converted to strain using the gross section modulus calculated from the original cross-section dimensions and a modulus of elasticity of 200 000 MPa (29,000 ksi).

The axial force influence lines for the diagonal are shown in Figure 3.5. The force was converted to strain by dividing by the gross cross-sectional area of the diagonal and Young's modulus. For the diagonal, the differences between the models are not very significant, which suggests that the response of the truss is not very dependent upon the type of connection assumed between members.

3.4.4 Loading

Once the influence lines obtained, the loads from the train listings were applied. Because this was a time-consuming and repetitive task, a computer spreadsheet was used. Railcar loads and lengths from the train listings were entered into the spreadsheet. This information was reduced in the spreadsheet to the load per axle and the axle location within each car. A macro program was then written to apply this information to the influence line. (A macro program is a program that runs on data in a spreadsheet).

Using the stringer influence line as an example, the macro started by moving the first axle onto the bridge. The moment was then calculated from the influence line and converted to strain using the theoretical section modulus and Young's modulus of elasticity. This strain was then stored back into the spreadsheet. The macro then moved more of the train onto the influence line, and a new strain was calculated. This procedure was repeated until the entire train had moved across the bridge. The final output is a list of strains, and these can then be compared directly with the measured strains for the same train.

3.5 Results

The results from the field measurements and the analytical models were in the form of lists of strains. The calculated and measured strains were plotted together in order to be able to examine the overall accuracy of each model. In addition to this procedure, a more precise comparison was done by converting the lists of strains to an effective strain range, using Eq. 2.3. This required that the maximum and minimum strains be identified and converted into list of variable amplitude strain ranges, which was done using the rainflow counting method [38]. All calculations were performed on a spreadsheet with a macro program. Both measured and calculated effective strains had strains ranges below two microstrain filtered out so as to disregard random fluctuations. Although these would only occur in the measured strains, the calculated strains were also filtered to be consistent.

The advantage of comparing the measured and calculated effective strain ranges is that all railcars are considered in the comparison, as opposed to randomly picking individual railcars and comparing the difference. Another reason is that it eliminates any errors from electronic zero shifts in the measurement equipment, which may occur in field testing environments. Shifting zero levels makes comparison of relative values of strain very difficult; however, effective strain ranges are absolute and are independent of the zero reference point. The final reason for using the effective strain range is that the resulting measured-to-calculated ratios can be used for more accurate estimates of the α-factor in the AREA standard [2].

3.5.1 Strains in the Stringer

Graphs comparing the measured and calculated strains are given in Figures 3.6 to 3.15. The names of the trains refer to the day and time that the strain measurements were made. For example, F100 refers to the particular train that ran on Friday at 1:00 p.m. This coding technique is essentially for the benefit of the author. For clarity, some of the graphs do not include all the railcars that were measured. For each train, there is a graph comparing the measured strains with the strains calculated using the Pinned and Continuous models, and another graph comparing the measured strains with the strains predicted by the Continuous-with-Springs model. The lengths and weights given on the graph are characteristic of most of the railcars in the train. The lengths are measured from hitch to hitch.

Some anomalies that could not be avoided exist in the graphs. In train F100 there were apparently four locomotives measured, but loads were obtained for only two, as seen in Figures 3.6 and 3.7. It was verified by CN Rail that two locomotives may have been added in Jasper for the trip through the mountains. To account for this, the plot of the calculated strains was begun at the start of the final two locomotives. For train F130, in Figures 3.8 and 3.9, the calculated strains between time 10 and 20 seconds are abnormally higher than the measured strains. This is very evident also in the corresponding diagonal strain measurement, Figures 3.20 and 3.21. It is believed that the train loads for this portion are erroneous. It is improbable that it was caused by a zero shift because of the different magnitudes of the measured and calculated strain ranges, and also by the fact that the measured strains for the rest of the railcars are comparable with those predicted by the models.

In some of the figures there is a slight shift in phase between the calculated strains and the measured strains. The reason for this is that the distance the real train traveled between each strain gage reading could not be exactly reproduced in the macro program that was written to represent the train movements. This meant that the calculated strains had to be lined up visually, and thus are prone to some error. The phase shifts that increase near the ends of the train may also have been caused by an acceleration of the train, since

the majority of the train would be past the local speed limit on the bridge. In any event, the phase shift does not hinder several important observations that can be made from the graphs.

All models predict the measured strains to about the correct magnitude. The Pinned model provides an upper limit and it would be appropriate for a preliminary calculation. The drawback of this model is that the negative strains are not represented at all. The effect of negative strains is shown by the Continuous model, wherein the strain range is essentially shifted downwards. The presence of negative strains indicates that, as expected, the end connections do indeed transfer some moment. The Continuous-with-Springs model is the most accurate model of the bridge. The spring stiffness used in the model was based upon the effective strain reading from train F658. As a result, this model plots almost directly on top of the measured strains.

The effect of impact could be considered to have been included in both the measured strains and the Continuous-with-Springs model, since they represent strains due to the actual loads. However, since full impact does not always occur with every railcar, it is unknown whether the train that the Continuous-with-Springs model is based on is truly representative of the normal impact, so it may not be appropriate to consider impact as included. Impact is not included in the Pinned and Continuous models since these models are based on theoretical behaviour only.

If we compare the number of calculated peaks with the number of railcars for trains F100, F130, and F658, there was generally one peak per railcar (Figures 3.6, 3.8, and 3.12). These peaks were caused by a pair of trucks from consecutive railcars on either side of the influence line peak. In trains that had longer railcar lengths, F430 and F717, close examination reveals that each peak is actually two peaks separated by a slight dip (Figures 3.10 and 3.14). In this case, the dual peaks are caused by each truck of consecutive railcars. Long railcars have the trucks placed more towards the center of the railcar in order to increase stability and reduce the span. The dual peak effect can also be seen in the strains that correspond to locomotives, where the trucks are also located closer to the center of the vehicle.

If the effects due to different weights of railcars are compared, for example, the 1 720 kN (194 ton) locomotives and the 840 kN (94 ton) railcars in Figures 3.6 and 3.7, we see that they produce about the same strain. This is because locomotives have three axles per truck, compared with two for the railcars, so the load is spread out more. The axle load for a locomotive is about 280 kN (63 kips), while for a railcar it is about 210 kN (47 kips). Thus, although the locomotive axle loads are higher than the railcar axle loads, the differences in the axle spaces means that the net effect of the loadings is about the same. Another reason for the similar effect is the dimensions of the truck. The locomotive truck has three axles spaced about 2 000 mm apart, and the last axle is about 1 850 mm from the hitch. The railcar truck has two axles spaced 1 800 mm apart, and the last axle is about 1 100 mm from the hitch. Therefore, the tighter grouping of railcar loads causes nearly the same strain as do the much heavier locomotives.

Table 3.1 shows the results of the measured and calculated effective strains for the stringers. The wheelbase is the typical distance between the center of the trucks of a single railcar. The Pinned model provides the most conservative prediction of the measured strains. The exception to this is train F130, where the measured-to-calculated ratio for the Pinned model (0.86) is slightly higher than that for the Continuous model (0.84). The reasons for this relate to the wheelbase and the weights of the railcars. Referring to Figure 3.4, the maximum strain range for the Pinned model will occur with a load moving from zero to the positive peak, a distance of 1.90 kN·m on the y-axis. For the Continuous model, the maximum strain range will occur with a load moving from one of the negative peaks to the positive peak, a distance of about 1.74 kN·m on the y-axis. However, the wheelbase of train F130, which is 14.30 m, is almost equal to the distance between the two negative peaks, which is 15.20 m. Hence, for this train the maximum negative strain will occur when both negative peaks are loaded simultaneously, at which point the strain range corresponds to distance of 1.89 kN·m on the y-axis. Thus, for trains with this critical wheelbase, the Continuous model can have strain ranges comparable to the Pinned model. This is seen in train F658 also, where its wheelbase is the same as F130, although in this case the loads only approach those predicted by the Pinned model, and do not exceed it.

However, care should be taken when assuming that a pinned model is an upper bound on the stress ranges in the stringer.

For trains F430 and F717, the Pinned model has significantly lower measured-to-calculated ratios than do the other trains. The main difference between these trains and the others has to do with the length and wheelbase of the railcars, as indicated in Figures 3.10 and 3.14, and Table 3.1. In these trains, each truck of the railcar produces a significant strain range, rather than each pair of consecutive trucks. Also, a reason for the difference between the measured and calculated strain ratios may be the inability of the Pinned model to reproduce negative strains.

The Continuous-with-Springs model provides the best strain predictions for all models. Because train F658 was the one used to establish the spring stiffness, its measured-to-calculated ratio is one, of course. However, the calculated strains for all the other trains are well predicted by this model. For the trains with the shorter wheelbases, the graphs essentially plot on top of one other, in both the positive and negative directions. For the trains with the longer wheelbases (F430 and F717, Figures 3.11 and 3.15), the measured-to-calculated ratios are just slightly less good. Based on these results, it is clear that the Continuous-with-Springs model will provide the most accurate prediction of stresses for use in the remaining fatigue life evaluation and the determination of any history of fatigue crack growth.

3.5.2 Strains in the Diagonal

Strains were measured in the diagonal for all the trains described in the preceding section. In addition to these, measurements were also made for a train T720, which crossed the bridge before strain gages were attached to the stringer.

Strain measurements in the diagonal were made from strain gage circuits in three locations. There was one circuit on each flange, and one on the web. The strains from the flanges were identified as either the North flange or the South flange. The North flange is the one that faced inside the bridge towards the rails. The web circuit was mounted on the underside of the diagonal, pointing downwards.

The calculated strains were obtained using the influence line of the axial force in the diagonal. The same bridge models that were used to develop influence lines for the stringer were also used for the diagonal. To recapitulate, these models were identified as Pinned, Continuous, and Continuous-with-Springs. Using the same influence line for all three circuits implicitly assumed a uniform axial force in the diagonal. Bending of the diagonal was not modeled.

The results of the measured and calculated strains for the respective trains are compared with one another in Figures 3.16 to 3.27. Measured and calculated strains were also converted into effective strain ranges, and these results are provided in Table 3.2. The anomalies arising from trains F100 and F130 that were mentioned in Section 3.5.1 (Strains in the Stringers) also apply to the strain measurements taken on the diagonal. These anomalies referred to the different number of locomotives identified in the measured and calculated strains (train F100), and abnormally high calculated strains for one part of a train (train F130). In addition, strains were not available from all three circuits at one time, due to technical difficulties, thus different combinations of the circuits are compared.

Examination of the measured-to-calculated ratios of the strains shows that all models generally predict the measured strains in the diagonal to the correct magnitude. The Pinned model provides the lowest prediction of the measured strains, and the Continuous-with-Springs model provides the highest. However, the difference between the models is not as large for the diagonal as it is for the stringer strains. It seems that the influence of the floor system stiffness does not have much effect on the loads in the diagonal. As was seen in Figure 3.5, the three influence lines of the three different models are very similar. All of the models are able to reproduce positive and negative strains, as opposed to the stringer influence lines, where the Pinned model could not produce negative strains.

The strains measured by the North flange circuit are generally higher than the calculated strains. Conversely, the measured South flange strains are generally lower than the calculated strains. This suggests that the diagonal is being subjected to some bending moment in addition to the axial force. The bending is probably caused by moment being

transferred between the floorbeam and the panel point gusset plate. This is very likely because the connection at this point is made using angles in the same manner as the stringer-to-floorbeam connection. The larger inside measured strains (North flange) and the smaller outside measured strains (South flange) are consistent with this type of applied moment.

Train F430 was the only train in which the North flange and South flange strains were measured simultaneously. Table 3.2 shows that for train F430, the measured-to-calculated ratios of the three models generally straddle the value 1.0. This indicates that the difference between the models is small, and that the average measured strain would be about equal to the axial strain.

Evidence of bending can also be seen in the results of the other trains. Referring to the Table 3.2, strains were measured only in the South flange for trains T720, F100, and F130. All of the calculated axial strains are more than the measured strains, which suggests that the measured flange strains are being reduced somewhat by bending. In trains F658 and F717, where the North flange and web strains were measured, the strains in the North flange are slightly higher than in the web, which again is consistent with bending.

The Continuous-with-Springs model, developed specifically for strains in the stringers, is quite unconservative in predicting the diagonal strains and is of no use. Considering the other two models, it is difficult to judge which of the two models would be the best to use for a fatigue evaluation. The Pinned model generally provides the most conservative strains, where the ratio of measured to calculated strains is at worst 1.01. If a simple analysis is to be done, it may be desirable to err on the conservative side, since the presence of bending would cause higher strains than calculated. Additional study is necessary to develop a more accurate model, but, for purposes of a conservative remaining fatigue life evaluation, it appears that the Pinned model is satisfactory.

Train	Wheelbase	Analytical Model	Measured $\Delta\varepsilon_{RMC}$	Calculated $\Delta\varepsilon_{RMC}$	Meas./Calc.
F100	18.90 m	Pinned	61.37	74.99	0.82
		Continuous	61.37	71.78	0.86
		Cont. w/ Springs	61.37	61.78	0.99
F130	14.30 m	Pinned	96.15	109.69	0.86
		Continuous	96.15	113.85	0.84
		Cont. w/ Springs	96.15	96.31	0.99
F430	17.00 m	Pinned	36.26	54.94	0.66
		Continuous	36.26	44.82	0.81
		Cont. w/ Springs	36.26	39.69	0.92
F658	14.30 m	Pinned	36.11	43.72	0.83
		Continuous	36.11	41.85	0.86
		Cont. w/ Springs	36.11	35.91	1.00
F717	21.00 m	Pinned	37.36	56.50	0.66
		Continuous	37.36	44.28	0.84
		Cont. w/ Springs	37.36	39.46	0.95

Table 3.1 Results of measured and calculated effective strain range for stringer

Train	Model	N. Flange $\Delta\varepsilon_{RMC}$	Web $\Delta\varepsilon_{RMC}$	S. Flange $\Delta\varepsilon_{RMC}$	Calc. $\Delta\varepsilon_{RMC}$	N. Flange/ Calc.	Web/ Calc.	S. Flange/ Calc.
T720	Pinned			63.73	88.04			0.72
	Continuous			63.73	72.01			0.86
	Cont. w/ Springs			63.73	69.76			0.91
F100	Pinned			51.34	67.45			0.76
	Continuous			51.34	60.03			0.86
	Cont. w/ Springs			51.34	57.03			0.90
F130	Pinned			55.89	80.17			0.70
	Continuous			55.89	65.88			0.85
	Cont. w/ Springs			55.89	63.75			0.88
F430	Pinned	68.09		59.91	67.23	1.01		0.89
	Continuous	68.09		59.91	64.48	1.06		0.93
	Cont. w/ Springs	68.09		59.91	60.00	1.13		1.00
F658	Pinned	45.57	43.90		44.97	1.01	0.98	
	Continuous	45.57	43.90		41.20	1.11	1.07	
	Cont. w/ Springs	45.57	43.90		39.33	1.16	1.12	
F717	Pinned	56.80	54.37		62.81	0.90	0.87	
	Continuous	56.80	54.37		54.27	1.05	1.00	
	Cont. w/ Springs	56.80	54.37		51.66	1.10	1.05	

Table 3.2 Results of measured and calculated effective strain range for diagonal

Figure 3.1 Bridge at mile 7.8 Albreda prior to removal

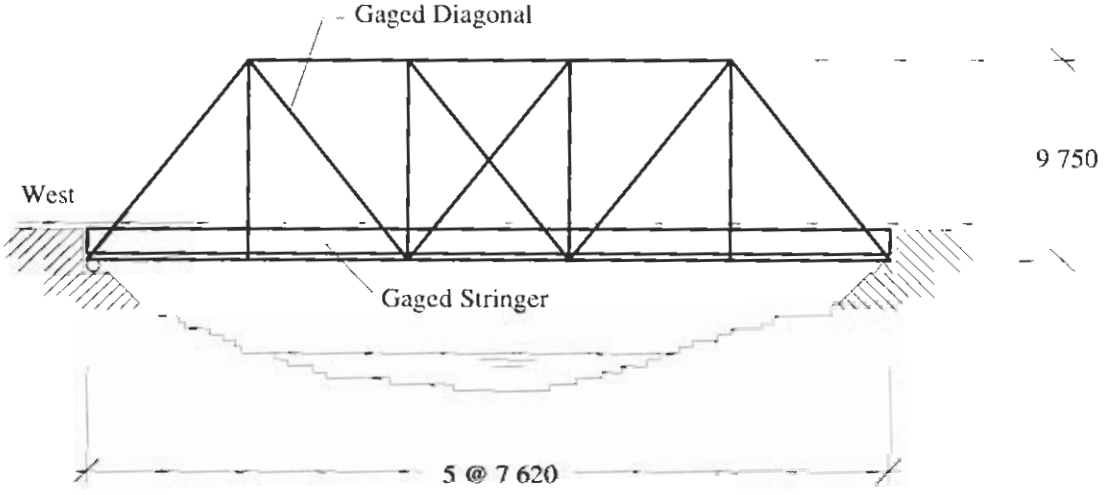

Figure 3.2 Bridge geometry and strain gaged members

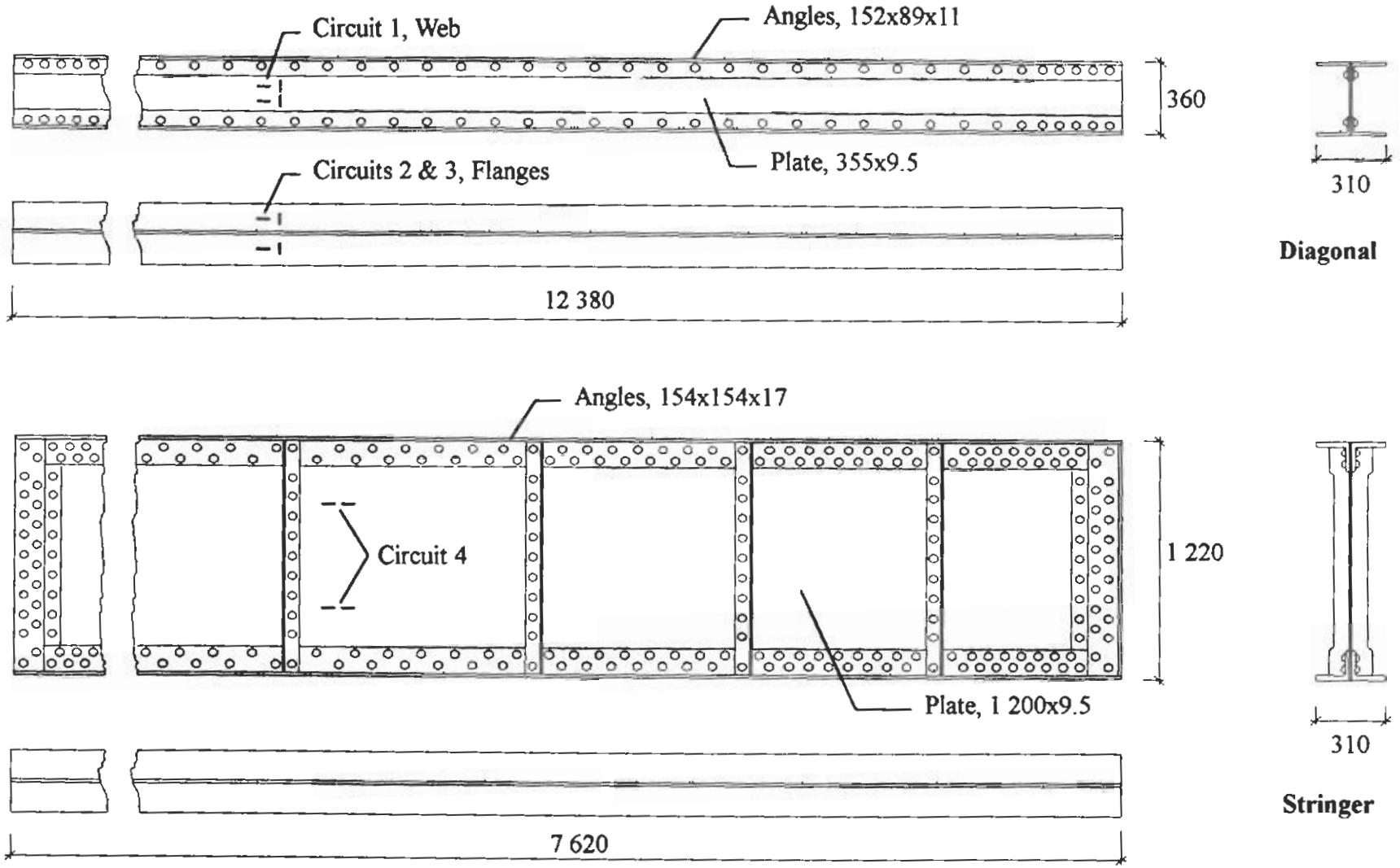

Figure 3.3 Details and strain gage arrangement

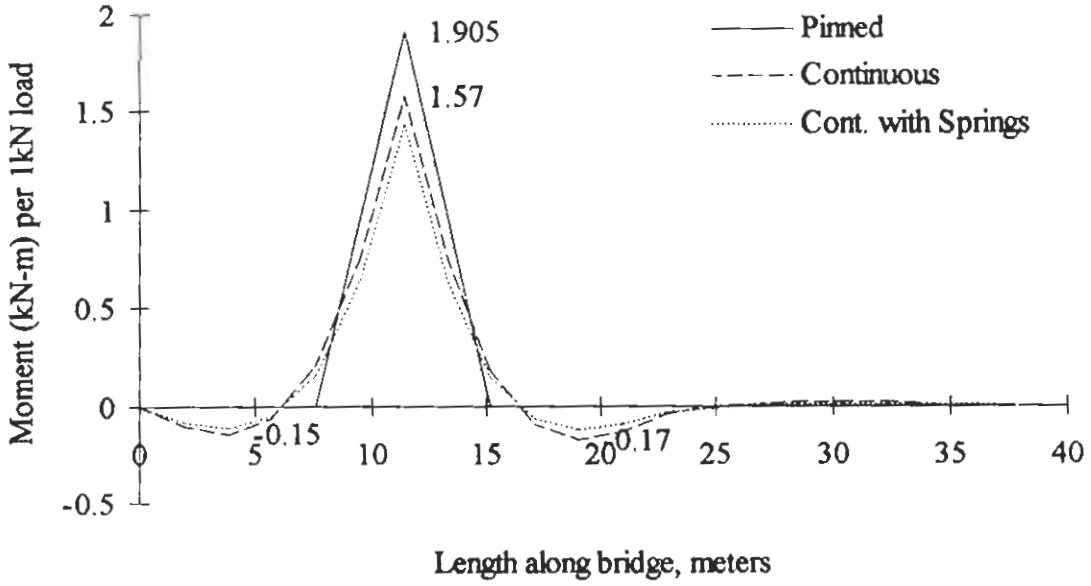

Figure 3.4 Influence lines for moment at stringer at strain gaged location

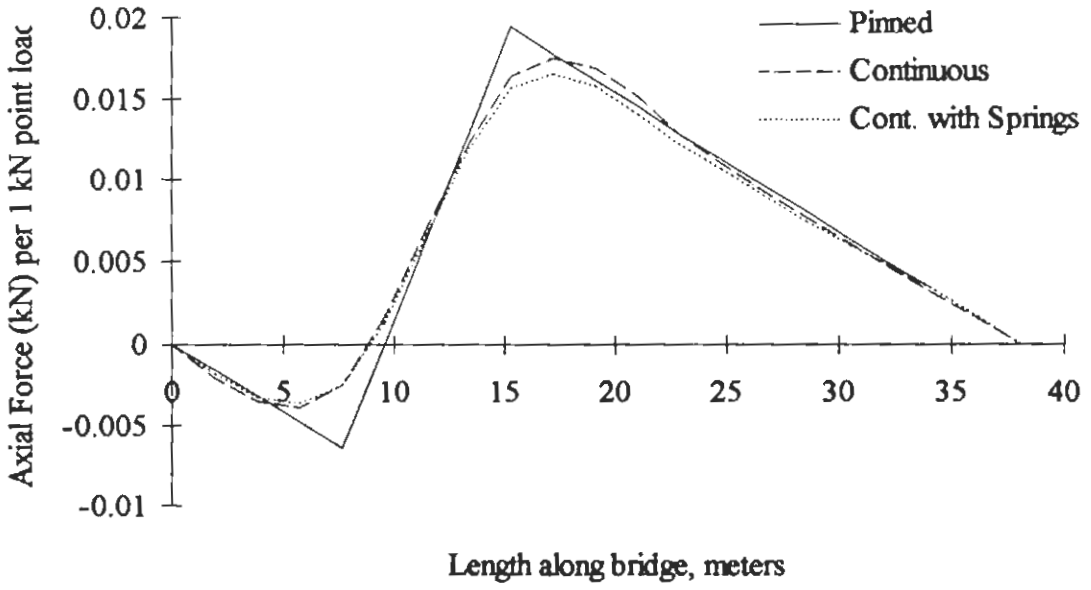

Figure 3.5 Influence lines for axial force in diagonal at strain gaged location

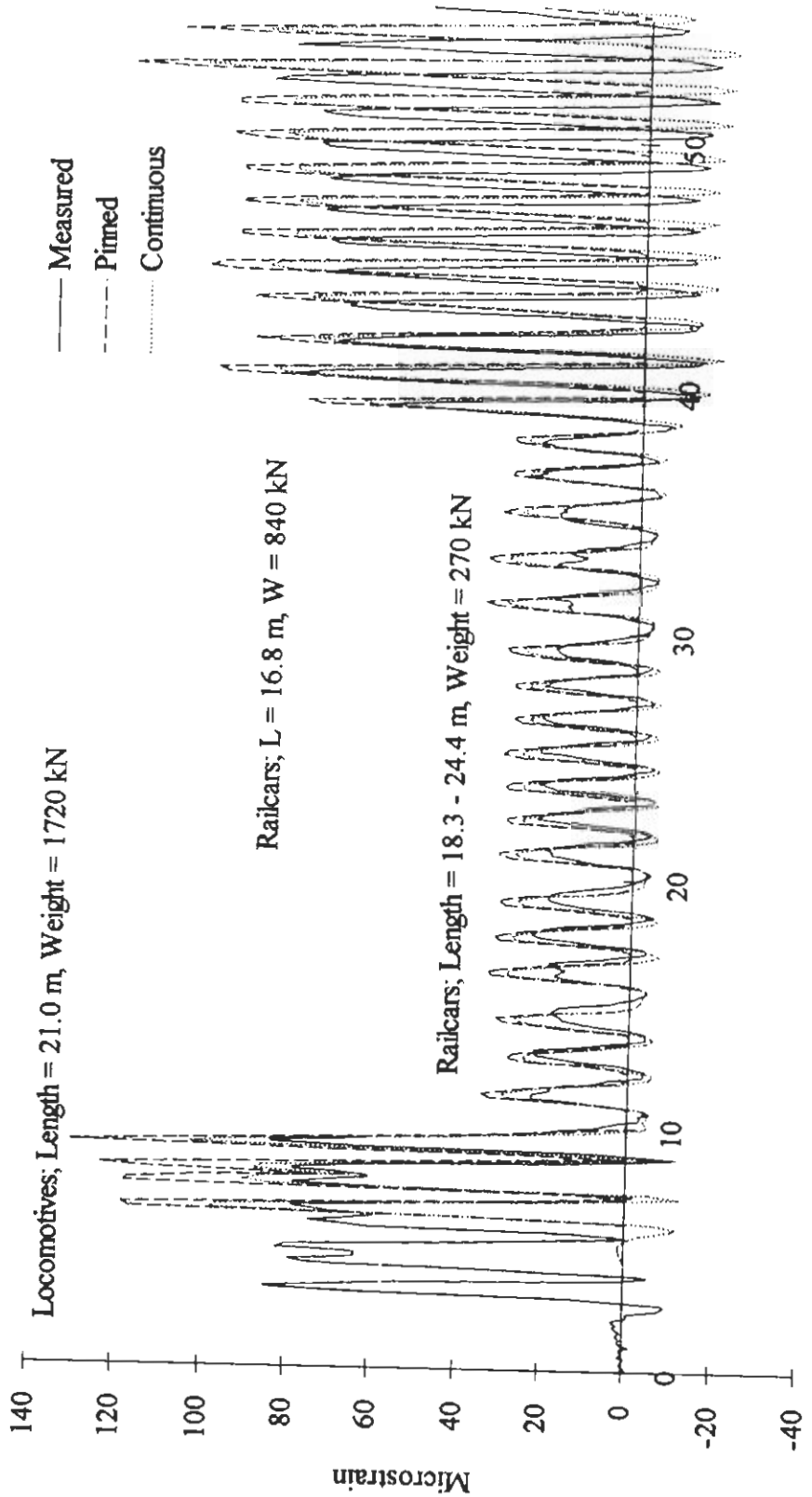

Figure 3.6 Train F100, Stringer strains compared with Pinned and Continuous models

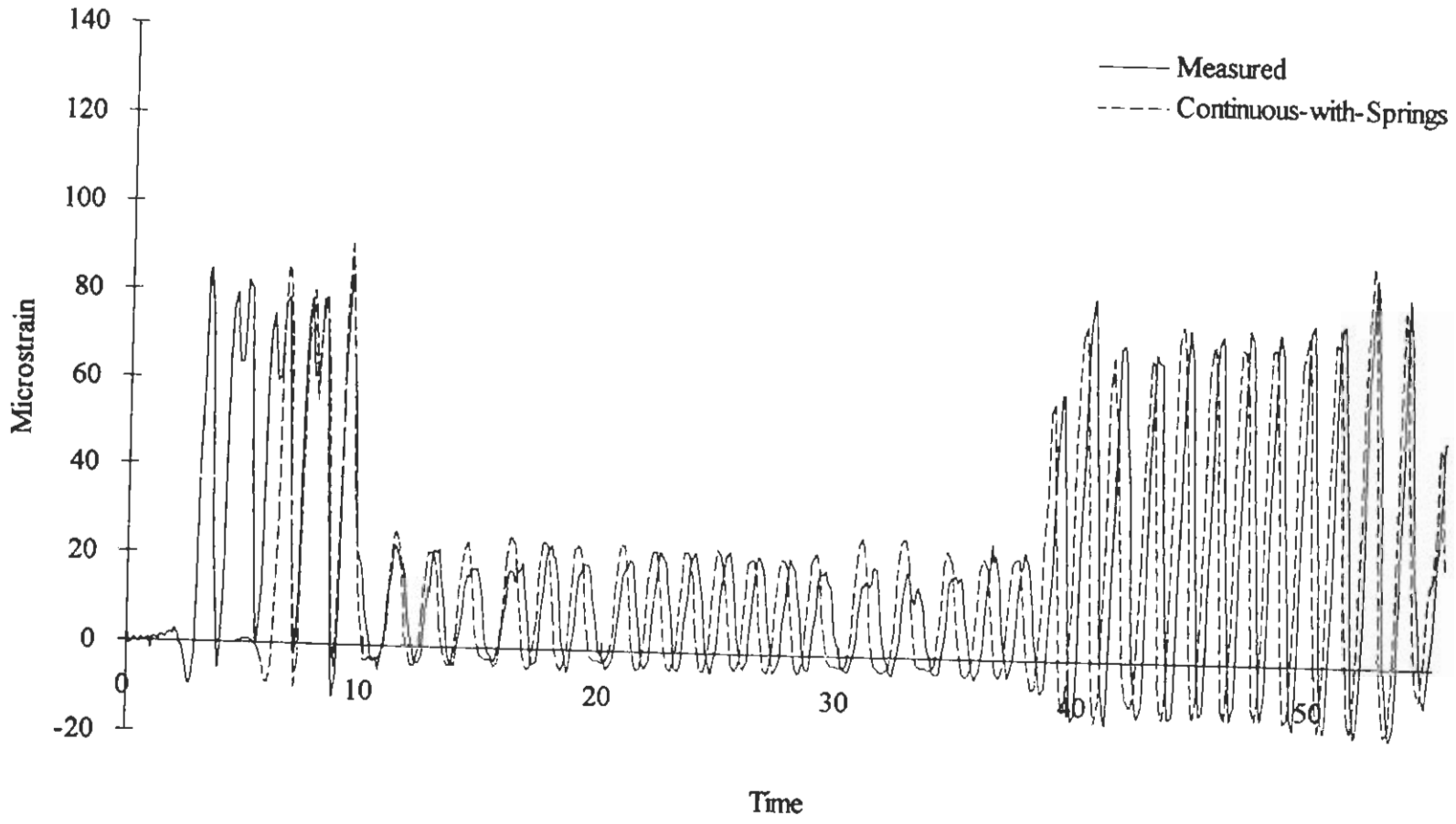

Figure 3.7 Train F100, Stringer strains compared with Continuous-with-Springs model

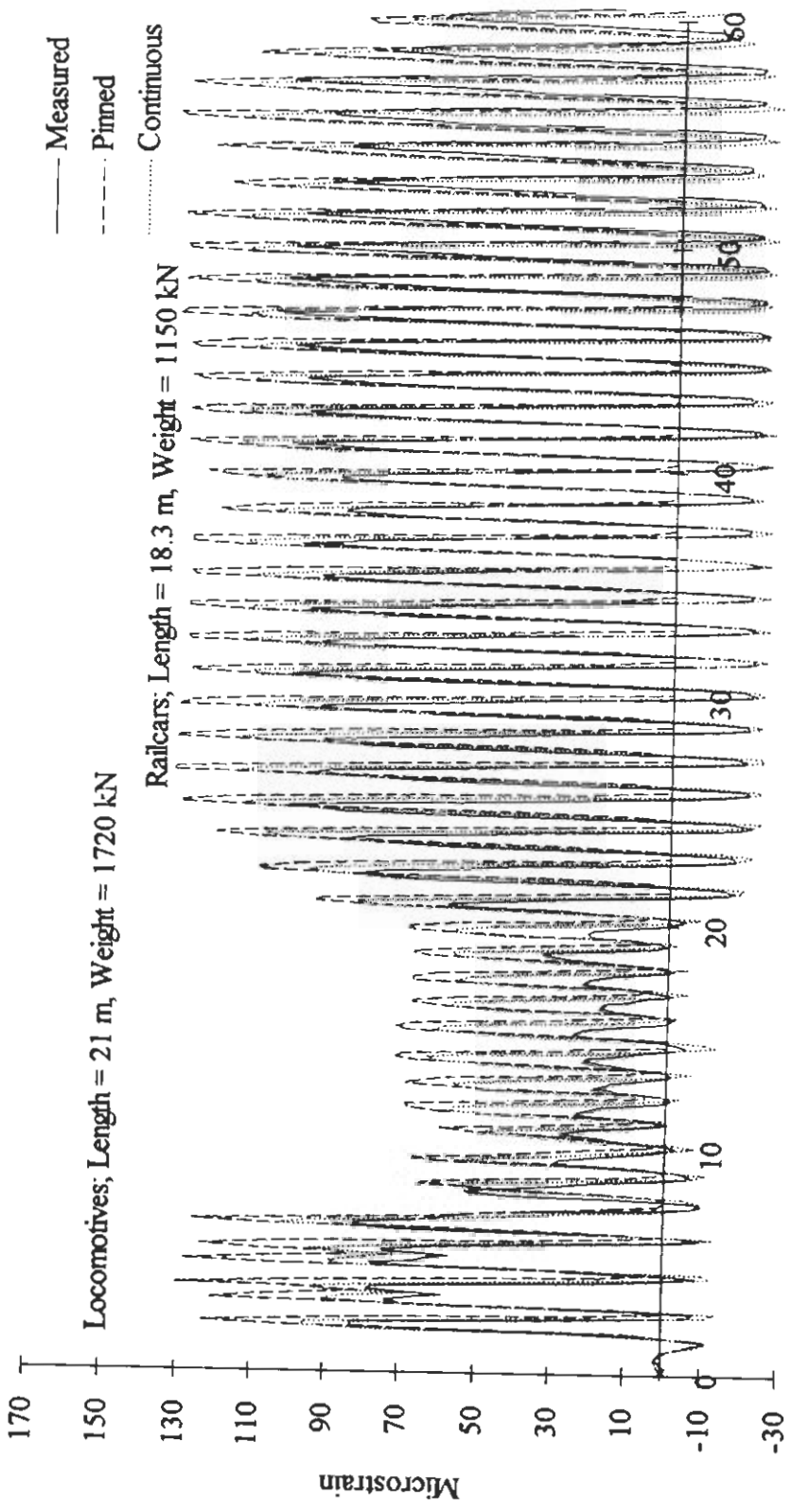

Figure 3.8 Train F130, Stringer strains compared with Pinned and Continuous models

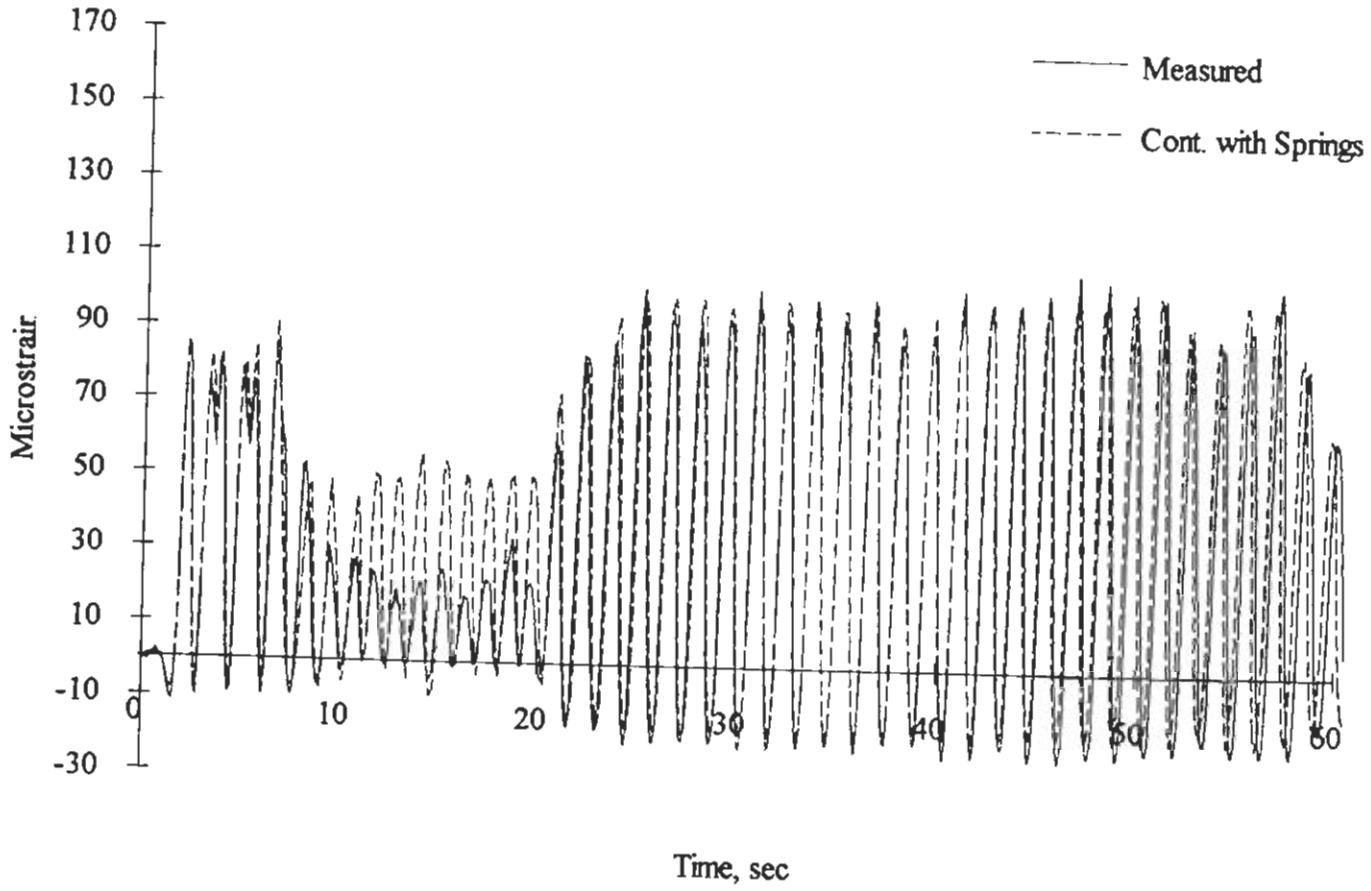

Figure 3.9 Train F130, Stringer strains compared with Continuous-with-Springs model

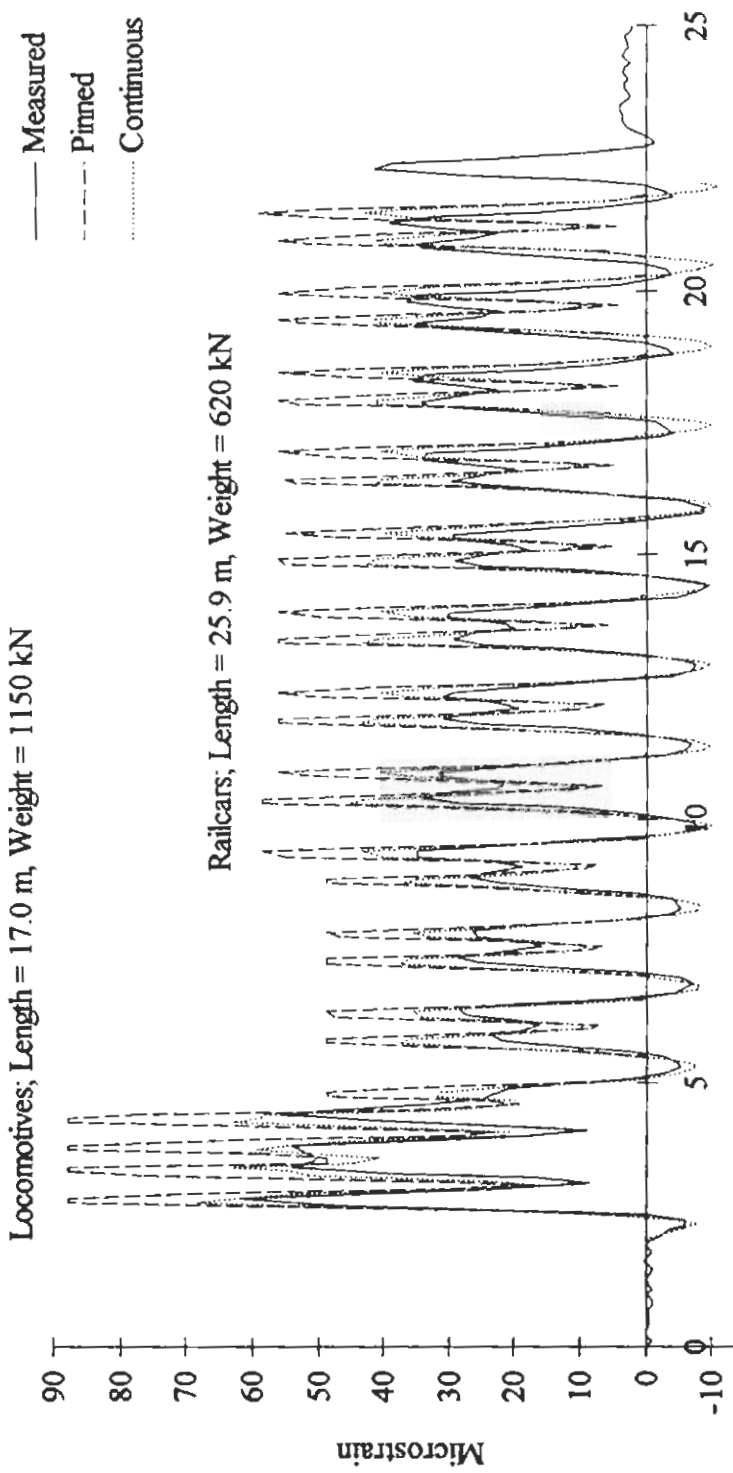

Figure 3.10 Train F430, Stringer strains compared with Pinned and Continuous models

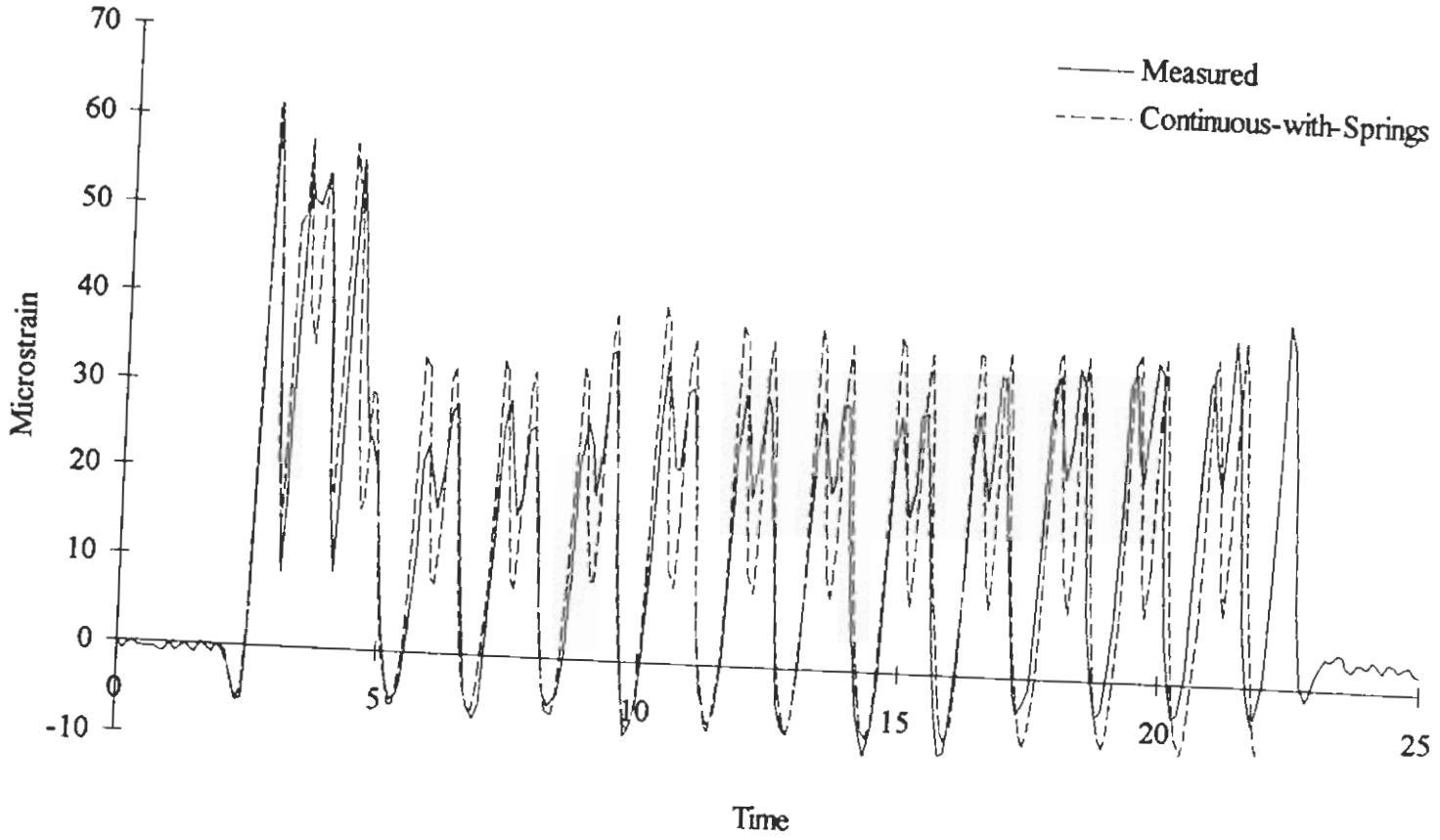

Figure 3.11 Train F430, Stringer strains compared with Continuous-with-Springs model

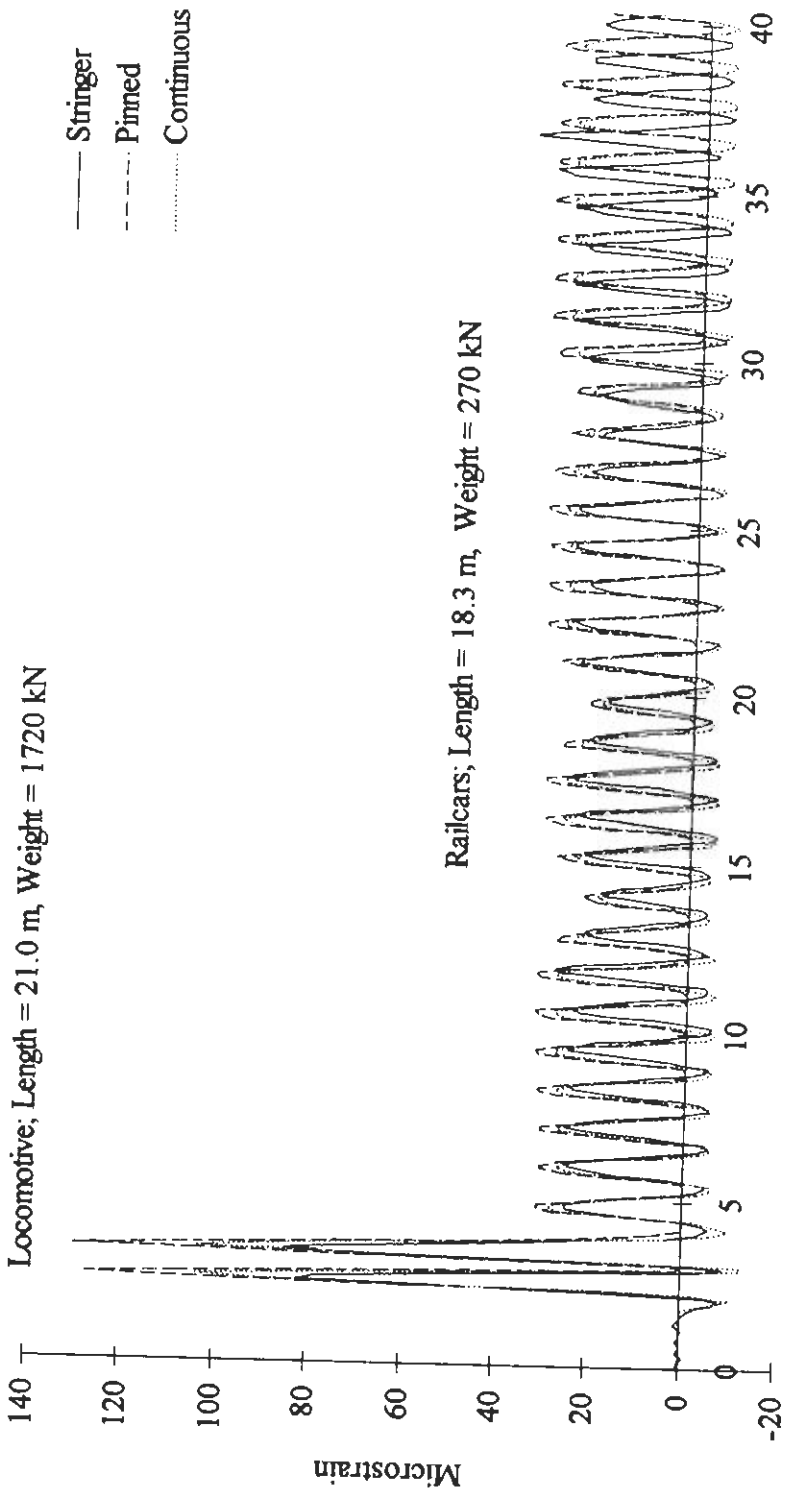

Figure 3.12 Train F658, Stringer strains compared with Pinned and Continuous models

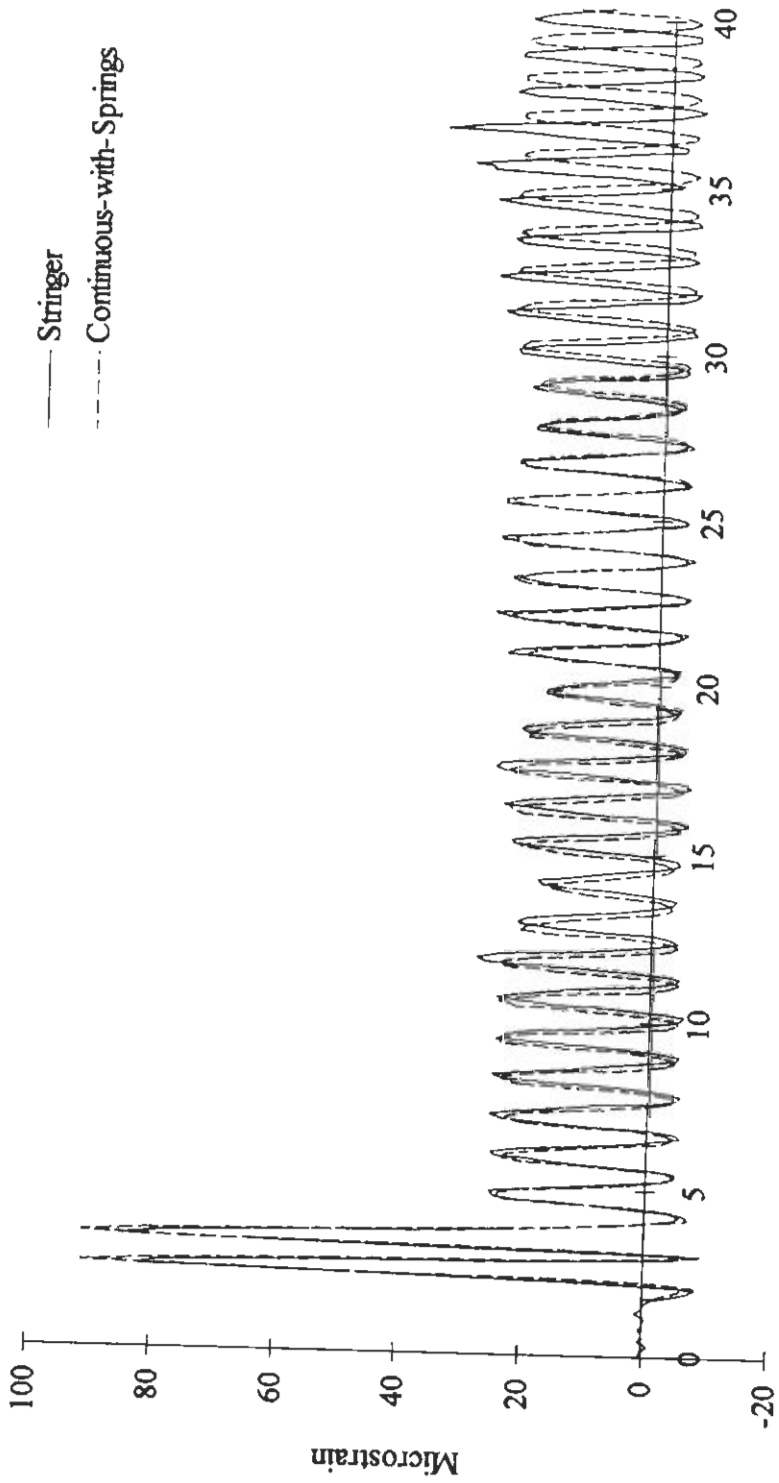

Figure 3.13 Train F658, Stringer strains compared with Continuous-with-Springs model

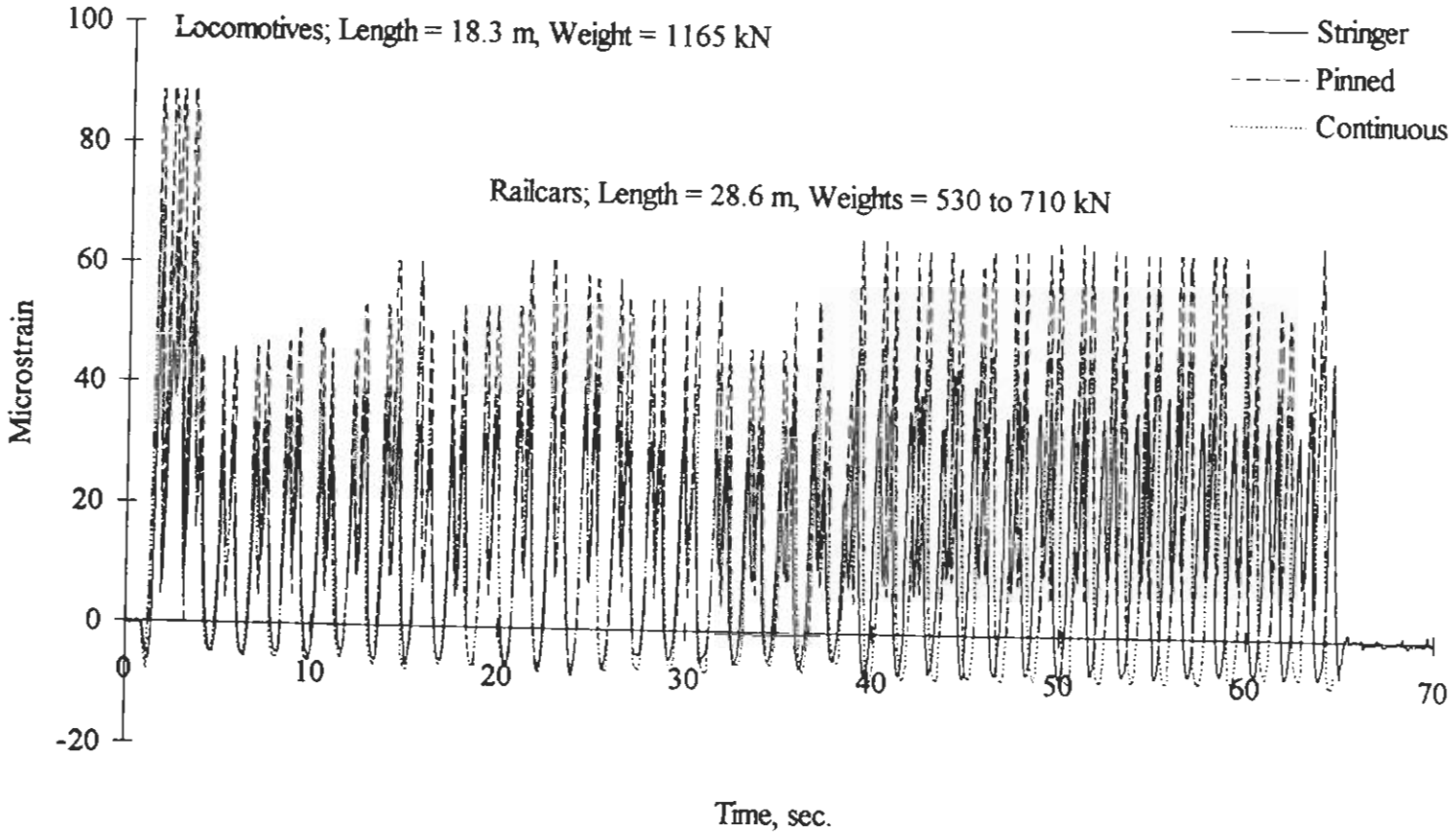

Figure 3.14 Train F717, Stringer strains compared with Pinned and Continuous models

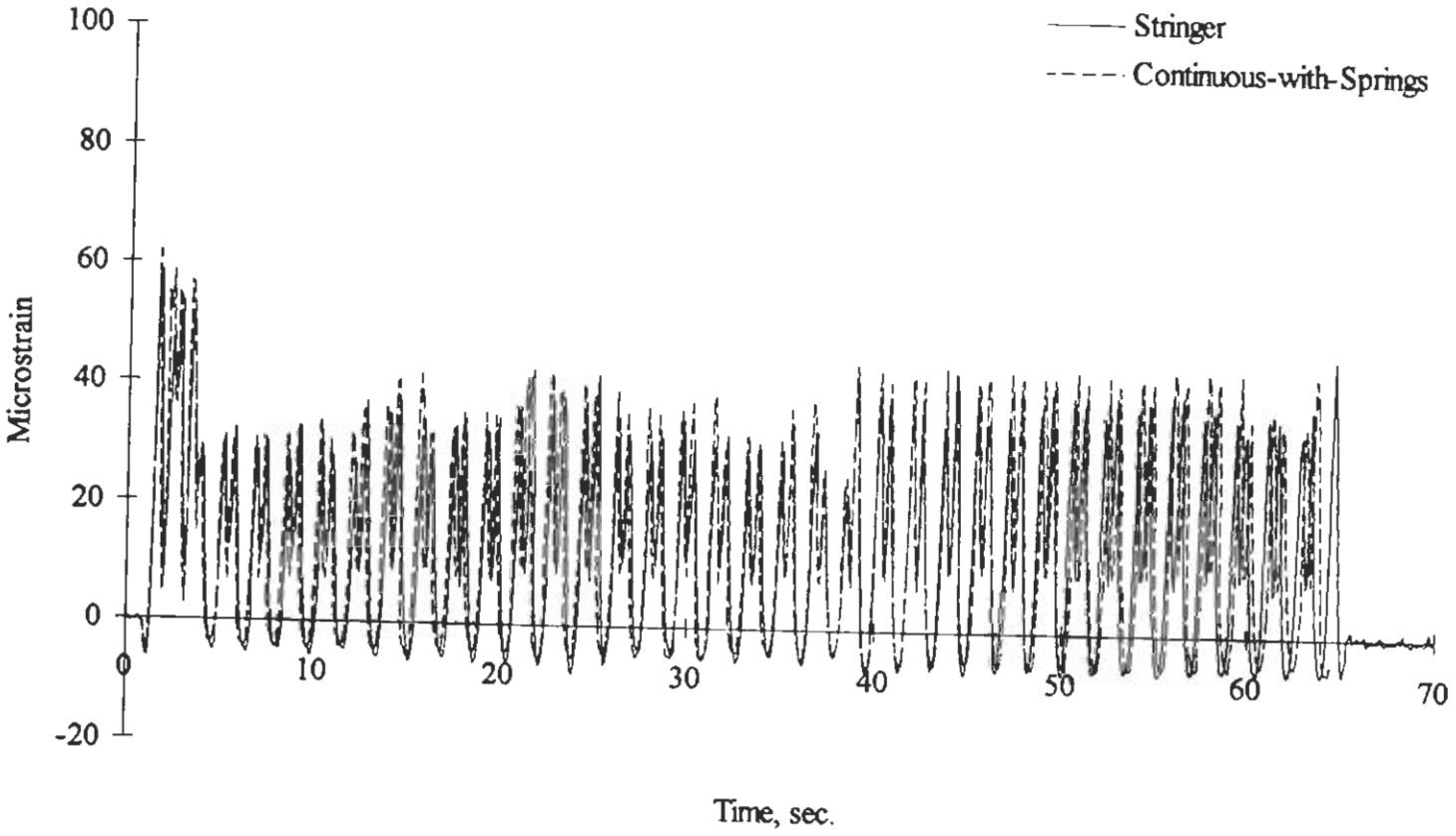

Figure 3.15 Train F717, Stringer strains compared with Continuous-with-Springs model

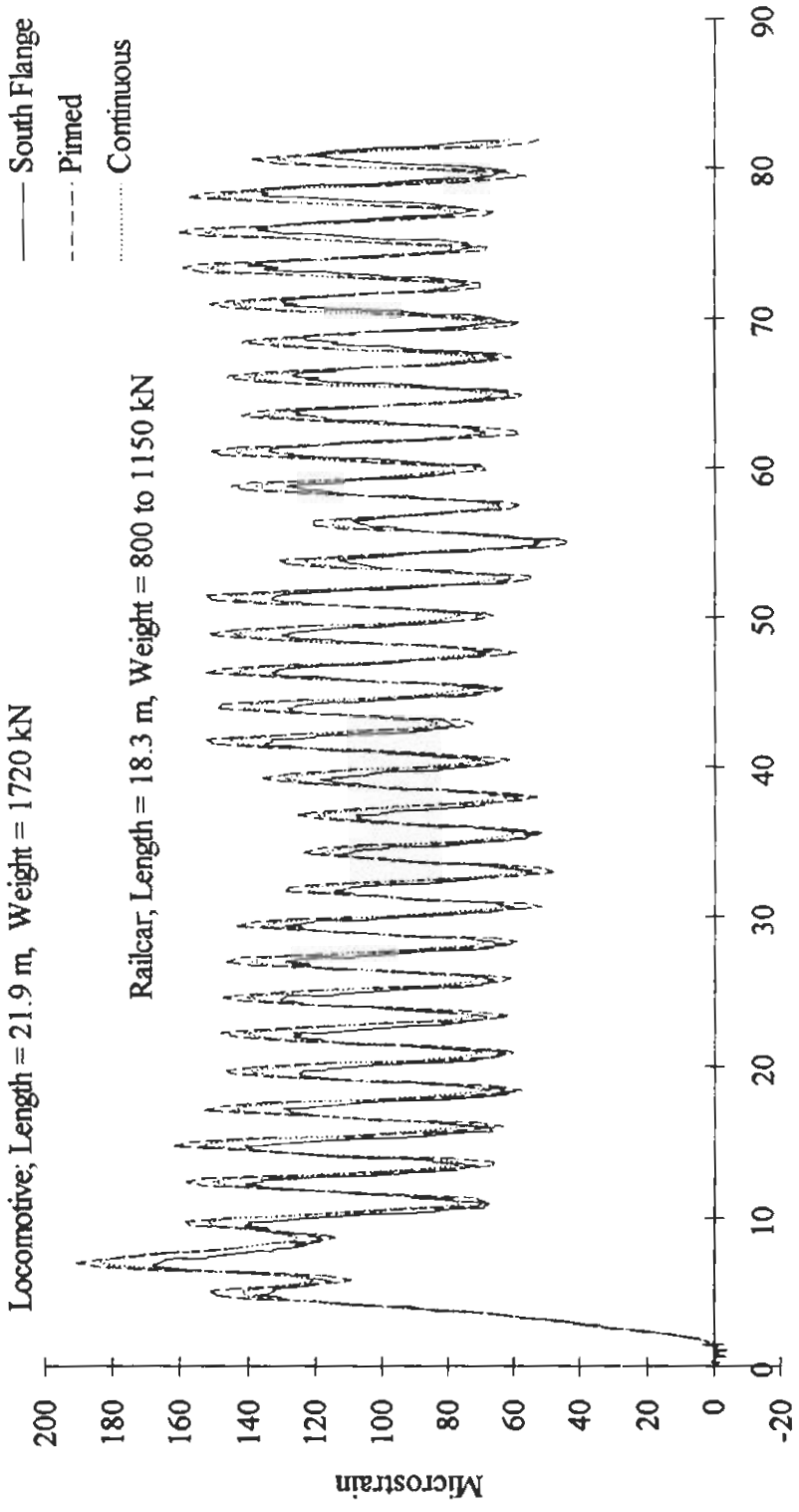

Figure 3.16 Train T720, Diagonal strains compared with Pinned and Continuous models

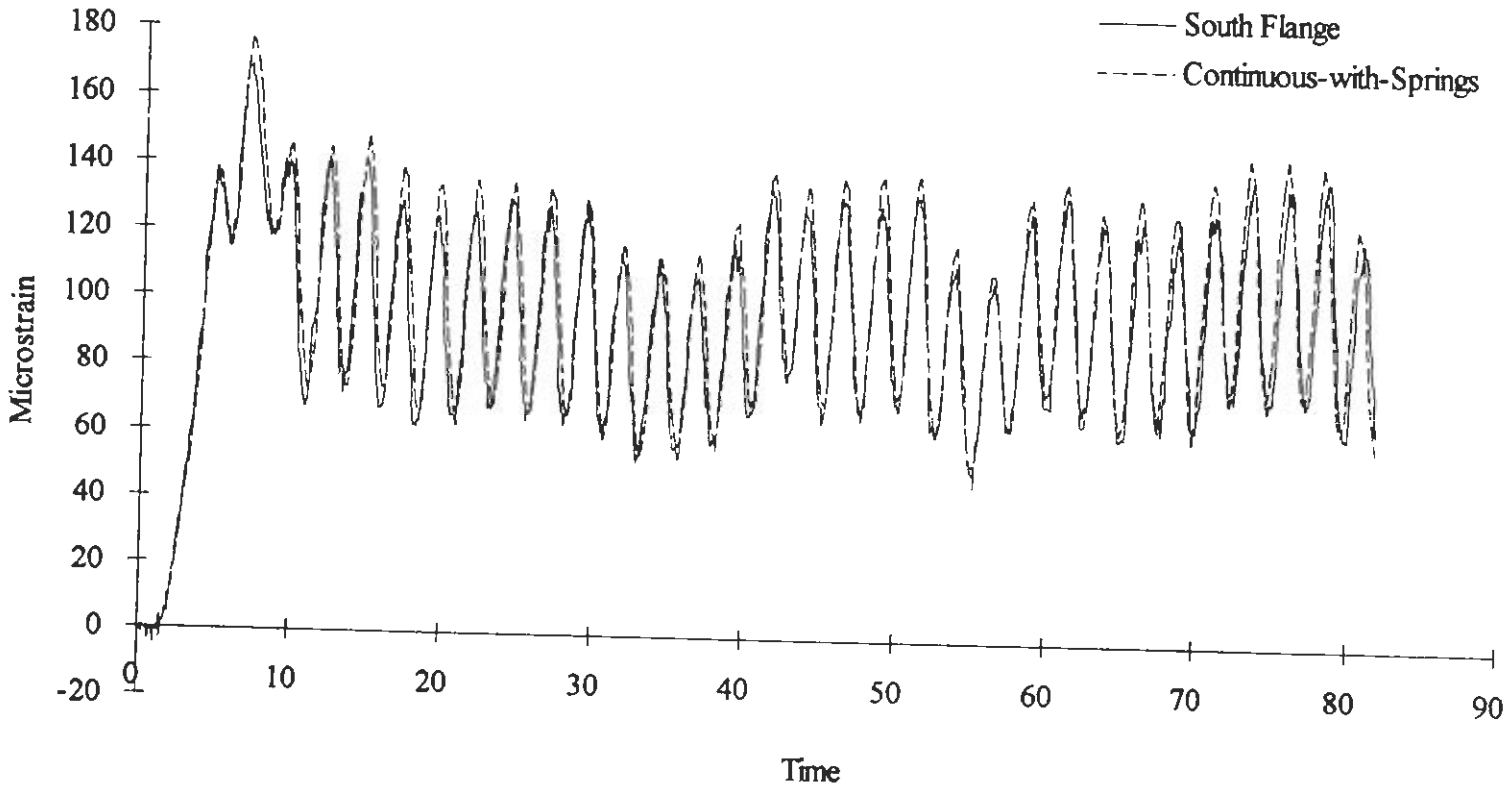

Figure 3.17 Train T720, Diagonal strains compared with Continuous-with-Springs model

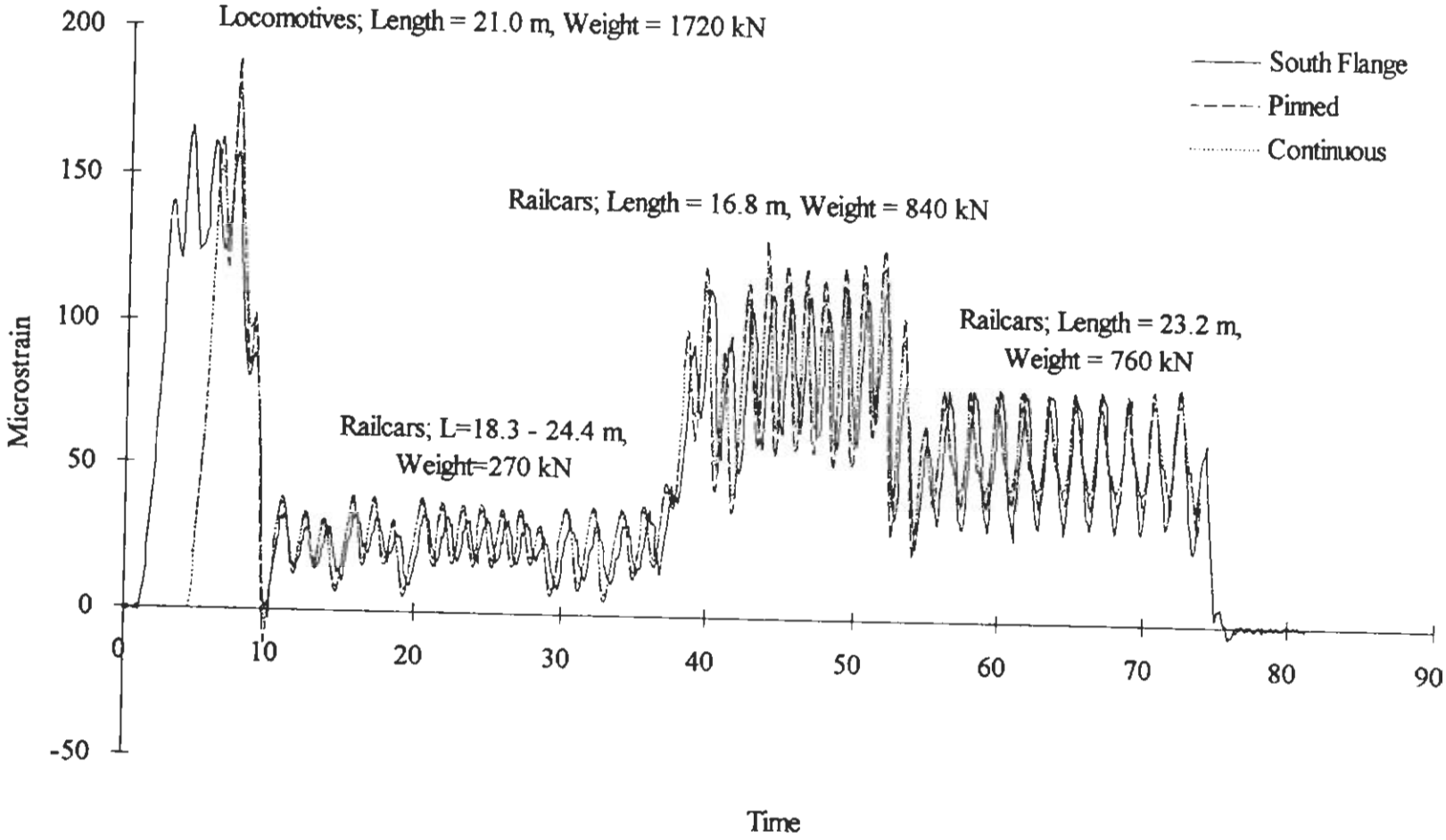

Figure 3.18 Train F100, Diagonal strains compared with Pinned and Continuous models

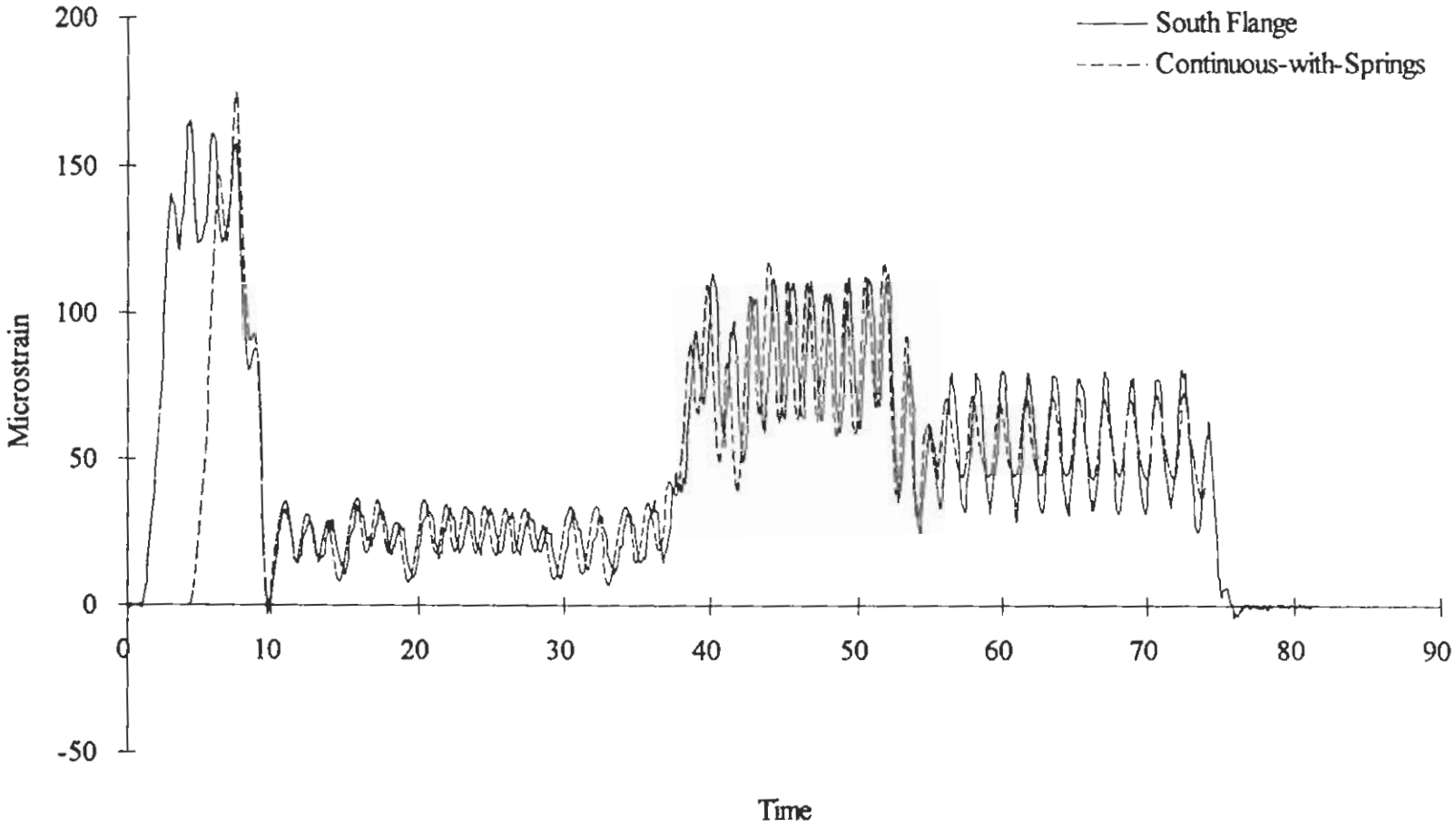

Figure 3.19 Train F100, Diagonal strains compared with Continuous-with-Springs model

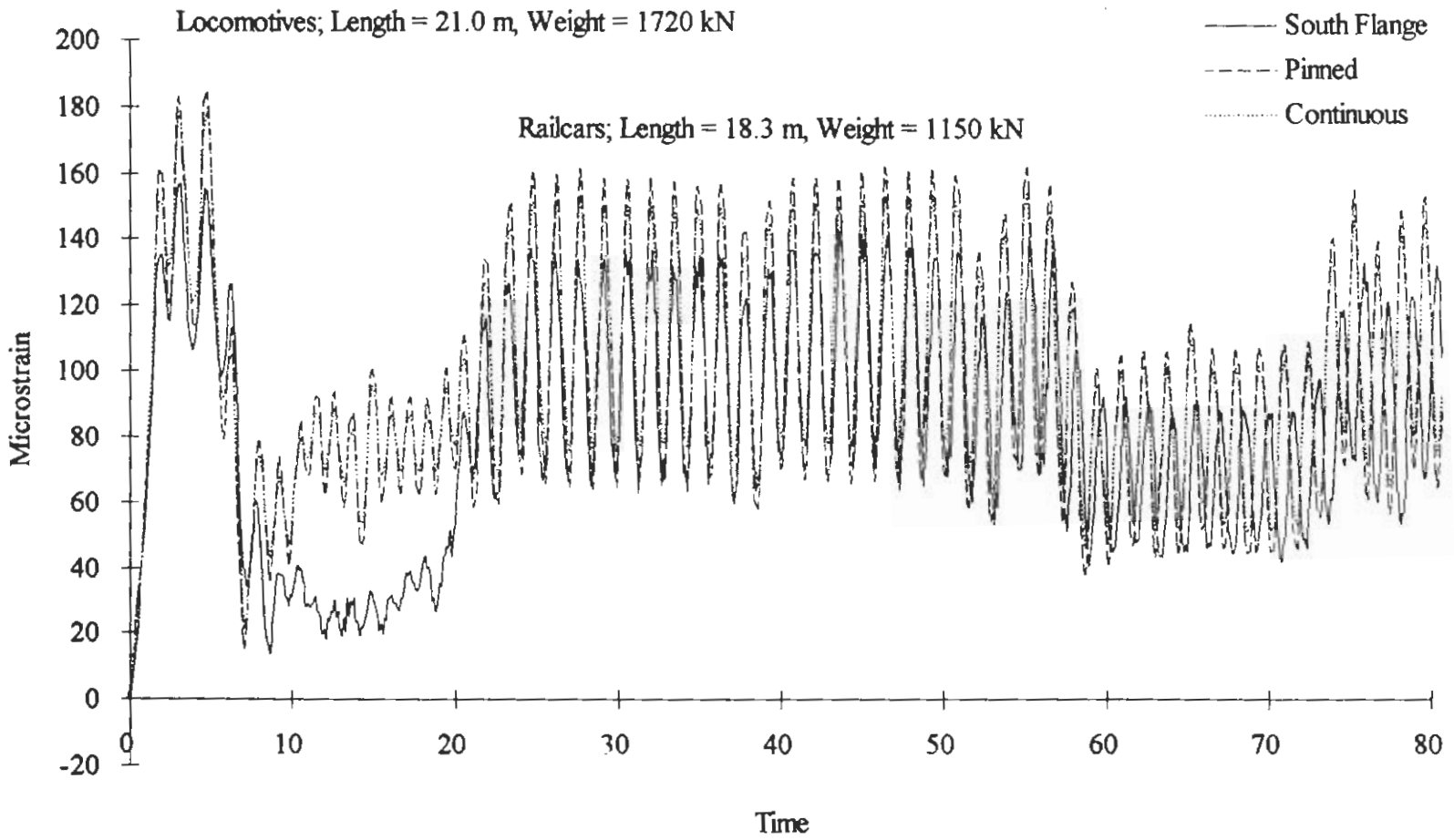

Figure 3.20 Train F130, Diagonal strains compared with Pinned and Continuous models

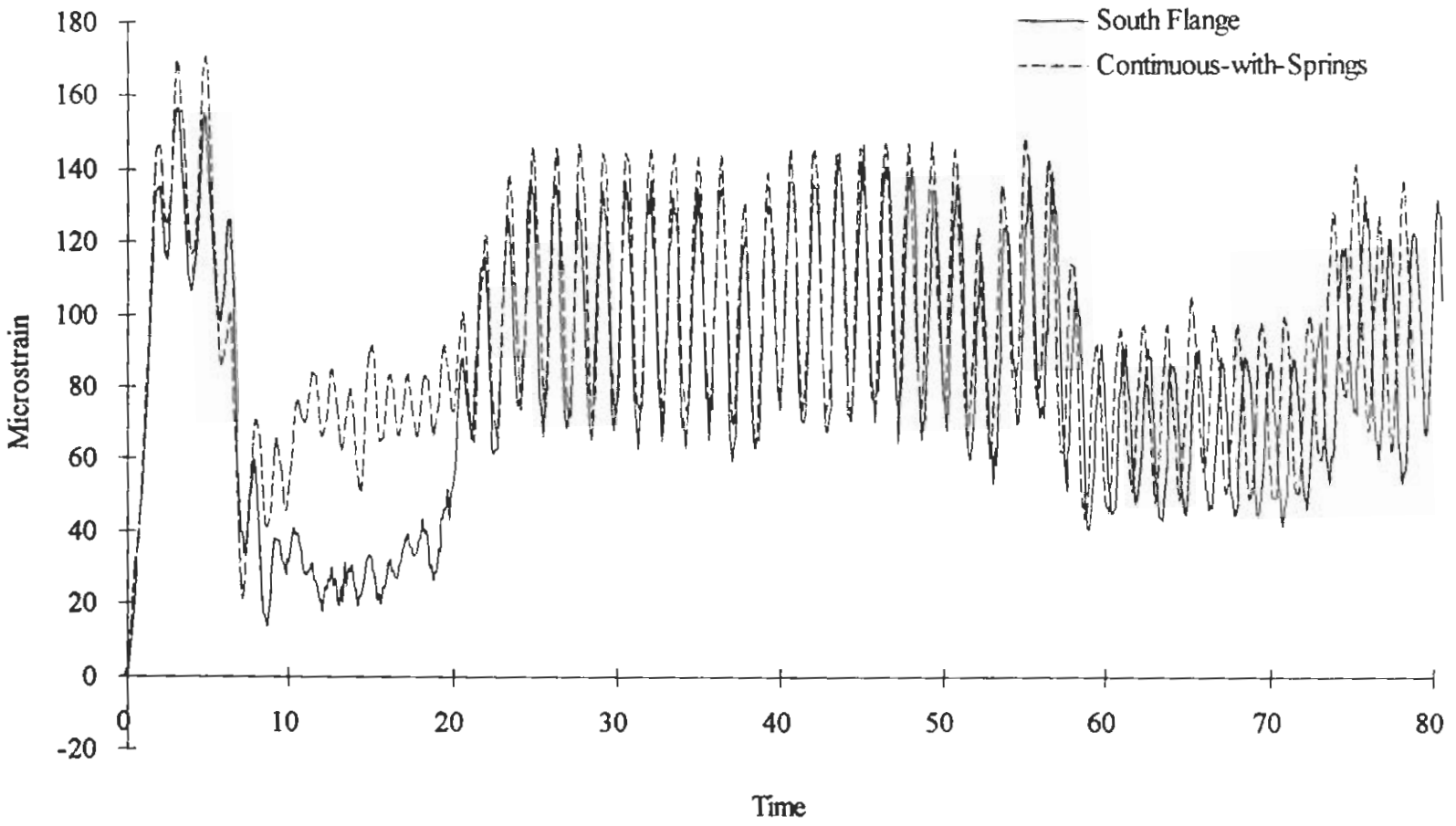

Figure 3.21 Train F130, Diagonal strains compared with Continuous-with-Springs model

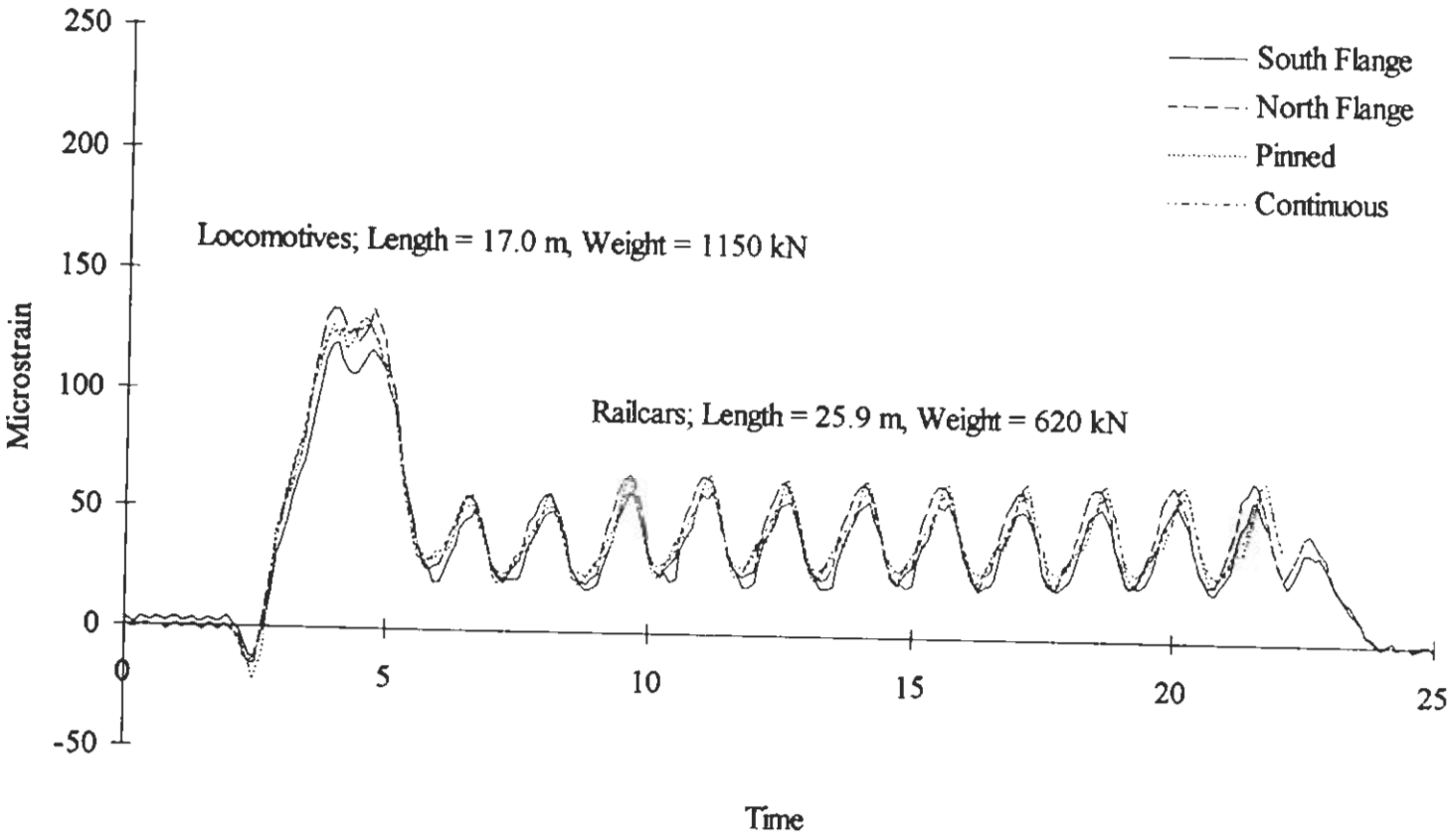

Figure 3.22 Train F430, Diagonal strains compared with Pinned and Continuous models

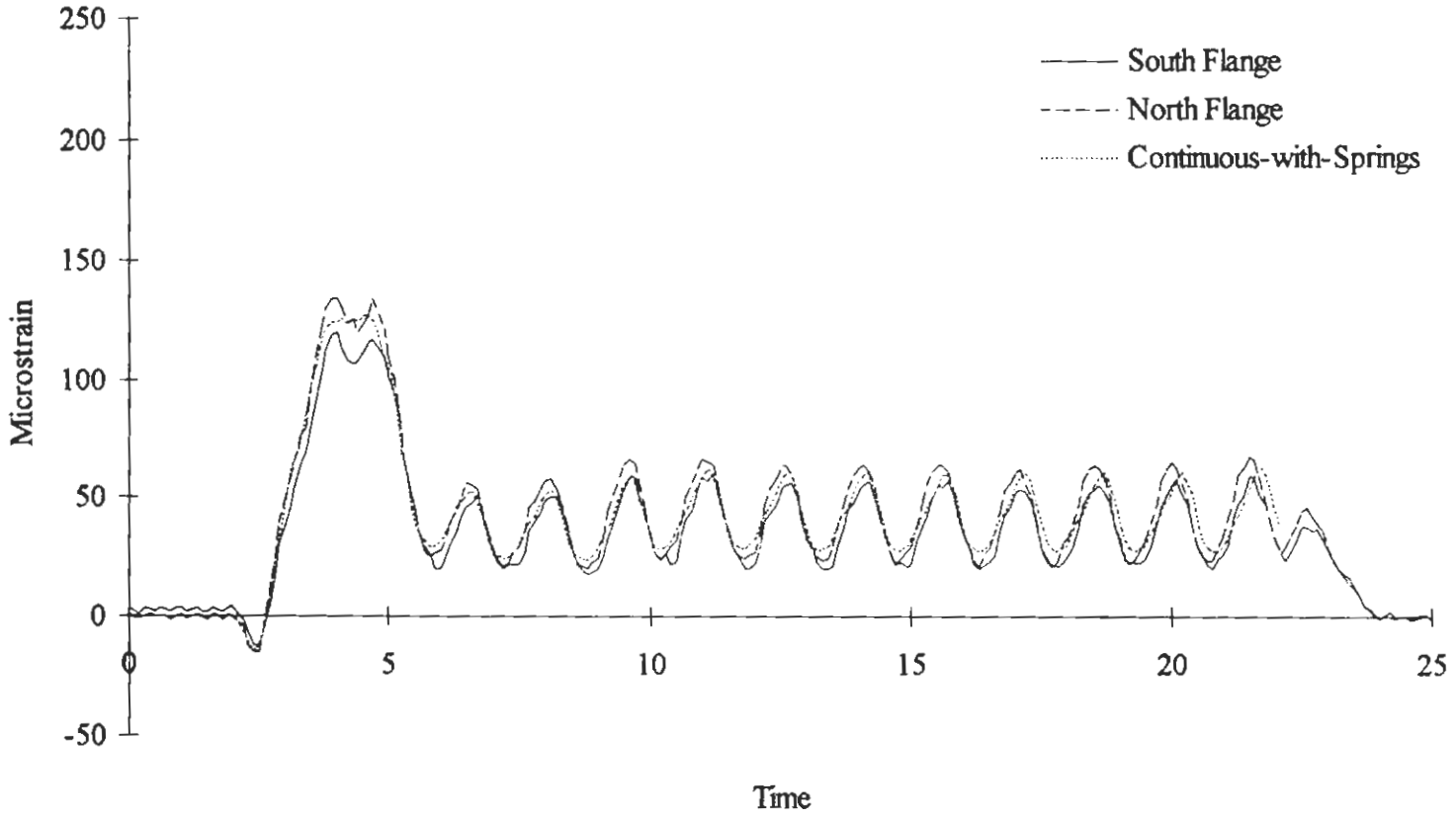

Figure 3.23 Train F430, Diagonal strains compared with Continuous-with-Springs model

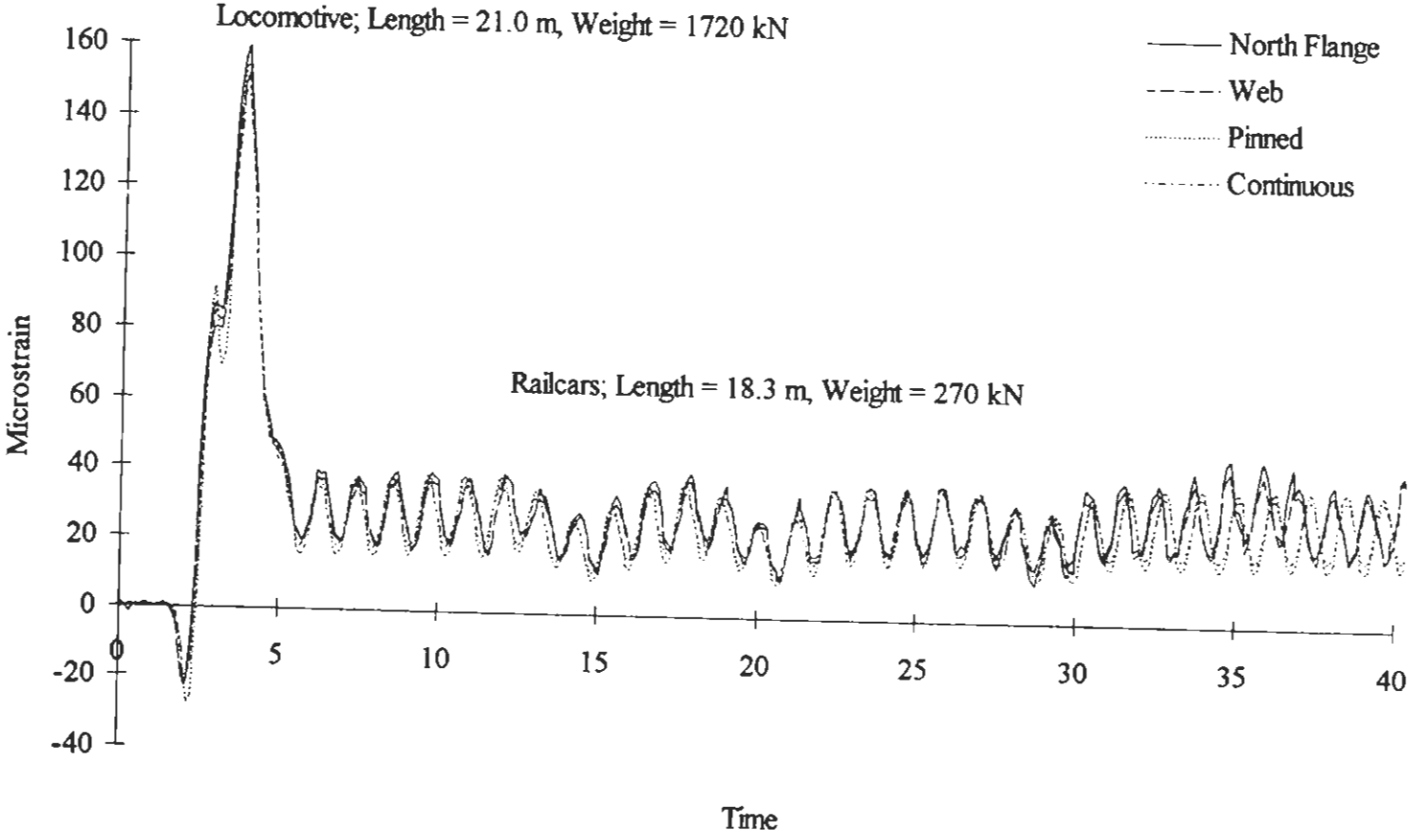

Figure 3.24 Train F658, Diagonal strains compared with Pinned and Continuous models

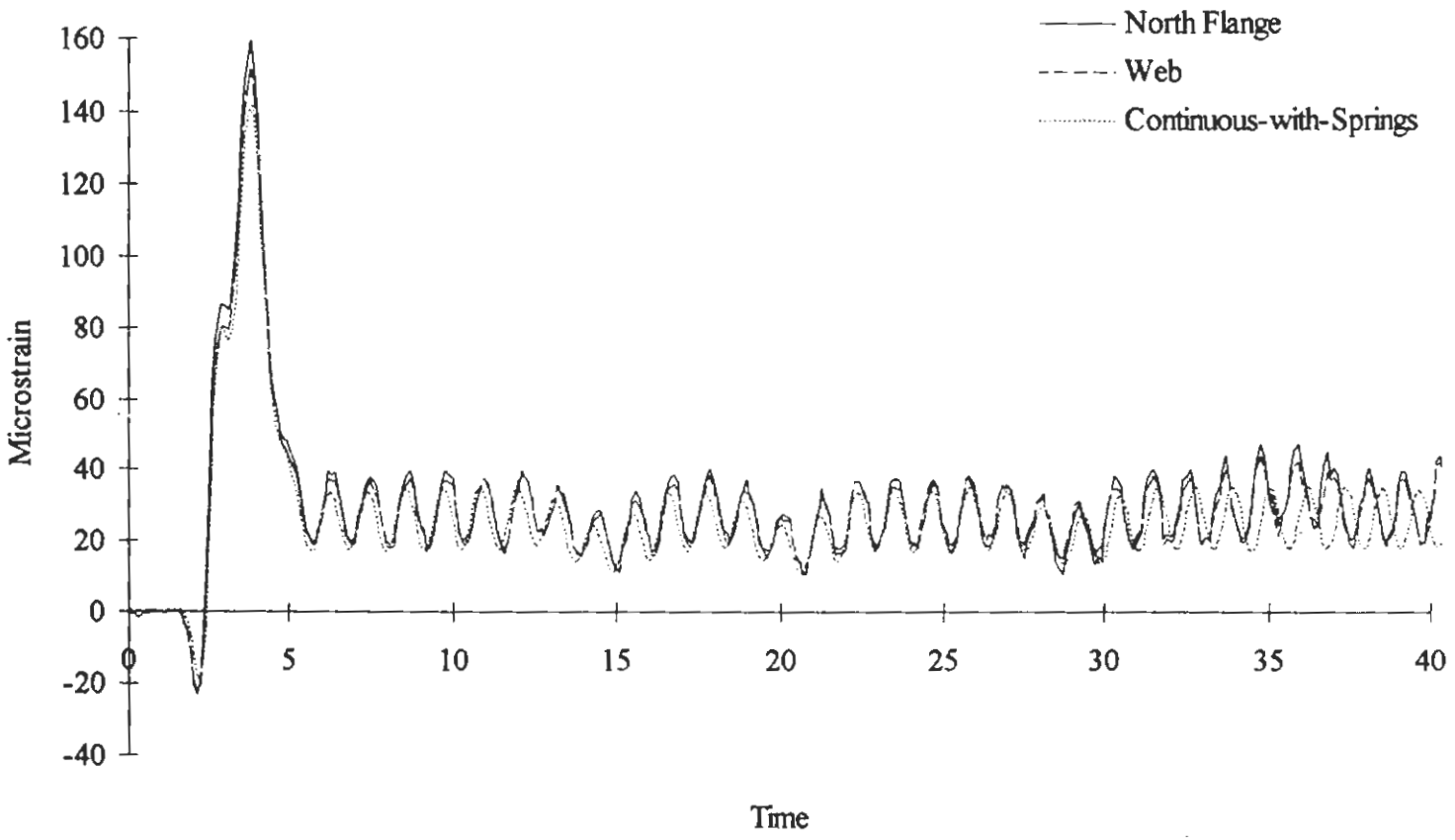

Figure 3.25 Train F658, Diagonal strains compared with Continuous-with-Springs model

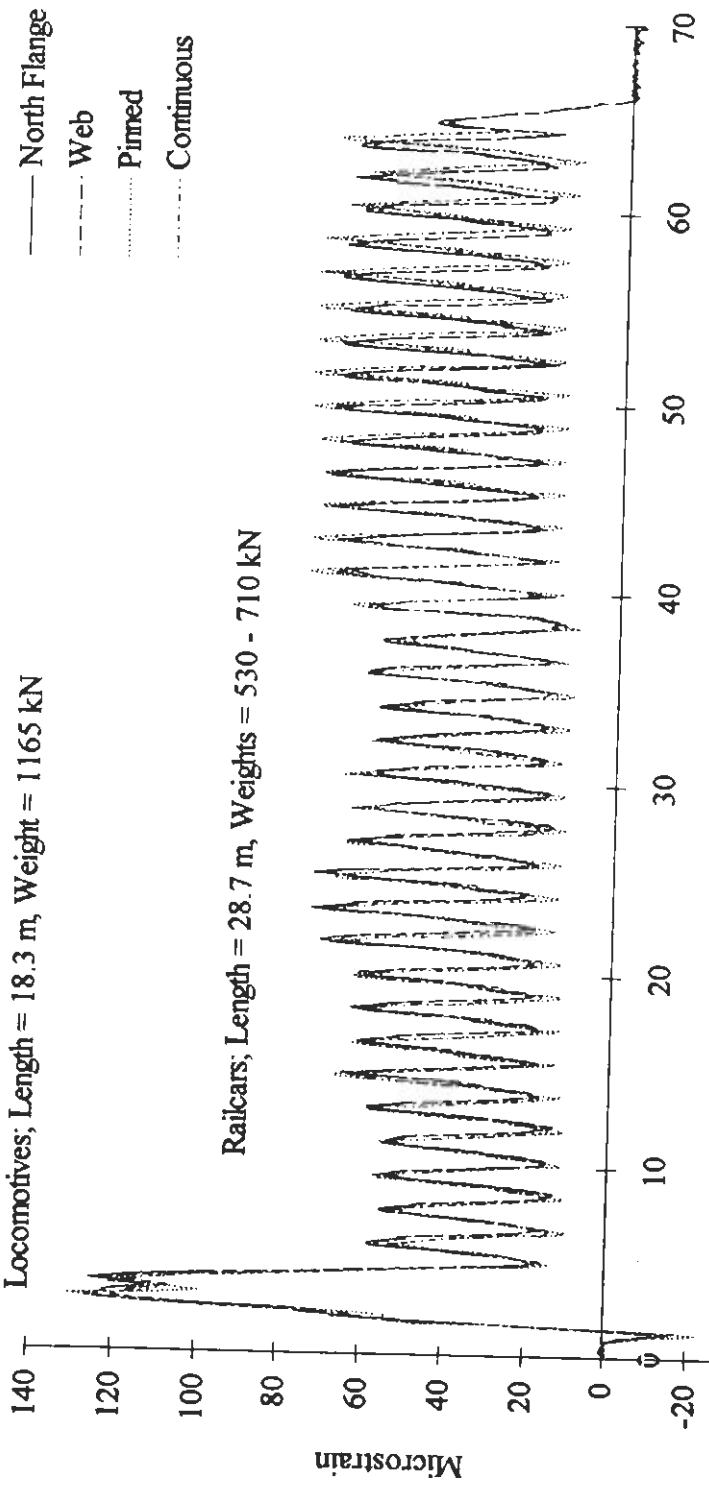

Figure 3.26 Train F717, Diagonal strains compared with Pinned and Continuous models

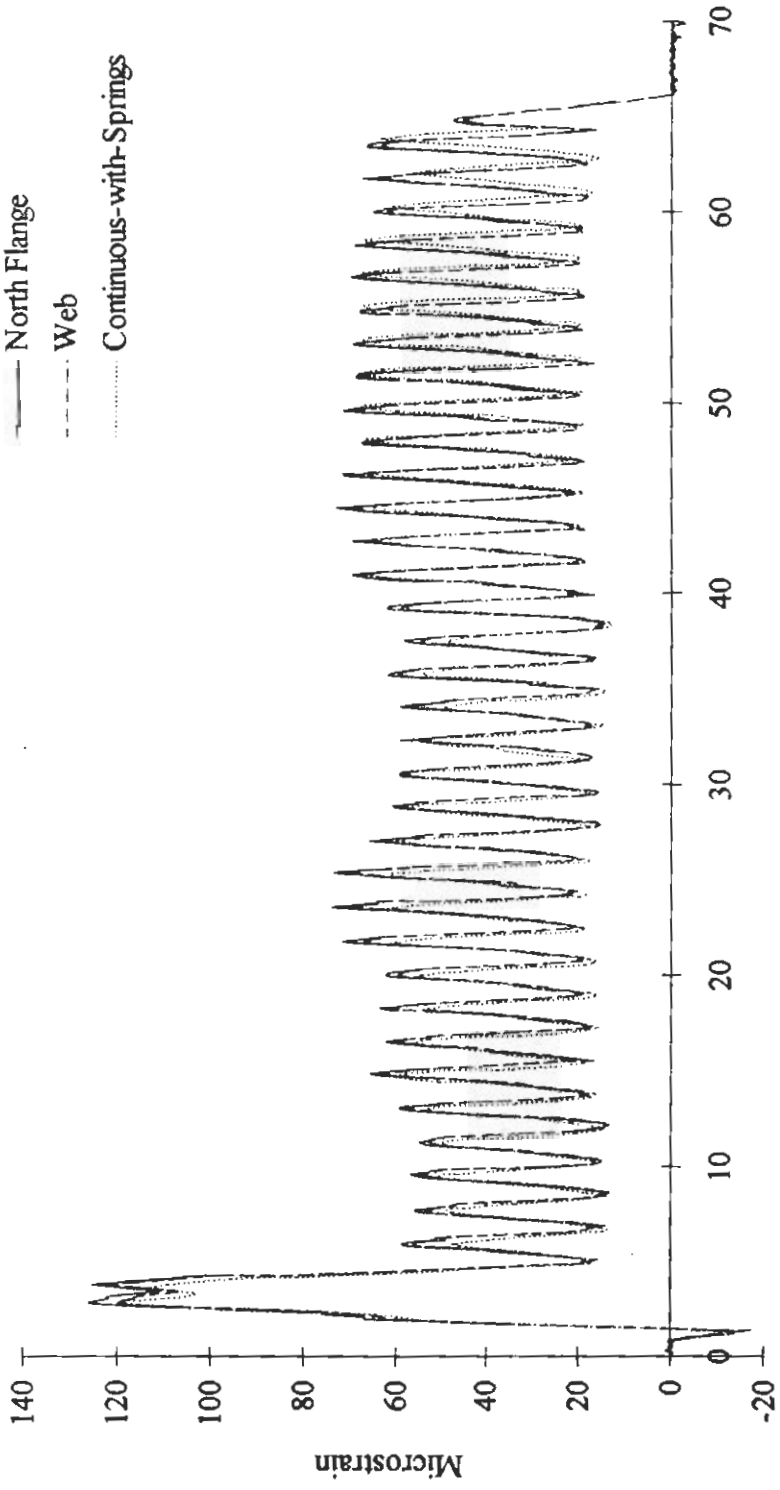

Figure 3.27 Train F717, Diagonal strains compared with Continuous-with-Springs model

4. EXPERIMENTAL PROGRAM

4.1 General

Once the field strain measurements on the bridge had been completed, the bridge was removed from service and dismantled. During the demolition, the ten stringers in the floor system of the bridge were carefully removed and kept intact. They were removed by carefully breaking off the heads of the rivets that fastened the stringer connecting angles to the floorbeam. After all the stringers were removed, they were transported to an outdoor storage yard where they remained for approximately two years, at which time the fatigue testing program was begun at the University of Alberta.

The main purpose of the experimental program was to obtain more information about the fatigue resistance of riveted details. Relatively less is known about the fatigue resistance of these details than about modern welded and bolted details. The information resulting from these tests will be used to supplement the existing database of fatigue tests on riveted details. More specific information about the fatigue life of riveted details will improve the accuracy of remaining fatigue life calculations. The information from these tests will also be used to determine the appropriate fatigue resistance so that it can then be used in the ensuing remaining fatigue life calculations.

The review of the literature identified a need for more testing below a stress range of about 75 MPa on the fatigue resistance graph shown in Figure 2.1. Information in this region is very important because it helps define the location of the constant amplitude fatigue limit, which is critical in determining crack initiation. This region is also the location of the fracture mechanics based transition region described by Kunz [33, 34]. Experimental verification of this region is needed if the benefits are to be used in remaining fatigue life calculations.

4.2 Material Tests

In the fabrication drawings of the bridge, the steel was specified as O.H. Steel, or Open Hearth Steel. The name *Carnegie* was imprinted on the web plate and the flange angles, identifying the supplier as the Carnegie Steel Company. (This company was

eventually merged into the United States Steel Corporation [39]). On the stiffeners, the name *Dorman Long & Co. Ld.* was imprinted. This was a large British steel maker and shape producer of the time [40].

In order to determine the material properties of the stringer steel, eight tensile coupons were saw cut from one of the stringers after it had been fatigue tested to failure (specifically, stringer ST4). Four of the coupons were cut from the web plate and two were cut from each flange angle, as shown in Figure 4.1. This region was selected because, as will be seen, this part of the stringer was not subjected to high fatigue stresses during the testing.

The tension coupon tests were carried out according to the CAN/CSA-G40.20-M92 and ASTM A 370-92 specifications [41, 42]. Coupons were approximately 420 mm long and 50 mm wide at the grips. The reduced section of the coupon was approximately 225 mm long and 40 mm wide. The gauge length for measuring the final elongation was approximately 200 mm. All coupons were initially cut from the full thickness of the flange or web. However, because the surfaces of the coupons cut from the flanges were affected by corrosion, they were milled down until no visible corrosion remained. The final dimensions of all coupons are given in Table 4.1.

During the testing, an extensometer with a gauge length of 25 mm (1 inch) was attached to the reduced section of the coupon in order to measure the strain. For two of the eight coupons, strain gages were attached to both sides of the coupon within the reduced section, as a check on the extensometer strains. The load applied to the coupons was measured by an in-line load-cell and was applied under stroke control. Once the coupon began to yield, the load was held constant for approximately three minutes to measure the static yield strength. The test was then continued until the coupon fractured. Final elongation of the coupon was measured by fitting the two pieces of the coupon back together and measuring the new gauge length.

4.3 Full-Scale Fatigue Tests

4.3.1 Specimen Description

Although ten stringers were obtained from the dismantled bridge, because of time constraints only six were used in this test program. The six stringers that were used were from the three interior panels of the bridge. These stringers were selected because they all had the same connection at each end, and thus should have experienced similar loading during the life of the bridge. The end panel stringers, on the other hand, framed into a floorbeam at one end and rested on a rocker or a roller at the other. This difference in boundary condition would have caused different behaviour in the end panel stringers. Also, there may have been more of an impact effect in the end stringers as trains moved from the approach onto the bridge, and it has been reported that track imperfections often occur at this location [8]. For these reasons, and in order to maintain simplicity in defining the previous history of the stringers, only the six stringers from the interior panels were tested. The identification and location of the stringers is shown in Figure 4.2.

A general description of the bridge and the stringers was given in Section 3.2 (Bridge Description), however the critical detail on the stringers was not discussed at that time. The critical detail is that feature where fatigue cracking occurs, and is usually at the location of the critical combination of structural detail, number of cycles, and high stress range. To identify the critical detail of these stringers, it was recognized that when they were in service they were primarily subjected to strong-axis bending moments. Therefore, it followed that the critical detail on these stringers was likely to be the horizontal gusset plate connection to the bottom flange. It is shown in Figure 4.3. This was the major disturbance along the length of the lower flange of the stringer. It was possible that fatigue cracking could also take place in the riveted connection of the flange angles to the web of the stringer.

Several conditions contributed to the potential that the gusset plate was the critical detail. The rivet holes that made the gusset plate connection were the farthest distance away from the neutral axis, as compared with other rivet holes, and therefore were subjected to the highest global bending stresses. The detail was at the centerline of the

stringer, which is where the moment is the highest (for beams that are not fixed-ended). The presence of rivet holes through the bottom flange is also a stress concentration, which increases the local stresses around the rivet holes. There also exists the possibility that strain compatibility would need to be maintained between the gusset plate and the bottom flange. This would require that load be transferred between the two components, either by friction, by shear in the rivet, or by a combination of both. However, the gusset plate connection is very short, and the question of strain compatibility cannot be defined with certainty.

The gusset plate connection in the bridge was used for lateral bracing between two parallel stringers. Two types of bracing were used between the stringers. One type was cross bracing, in which single cross-angles connected the bottom of one stringer with the top of the other. This angle can be seen in Figure 4.3, where it is at about 45 degrees to the bottom flange. The angle does not connect directly to the bottom flange, but rather is connected to the bottom of the stiffener by a plate. The second type of bracing was a strut between the bottom flanges of adjacent stringers which used two back-to-back angles. These angles were connected to the flange by the critical gusset plate detail shown in Figure 4.3. There were also gusset plate connections to the bottom flange at the third points of the stringers; however these were not considered to be critical because the bending moment is usually not as high at this point as compared with the center of the stringer.

The gusset plate was 9.5 mm thick (3/8 inch) and was connected to the underside of the bottom flange with four 22 mm diameter (7/8 inch) rivets. The rivet holes were 43 mm (1-11/16 inch) from the toe of the flange and were spaced 102 mm apart (4 inch) in a longitudinal line, two rivets on each side of centerline. According to the drawings for the bridge, the holes were to have been punched to 17.5 mm (11/16 inch) and then reamed to 24 mm (15/16 inch).

For four of the six stringers, the gusset plate that extended beyond the bottom flange had been flame cut off next to the flange during the demolition of the bridge. Only the part of the gusset plate that was directly underneath the flange remained. This can be

seen in a later figure (Figure 4.5). Fortunately, no damage appeared to have been done to the flange by the cutting torch, therefore this loss of material was assumed not to have any effect on the tests. For the other two stringers, the bracing was cut about 300 mm away from the flange (as was shown in Figure 4.3).

Corrosion existed on both the top and bottom flanges of the stringers. The top flange corrosion was essentially uniform under the original location of the ties, but between the ties there was more severe pitting. At the worst points, the 17.5 mm thick (11/16 inch) flange was reduced to about 15 mm (9/16 inch). The bottom flange corrosion was on the topside of the bottom flange angle. It was concentrated around the bracing connections, and was probably due to accumulation of dirt and water at these locations. Another source of corrosion could have been brine. Brine was employed as a cargo refrigerant prior to the advent of sealed cooling systems. This substance, which is a mixture of salt and ice, tended to melt and drip on the track and bridge structures, where it could have contributed to the corrosion.

A thin layer (1 or 2 mm) of corrosion also was present between the critical detail (horizontal gusset plate) and the bottom flange angle. This corrosion was located under the edge of the angle toe, and was probably caused by water or brine collecting on the outstanding part of the plate. The furthest that the corrosion penetrated towards the heel of the angle was about 10 mm (3/8 inch) at the centerline of the plate.

Through analytical calculations, which are discussed in more detail in Section 6.0, previous fatigue stress cycles applied to the critical detail were considered to have had a negligible effect. However, for one test, the stringer was inverted so that any possibility of previous fatigue damage was eliminated, since the top flange was loaded in compression during its service life and no fatigue crack growth was likely to have happened. The inverted test also allowed examination of the fatigue resistance of a different detail, the continuous web-to-flange connection (described in Section 3.2). For the inverted stringer subjected to bending, these rivet holes were the farthest fatigue-prone element from the neutral axis, and hence were subjected to the highest stress range. Another reason for studying this detail is that it is similar to details reported in the literature [25].

4.3.2 Test Setup

The objective of the test was to apply a stress range to the critical detail in a manner similar to the stresses it had experienced in the bridge. Since the stringer was primarily loaded in strong-axis bending, the test setup was designed to load the stringers in four-point bending, as shown in Figure 4.4. Note that in this figure the frame columns in front of the stringer have been removed for clarity. The original location of the columns can be seen by the open channels on the top of the frame, and the symmetrically located columns behind the stringer. The critical detail was located on the bottom flange, between the two load points.

The top flange of the stringer was laterally braced at the load points and at the ends of the stringer. Rollers were used between plates at the reaction points to ensure simple supports. Plaster was placed between the end support plates and the bottom flange of the stringer, and between the loading piston and the top flange of the stringer, in order to maintain uniform contact and proper load distribution. No cracking of the plaster was observed during the testing.

Fatigue loads were applied using a Pegasus Servo-Load Simulation system. This system uses hydraulic power controlled by electronic servovalves to apply load. Loads are applied using hydraulic linear actuators. Load-cells mounted between the actuator and stringer monitor the application of load. Static and dynamic electronic signals are used to control the servovalves and apply the fatigue loads. Fatigue loads up to 489 kN (110 kip) per actuator, at a rate of about 4 Hz, can be applied with this system.

4.3.3 Test Preparation

All paint and loose corrosion was removed from around the critical detail to make it easier to find cracks. This was done with a commercial paint stripping compound and a scraper, which was used with care so as not to damage the surface with nicks or cuts. After most of the paint had been removed, the remaining paint and the mill scale surrounding the rivet heads was lightly sandblasted.

The corrosion around the detail was mapped by taking impressions at sections along the flange with a metal comb. These impressions were then traced onto a paper, wherein measurements of the material loss could be estimated.

For the stringers that were tested in the normal orientation, eight strain gages were attached to the bottom flange, as shown in Figure 4.5. These strain gages were located approximately 450 mm (18 inch) on either side of centerline, in the gross section of the stringer. They were approximately 250 mm (10 inch) from the nearest rivet in the gusset plate detail.

The strain gages were used to monitor the strain range applied to the critical detail during testing, however, their measured values needed to be modified in order to reflect the correct strain range. Normally, strains along the bottom flange of a beam within a constant moment region are constant. However, due to changes in cross-sectional area caused by the presence of corrosion and rivet holes, the strains measured in gross-section were slightly lower than those measured in the net-section. Since the desired stress range at the critical detail is a net section stress range, the bottom flange gross-section strain measurements were modified by a factor to convert them to a net-section strain. This factor was a ratio of the gross and net section modulii, calculated using the original dimensions of the stringer. The calculation assumed that only the rivet holes on the tension side of the neutral axis deducted cross-sectional area from the net-section. Rivet holes on the compression side were assumed to directly carry load via the rivet shanks.

The effect of section loss due to corrosion was not considered in the net-to-gross section conversion factor. It was found during the examination of the corrosion profiles that the area lost due to corrosion was, for the worst case, about 4 % of the area lost due to the rivet hole. Therefore, the ratio of section modulii for the net and gross sections was calculated for the presence of the rivet hole only: it is equal to about 0.97. When the area lost by corrosion was included in the calculations, the difference was negligible. Since the measured area lost by corrosion is an estimate in any event and has room for error, its effect was neglected when converting the gross-section strains to the net-section strains.

For the test in which the stringer was inverted, the critical net-section was at the lower row of rivets in the continuous web-to-flange connection detail. The strain gages were attached to the web as shown in Figure 4.6, where they measured the gross section strain. This was necessary because, due to the close proximity of the rivet holes to one another in the detail, any strain gages attached near the detail would have been affected by the local strain concentrations.

To determine the strain at the critical detail for the inverted test, the web gage readings were first used to locate the neutral axis by applying a static load to the stringer. Assuming plane sections remain plane, the gross-section strain at the lower row of rivets was calculated by a linear extension of the strains measured by the web gages. Since this strain was a gross-section strain, it was converted to a net-section strain by using the ratio of section modulii, as was done in the normal orientation tests.

Once the critical detail was cleaned and the strain gages attached, the stringer was inserted into the test frame where it was aligned and plastered into place. The strain gages were connected to a voltage excitation and amplification system similar to the one described in Section 3.3 (Strain Measurement). A computer program sampled the output of the gages 75 times per second, calculated maximums and minimums, and displayed this result on a computer screen. These maximums and minimums were updated every few seconds, which enabled monitoring of the applied strain range to the critical detail while it was under fatigue loading.

4.3.4 Test Procedure

For the testing of the stringers in the normal orientation, the target net-section stress range was converted into its equivalent gross-section strain range. Static load was then applied to the stringer by both actuators until the average of the eight strain gages was just over one-half the target gross-section strain. At this point, both the maximum and minimum strains on the computer screen were about equal. Dynamic load was then applied to the stringer. This caused the minimum strain to be reduced and the maximum strain to be increased. The dynamic load was amplified until the difference between the maximum and minimum strains was equal to the target strain range. The load that was

being applied at this point was fixed and then used throughout the test. The cycle counter was started as soon as the target strain range was reached.

For the inverted test, static load was first applied to the stringer to determine the location of the neutral axis and the distribution of the strain plane from the web gages. The target net-section stress range was then converted into an equivalent gross-section strain range at the location of each web gage. Static load was applied until each web gage read just over one-half of its target strain range. Once again, at this point the maximum and minimum strains for each gage were about equal. Dynamic load then was applied until the difference between the maximum and minimum strains was equal to the target strain range. The corresponding loads were fixed and applied throughout the test.

The net-section stress ranges for the six tests done in the normal orientation were one test at 73 MPa, two tests at 68 MPa, two tests at 66 MPa, and one test at 62 MPa (10.6 ksi, 10.0 ksi, 9.6 ksi, and 9.0 ksi, respectively). These stress ranges were selected for the reasons outlined earlier, namely to provide information near the Category C and D fatigue limits and in the transition region. The one stringer tested in the inverted position was loaded at a stress range 73 MPa, so that it could be compared with a normal orientation test.

As much as possible, tests were run 24 hours a day, seven days a week. An automatic shutdown circuit monitored the stroke of the actuators to guard against large deflections. Regular inspection for cracks was performed visually, with chemical dye penetrant, and with magnetic particle detection.

The definition of failure, that is, when to stop the test, is very important. The failure criteria in previous investigations have ranged from a specified amount of additional deflection to complete loss of load-carrying capacity. In order to maintain consistency between reported test results, discussions were held with CN Rail, sponsors of the work, and with Lehigh University, who were conducting similar tests. The consensus reached was that fatigue failure would be defined as that condition wherein one component was completely severed by a fatigue crack and new cracking was detected in another

component. For example, failure would be considered to have taken place when the flange angle was completely severed and a new crack was found in the web.

4.3.5 Post Test Examination

After failure had been reached and the testing stopped, the stringers were removed from the test frame. For several stringers the critical detail rivet holes and crack surfaces were opened up for examination. To do this, the rivet hole where the crack had initiated was cored out using a hole saw of about 2-1/2 times the diameter of the rivet hole. The rivet head was then milled off and the crack surface was opened up. For one crack, the section around the crack was sawn out.

The purpose of the examination was to inspect the surface of the rivet holes, the fracture surface, and the microstructure of the steel. This was done to determine the method of hole preparation and to see if any abnormalities contributed to the initiation of fatigue cracks. The inspection of the rivet holes was done visually and with a stereobinocular microscope.

Inspection of the microstructure and fracture surface was carried out with optical and scanning electron microscopes. This was done to closely inspect the fatigue initiation sites, determine the presence and effect of microstructural defects, and to inspect the crack propagation patterns. The inspections were carried out on polished and etched samples taken from sections of the cores, and on the fatigue fracture surfaces.

Coupon	Original Depth, mm	Milled Depth, mm	Width, mm
1	0.375	–	40.04
2	0.375	–	40.10
3	0.375	–	40.04
4	0.375	–	40.08
5	17.46	16.40	40.05
6	17.46	16.45	40.04
7	17.46	14.70	40.08
8	17.46	14.86	40.05

Table 4.1 Dimensions of tension coupons

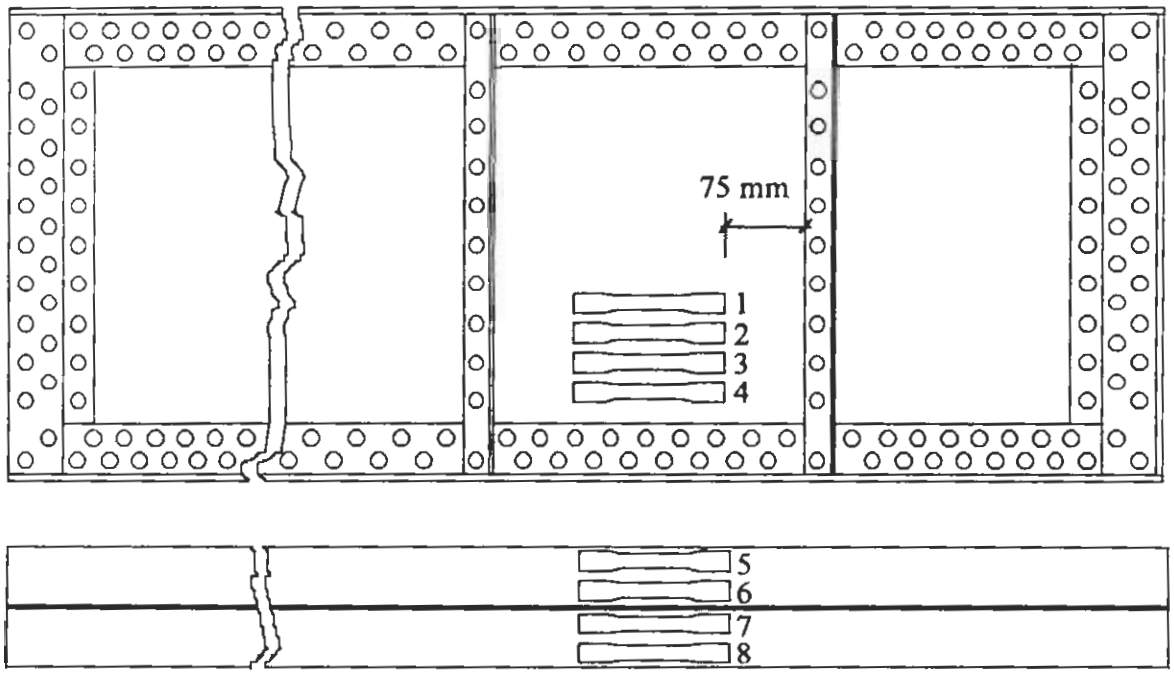

Figure 4.1 Location of tension coupons

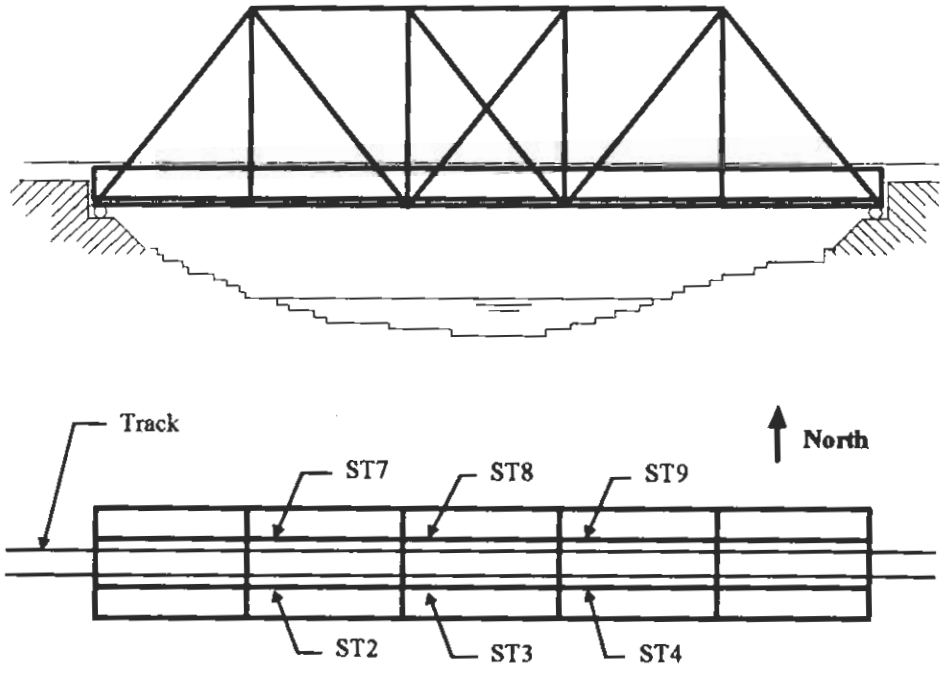

Figure 4.2 Identification of stringers in the bridge

Figure 4.3 Gusset plate connection, critical detail

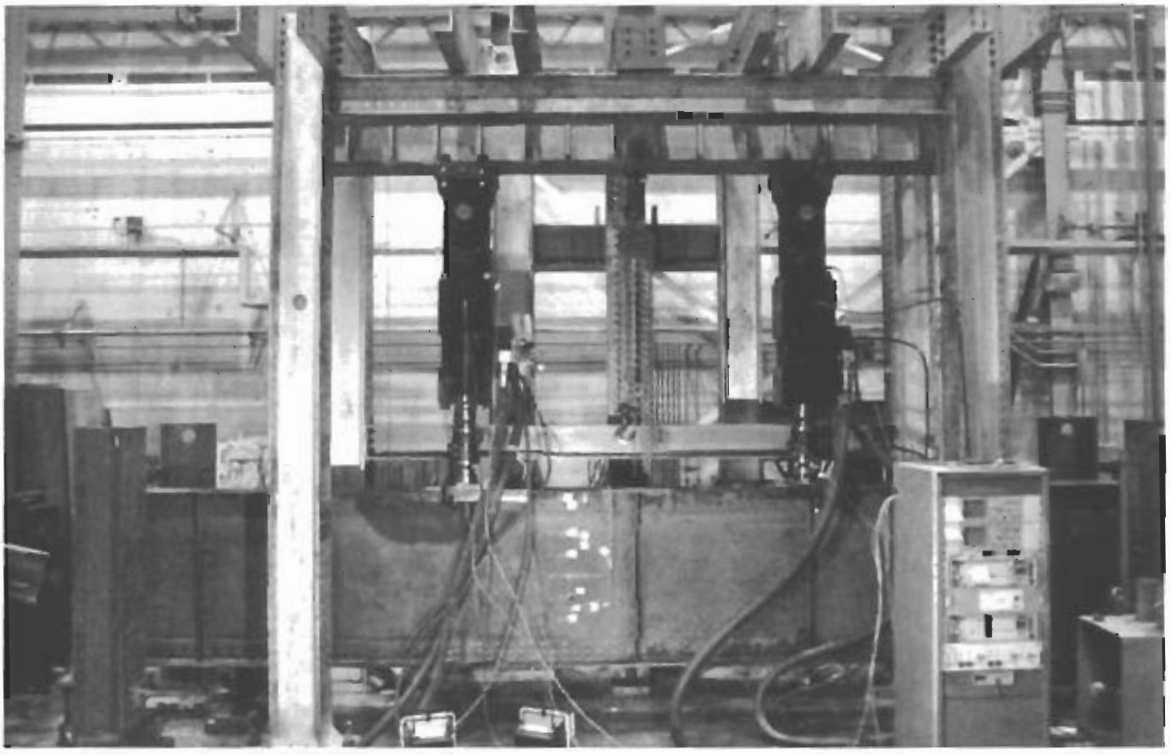

Figure 4.4 Test setup, four-point bending

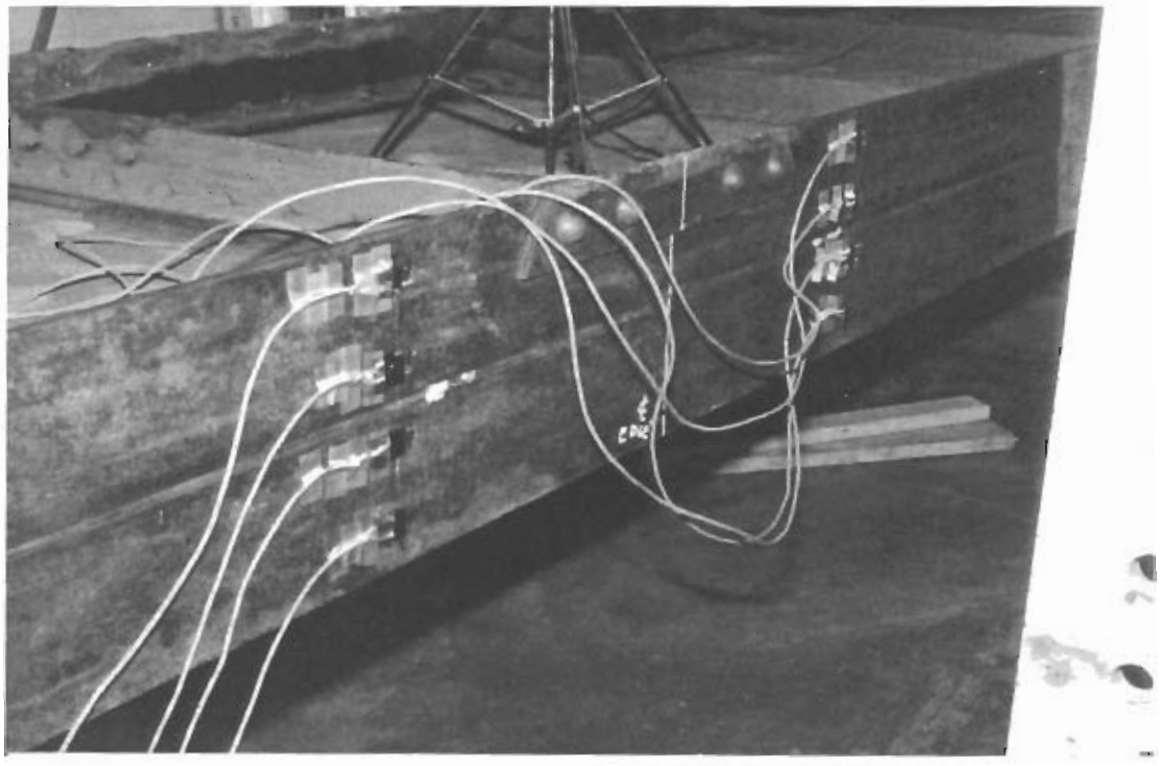

Figure 4.5 Test gages on bottom flange

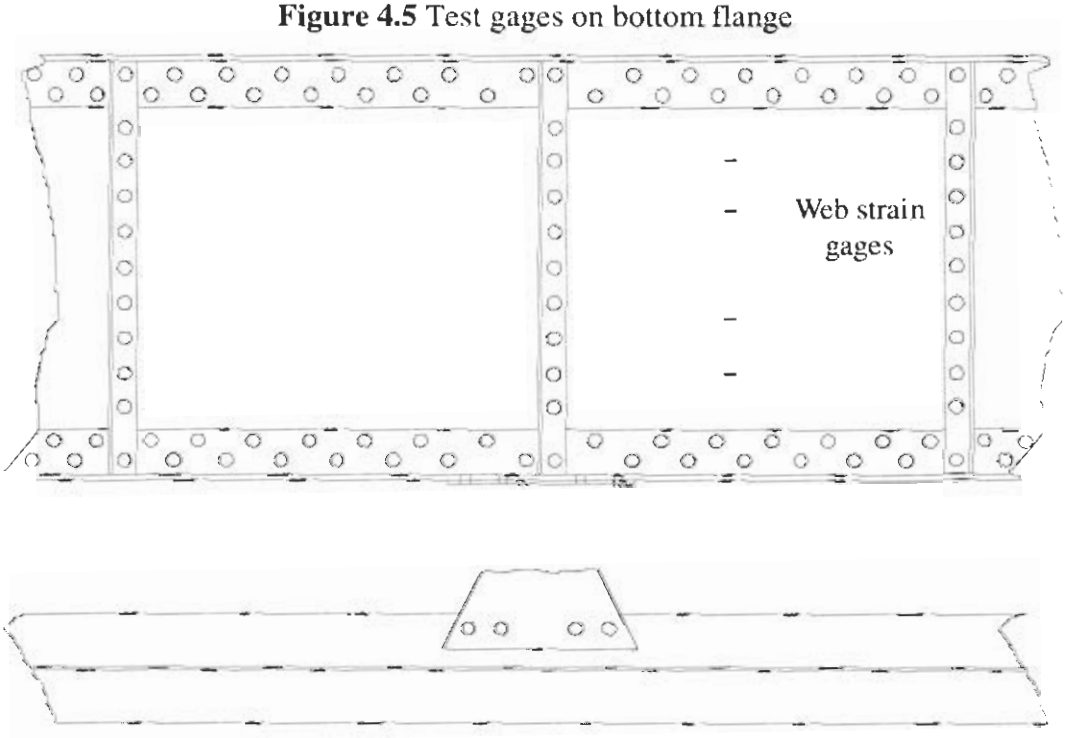

Figure 4.6 Inverted test strain gage arrangement

5. RESULTS OF EXPERIMENTAL PROGRAM

5.1 Material Tests

The static yield level, ultimate strength, and other material properties are summarized in Table 5.1. Canadian specifications from about the time the bridge was built indicate that so-called Open Hearth Steel, when used as structural steel for bridges, should have a tensile strength (ultimate yield stress) of between 380 MPa and 450 MPa (55 ksi and 65 ksi), and a minimum yield strength (lower yield strength) of one-half the tensile strength, which is between 190 MPa and 225 MPa (27.5 ksi and 32.5 ksi) for this grade [35]. The specified minimum elongation for the steel is calculated by dividing the tensile strength (in psi) by 1 500 000. The results are presented in the table for each coupon, where it is seen that the tests indicate the stringer steel meets the specifications. (Static yield strength is slightly less than the so-called lower yield strength. Since the steel tested has a static yield strength greater than the specified minimum lower yield strength, it can be concluded that the requirement has been met). The average modulus of elasticity was 201 182 MPa for the steel in the web and 199 187 MPa for the steel in the flanges.

The strain gages that were mounted on two test coupons measured essentially the same strain as did the extensometer. This confirms that the measurement devices were functioning properly during the test.

5.2 Full-Scale Fatigue Tests

5.2.1 General Observations

Monitoring of the strain gages during the tests showed that the strains stayed essentially constant for the duration of the fatigue tests. However, just prior to visual detection of the first crack, the strain measurements from the gages in-line with the critical detail would show a decrease and the strains from the other gages would increase. This apparently was the result of the change in cross-sectional area caused by the crack, and the subsequent strain redistribution. This change in strains that was observed during the tests was significant and it was therefore useful as a signal that a crack was about to appear.

No movement between the components of the stringer was observed during the tests. The rivets appeared to be tight and apparently had some appreciable clamping force.

The paint that spanned adjacent components (e.g., at the continuous web-to-flange connection) or corrosion that was present between components (e.g., the gusset plate connection) remained undisturbed throughout each test. There was a small movement of the flange angle relative to the web observed at the end reaction points, which was indicated by a grinding sound and accumulation of fretting dust.

Most initial cracks were identified visually, either by the naked eye or with the help of a magnifying device. The magnetic particle or dye-penetrant crack detection methods performed satisfactorily, although they were generally only used in this program to determine the location of a crack tip. Some cracks that occurred in areas where the paint was not removed did, in fact, crack through the paint, although by the time they were discovered they were quite long. In a painted area where there was a known crack, the magnetic particle procedure was successful in identifying its location through the uncracked paint.

After the crack was discovered, fretting dust usually had begun to appear around the head of the rivet. This clue could be useful for detecting large cracks, providing that the overcoat of paint would not hide the dust. For small cracks, fretting of the moving parts had yet to develop any dust, so this clue was not useful for initial crack detection.

Comparison of the measured strains with those calculated from the applied loads gave values generally within 5 MPa (stress terms) of each other. This is quite good considering that the effect of corrosion had not been taken into account; the section modulus was calculated using the original dimensions of the stringer. The deflection of the beam was calculated to be about 3 mm and it was observed in the test to be about 5 mm.

5.2.2 Test Results

The results of the full-scale fatigue tests are presented in Table 5.2 and Figure 5.1. All tests were conducted on stringers in the normal orientation except for stringer ST8i, which was tested in the inverted position. For stringers ST8 and ST2, testing was stopped before any cracks had been detected. Data points ST7s and ST8s represent cracks that developed in the shear span of the stringer, at a detail similar to the critical detail, however these were not the cause of failure. In the rest of the tests done in the normal orientation position, the crack occurred through the outer rivet hole in the critical detail, as shown in Figure 5.2. Typically, the crack started at this hole and then propagated though the angle

until it was completely severed. As testing was continued, usually the next crack was discovered in the web, at which point failure was deemed to have occurred and the test was stopped.

Stringer ST3 was tested at a net-section stress range of 73 MPa (10.6 ksi). In this test, the crack was discovered late due to improper setup of the automatic shutdown device. As a result, the number of cycles at the time of the initial crack is unknown. Fortunately though, the test was stopped at the correct definition of failure, at 1 874 730 cycles. The final appearance of the crack is shown in Figure 5.2. Most likely the crack began at the rivet hole in the gusset plate detail and propagated through the angle. The second crack was discovered in the web, in line with one of the continuous web-to-flange connecting rivets. The web crack is identified in the figure by the dark spot of dye-penetrant on the white developer.

Stringer ST4 was tested at 69 MPa (10.0 ksi). The first crack was found at 1 521 450 cycles on the toe side of the critical detail rivet hole. It had fully propagated to the toe of the angle by the time it was discovered, as shown in Figure 5.3. Fatigue loading was continued and another crack was detected on the other side of the rivet hole at 1 523 270 cycles, that is, 18 200 cycles after the first crack was detected. This crack continued to propagate until it severed the angle at 1 766 880 cycles. The next new crack was discovered in the angle on the other side of the stringer at 2 168 570 cycles, 647 120 cycles after the first crack had been detected. The crack was at a lower rivet hole in the continuous web-to-flange connection. This rivet hole was the closest hole to the first crack in the other angle. The test was again continued, and a third crack was discovered in the web, in line with the same rivet hole, at 2 172 570 cycles. These last two cracks can be seen in an extremely propagated form in Figure 5.4, far beyond the normal definition of failure. The deflection of the stringer was very large (about 50 mm) at this number of cycles.

Stringer ST9 was tested at 69 MPa (10.0 ksi), which is the same stress range as used for ST4, and it failed at 3 336 700 cycles. The first crack was found at 2 486 070 cycles on the toe side of the rivet hole, similar to that shown in Figure 5.3, except that it had not propagated all the way through to the toe. At 2 743 240 cycles, 257 170 cycles after the first crack was detected, another crack was discovered on the side of the rivet

hole that faced towards the heel of the angle. At this point a repair was attempted by clamping a plate over the crack. Crack growth slowed considerably, but was not halted. The plate was removed at 2 950 860 cycles, 207 620 cycles after it had been installed. This number of cycles is small compared to the final number at failure, therefore the influence of the slowed crack growth was considered negligible. The crack propagated through the flange and continued up the vertical leg of the angle. The angle was severed at 3 157 670 cycles, and a second crack was discovered in the web plate at 3 336 700 cycles. Failure was 850 630 cycles after the first crack was discovered.

Stringer ST7 was tested at 66 MPa (9.6 ksi). The first crack was detected at 2 364 230 cycles on the heel side of the critical detail rivet hole. At 2 856 410 cycles, another crack was detected on the other side of the rivet hole, fully propagated to the toe of the angle. The crack on the heel side of the rivet hole continued to propagate until it severed the angle at 2 971 950 cycles. A crack was found in the web at 3 240 180 cycles, or 875 950 cycles after the first crack was discovered.

There was also a crack discovered in the shear span of ST7 at a detail similar to the critical detail, that is, at a gusset plate attached to the underside of the bottom flange. The crack began at the rivet hole in the flange and propagated into the vertical leg of the angle. On the vertical leg it curved towards and into a web-to-flange connection rivet hole and stopped. It was at this point that the crack was discovered. The number of cycles was 3 213 710 and the net-section stress range due to bending at this location was about 61 MPa. The results are identified in Figure 5.1 and Table 5.2 as ST7s.

Stringer ST8 was tested at 66 MPa (9.6 ksi), the same stress range as ST7. No cracks were detected at the critical detail for the duration of the test. The test was stopped at 12 017 640 cycles and the stringer was removed. At this number of cycles, the data point plotted well right of the Category C fatigue resistance line. Since a main region of interest for this report was the transition region, it was felt that the information provided by starting a new test would be more beneficial than continuing with the uncracked one.

One crack was discovered in the shear span of ST8 at the same type of detail as was discussed in connection with stringer ST7. The number of cycles was 10 850 670 and the net section stress range was about 61 MPa. However, an important difference between this detail and the one in ST7 is that this detail did not have any rivets present in the holes,

because the gusset plate had been removed during the demolition of the bridge. To repair the crack, two splice plates were bolted to both sides of the horizontal leg of the angle. No further crack growth was detected after the repair was made.

Stringer ST2 was tested at the lowest stress range, 62 MPa (9.0 ksi). No cracks were detected in this stringer and the test was stopped at 12 178 930 cycles.

After all the testing of the stringers in the normal orientation was complete, stringer ST8 was inverted and reinserted into the testing frame. Under the new designation ST8i, it was tested at the same net-section stress range as ST3, 73 MPa (10.6 ksi). The first crack was detected at the lower rivet hole in the continuous web-to-flange connection at 7 577 300 cycles. The rivet in this hole also fastened a stiffener to the web plate, as shown in Figure 5.5. The second crack was discovered in the web at 8 073 460 cycles. Since the crack appeared in line with the stiffener holes, the test stress range was adjusted to reflect the net section stress range at the stiffener detail.

5.2.3 Discussion of Results

Table 5.3 compares the test results at failure with predicted fatigue lives according to the AASHTO Category D fatigue resistance line and the prediction line for this same category as modified by Kunz. The fatigue resistance curves are also plotted in Figure 5.1.

All of the test results obtained from the gusset plate detail exceed the Category D fatigue resistance curve at least slightly. This is consistent with most of the results on shear splices and full-scale fatigue tests obtained in the literature, but it must be remembered that the Category D line is two standard deviations less than the mean, whereas the test results are absolute. Note that most of the test results do not support the modified AREA fatigue resistance curve for rivets with normal clamping force (the shift to Category C at 83 MPa).The two test specimens that were stopped before cracking was detected ran significantly longer than the other tests. This could be due to scatter, which is common in fatigue testing of details that do not present particularly large stress concentrations. In addition to the type of initial flaw, scatter can also be attributed to the variation in rivet clamping force.

The stringer tested in the inverted position (ST8i) had a much higher fatigue strength as compared with the results from the stringers done in the normal orientation. Although this could be due to inherent scatter in the results, the fact that it is a different

detail must also be considered. It could be that this type of detail, the continuous web-to-flange connection, has a different fatigue resistance than the gusset plate detail. Compared with the standard fatigue strength curves, it seems that this test is better represented by a line closer to category C, than by category D.

There was generally a large number of cycles between when a crack was first detected and when failure occurred. Usually between one-half and one million additional cycles were applied to the stringer past the time of the initial crack and until the point of defined failure was reached. There was no noticeable increase in deflection in any of the stringers tested in this program during this interval. As pointed out in the literature, riveted members have an internal redundancy. After one component has cracked, the load may be able to be carried for a relatively long period of time by the remaining components of the cross-section. In remaining fatigue evaluations, these additional cycles can translate into a significant amount of remaining serviceable time.

The test results appear to support the concept of the transition region. Test ST4 is marginally lower than the transition line predicted by Kunz, but the rest of the tests are above this line. However, it is recognized that the fact that the fatigue failures are higher than this transition region is not conclusive proof that it exists. The concept that this region is significant should be explored further with additional testing.

The cracks that developed in the shear span are also plotted in Figure 5.1. The number of cycles plotted corresponds to when the crack was discovered, not failure as defined by the detection of a second crack. Therefore, there would be still more cycles that could be added to the data point. With this in mind, the data points generally agree with those of the other tests. Crack ST7s plots right of the Category D resistance curve, and with the additional cycles it would probably exceed the transition region. ST8s also plots well right of the resistance curves.

These fatigue life data support the use of the category D fatigue resistance curve to represent the gusset plate detail in the remaining fatigue life evaluation. It would also be beneficial to include the transition region, since the data tend to support its existence. The test of the inverted stringer suggests that there might be a different fatigue resistance between types of riveted details, although the number of data to support this possibility is small.

5.2.4 Post Test Examination

Rivet holes that had fatigue cracks were cored out of stringers ST3, ST9, ST7, and ST8i. The crack in stringer ST4 was sawed out. Two cores were also taken from the uncracked stringer ST2, and were sawed open. All cores had the rivet holes examined, and samples of cores from ST7 and ST8i were used for optical and scanning electron metallographic examinations. The post-test examination of the rivet holes and crack surfaces was carried out by others, and the complete report is given in the Appendix A. brief summary of the findings is discussed below.

Examination of the rivet holes showed them to be fairly corroded in the gap between the rivet shank and the edge of the hole. Parallel grooves normal to the plane of the plate indicated that the holes were punched, and circumferential marks in the plane of the plate indicated the holes were subsequently reamed. Since some punch rub marks were visible, this suggests that the reaming operation may not have been totally effective. However, for all the cores examined, there was no association between the punch rub marks and the initiation of the fatigue cracks.

In specimens ST7 and ST8i, microstructural examination of the steel revealed that it was consistent with steels from the time the bridge was built. Carbon content was estimated at about 0.2 %, and there were significant amounts of manganese sulphide and silicate inclusions, which makes it dirty by modern standards. Examination of the fracture surface showed it to be covered with typical fatigue striations. Microstructural examination of the initiation sites showed no defects were present, and the crack initiation and propagation behaviour appeared to be normal.

Coupon	Location	σ_{ys}, MPa	σ_u, MPa	E, MPa	% Elongation Specified	% Elongation
1	Web	241	451	199 380	22.9	27.8
2	Web	239	446	199 390	23.2	28.0
3	Web	239	447	198 640	23.1	27.6
4	Web	240	447	199 340	23.1	27.1
Average	Web	225	438	201 180	–	28.5
Std. Deviation	Web	6	8	2 460	–	1.8
5	Flange	228	442	202 500	23.4	27.0
6	Flange	217	433	197 790	23.9	31.1
7	Flange	232	448	203 410	23.1	28.4
8	Flange	223	431	201 030	24.0	27.4
Average	Flange	240	448	199 190	–	21.6
Std. Deviation	Flange	1	2	360	–	0.4
Average (web & flange)	–	232	443	200 180	–	28.0
Std. Deviation (web & flange)	–	9	7	1950	–	1

Table 5.1 Material test results of ST4

Stringer No.	Stress Range MPa (ksi)	Cycles to Initial Crack	Cycles to Failure	Difference
ST9	69 (10.0)	2 486 070	3 336 700	850 630
ST3	73 (10.6)	–	1 874 730	–
ST4	69 (10.0)	1 521 450	2 168 570	647 120
ST7	66 (9.6)	2 364 230	3 240 180	875 950
ST8	66 (9.6)	–	12 017 640*	–
ST2	63 (9.1)	–	12 178 930*	–
ST7s	61 (8.7)	–	3 213 710	–
ST8s	61 (8.7)	–	10 850 670	–
ST8i	73 (10.6)	7 577 300	8 073 460	496 160

* Test stopped, no cracking

Table 5.2 Results of full-scale fatigue tests

Stringer No.	Stress Range MPa (ksi)	Cycles to Failure	AASHTO Category D	Kunz Prediction
ST3	73 (10.6)	1 874 730	1 688 920	1 835 700
ST9	69 (10.0)	3 336 700	2 000 000	2 213 800
ST4	69 (10.0)	2 168 570	2 000 000	2 213 800
ST7	66 (9.6)	3 240 180	2 285 310	2 575 200
ST8	66 (9.6)	12 017 640*	2 285 310	2 575 200
ST2	63 (9.1)	12 178 930*	2 627 580	3 030 300
ST7s	61 (8.7)	3 213 710	2 894 590	3 398 100
ST8s	61 (8.7)	10 850 670	2 894 590	3 398 100
ST8i	73 (10.6)	8 073 460	1 688 920	1 835 700

* Test stopped, no cracking

Table 5.3 Test results compared with fatigue resistance curves

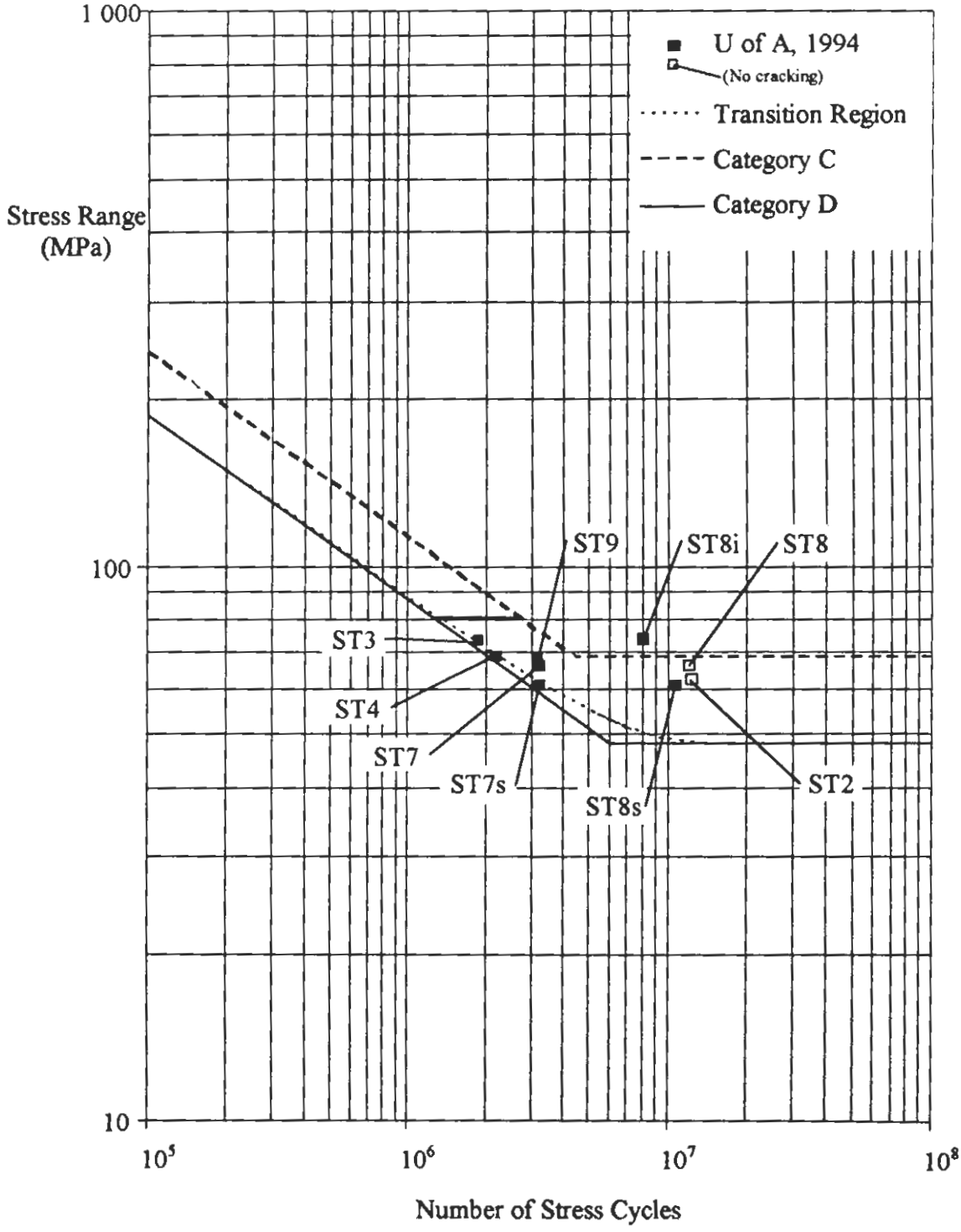

Figure 5.1 Results of full-scale fatigue tests at failure

Figure 5.2 Stringer ST3 at failure

Figure 5.3 First crack in stringer ST9

Figure 5.4 Cracks in stringer ST4, past defined failure

Figure 5.5 First crack detected in stringer ST8i

6. REMAINING FATIGUE LIFE

6.1 General

The remaining fatigue life evaluation will be limited to that of the stringers, and it specifically reflects the lateral bracing gusset plate detail tested in the experimental program. Stress ranges will be calculated using the influence lines developed in Chapter 3.0, and traffic levels will be estimated from traffic information provided by CN Rail. Note that this exercise does not represent a complete remaining fatigue life evaluation of the bridge because it is likely that there are other fatigue-critical details and members that must be examined. The objective of the evaluation is to examine the sensitivity of the influence line and fatigue resistance information developed in this report, and to determine the amount of previous fatigue damage, if any. For the latter objective, the traffic models applied to the bridge were selected conservatively so as to ensure a worst-case scenario.

6.2 Evaluation Methods

Three methods were used to evaluate the remaining fatigue life of the stringers. The first two were based on the current AREA and ECCS standards, which were described in Section 2.3. The specific information from these standards required for the evaluation is the method of damage accumulation and the fatigue resistance curves. The Miner summation is used by both standards for damage accumulation (Eq. 2.3), and their respective fatigue resistance curves are shown in Figures 2.3. and 2.4. For variable amplitude stress ranges, AREA discards the constant amplitude fatigue limit and extends the fatigue curves downwards at the standard slope, i.e., a slope of 3. In the ECCS standard, the user has the option of either extending the curves downwards at the standard slope (3) or, alternatively, using a combination of two slopes. The latter option will be used in this evaluation.

A possible limitation of the AREA and ECCS evaluation methods is the way in which they deal with variable amplitude loads when a few stress cycles exceed the constant amplitude fatigue limit. When AREA recommends extending the fatigue resistance line downward at the standard slope, it is the same as saying that all cycles will contribute to crack propagation. This is very conservative. The ECCS standard tries to

take this into account by means of the dual slope concept. However, even this may not correctly predict the correct amount of damage because crack propagation depends to some extent on the sequence of the applied loading.

The third method of evaluation will be the alternative method described in Section 2.3.3 of this report, i.e., the method developed by Kunz. The two main components of this evaluation technique are (a) a new method of damage accumulation and (b) a modified form of the fatigue resistance curve, both of which are based on fracture mechanics. The new method of damage accumulation assumes that when all stress ranges are below the constant amplitude fatigue limit, they do not contribute to crack propagation. However, as soon as this limit is exceeded, a new, slightly lower, limit, called the damage limit, is calculated. The new damage limit is then used in the same manner as was the constant amplitude fatigue limit. Stress ranges below the calculated damage limit are discarded until it too is exceeded by a stress range, at which point another damage limit is calculated. This process is continued until the calculated damage is equal to unity (as per the Miner summation).

The modified form of the fatigue resistance curve, also developed by Kunz, includes a transition region between the sloping portion of the fatigue resistance line and the constant amplitude fatigue limit. As explained in the literature review, this region is observed in experimental fracture mechanics data. The specific numerical information required in this method, the detail category and the initial constant amplitude fatigue limit, will be taken from the AREA standard.

6.3 Computer Program Remaining Fatigue Life (RFL)

The calculation process for the remaining fatigue life evaluations in this study has been greatly simplified for the authors by the creation of a computer program. The computer program, called "RFL" or "Remaining Fatigue Life," determines the remaining fatigue life of a specific detail by calculating the damage accumulation due to past, present, and future traffic models [43]. Using this program, each of the evaluation methods mentioned in the previous section can be run using the same input data. This enables the user to examine different fatigue life scenarios and methods of evaluation without spending a lot of time on calculations. RFL was written in FORTRAN and can be

run on a UNIX-type operating platform or, in a more restricted form, on a PC 386 level or later machine.

The RFL program requires a variety of information in order to perform the remaining fatigue life calculations. The five general areas for which input is required are: the geometry of the locomotives and railcars, typical trains made up from these geometries, traffic models of the typical trains, influence lines of specific details, and fatigue resistance curves of these same details.

The geometry of the locomotives and railcars are put into the program and stored in a data file. The number of axles, the load on each axle, and the location of each axle with respect to the coupling are defined. Once this information has been input, the user uses it to build typical trains. Typical trains may be defined as freight or passenger trains, and many different arrangements may be used in order to accurately reproduce traffic loading sequences. All of the typical trains are then stored in a data file, which will subsequently be used to build the traffic models.

The traffic models define which typical trains have used or will use the bridge. Traffic models are defined on a yearly basis, and the process begins by specifying the total number of trains that cross the bridge, followed by the percentage of the total accounted for by each typical train. If traffic is essentially the same for a specific time period, yearly traffic patterns can be repeated from year to year. The starting year of the traffic model is usually taken as the year the bridge was constructed, but any year may be selected. A reference year must also be specified, which is the year from which the remaining fatigue life is to be calculated. This is usually the current year, that is, the date at which the examination is being made. In addition to the arrangements of the typical trains in the total traffic, the speed of each typical train must be input in order that dynamic effects can be calculated. The program RFL calculates impact for all trains using a method that relates impact to the speed of the train. Impact factors obtained from the standards are not used. It has been judged that it would be overly conservative to apply them to every force.

Information about the structural detail to be evaluated is input in the form of an influence line and the appropriate fatigue resistance curve. The influence line is input as two dimensional coordinates, and a multiplication factor is used to convert the units of the influence line to stresses at the detail. For example, if the influence line is for the bending

moment, the multiplication factor would simply be the inverse of the section modulus, assuming consistent units. Selection of the fatigue resistance curve can be made from a suite of eight possible internally-defined fatigue resistance curve variations of the standard AREA single slope and ECCS dual slope curves. The curves can be specified either with or without the associated constant amplitude fatigue limit or the cut-off limit. The Kunz fracture mechanics based curve with the decreasing fatigue limit is also included, and it can be selected either with or without the transition region. Once the curve format has been selected, the user enters the specific numerical values for detail category (i.e., the fatigue resistance at 2 million cycles), the constant amplitude fatigue limit, if any, and the cut off limit, if any.

When all the input data has been entered, the RFL program begins by applying the typical trains in the traffic models to the influence line. This operation yields the maximum and minimum stresses, which are then converted into stress ranges using the rainflow counting method. The resulting stress ranges can then be used for the damage accumulation calculation. If the AREA or ECCS fatigue resistance curves are selected, the damage accumulation is done using the Miner summation. If the Kunz fatigue resistance curve is selected, calculations are performed as outlined in Section 6.2. In any case, damage is accumulated until the sum of unity is reached.

When unity is reached, the RFL program identifies the amount of damage that has occurred up to the reference year and the remaining fatigue life in years, relative to the reference year. This remaining fatigue life assumes that the traffic patterns in the last model year remain constant. Obviously, if traffic patterns change, the remaining fatigue life would need to be recalculated by updating the traffic model with the new information.

6.4 Calculation of Remaining Fatigue Life

The computer program RFL was used for all remaining fatigue life calculations. Numerical input data was obtained from Chapter 3 (influence lines), Chapter 5 (fatigue resistance curve for the gusset plate detail), from CN Rail (traffic information), and from the AREA and ECCS standards (current detail categories and fatigue limits). Some of the input data remained the same for all of the remaining fatigue life calculations, and some was changed in order to examine the influence of certain parameters. The input data that was constant consisted of the locomotive and railcar geometry and weights, the

arrangements of the typical trains, and the traffic models. The input data that varied consisted of the influence lines, the methods of damage accumulation, and the fatigue resistance curves.

6.4.1 Input Data: Constants

The first piece of information required by the RFL program is the locomotive and railcar weights and geometry. Typical geometry was provided by CN Rail and are shown in Figure 6.1. One type of locomotive was used for all trains, whereas the railcars were divided between freight type and passenger type. The locomotive had four axles and weighed 1 157 kN (130 tons). The freight railcars had four axles and had weights ranging from 267 kN (30 tons) to 1 263 kN (142 tons). The length of all freight railcars was 18.3 m (60 feet). This was the shortest length of railcar found in the train listings and it produced the most critical loading on the bridge. Use of this length for all the typical freight cars was considered reasonable because this type of railcar is very commonly used on the CN mainline. A passenger railcar was input with four axles, a total length of 25.9 m (85 feet), and a weight of 623 kN (70 tons).

The locomotive and railcar weights were obtained from traffic information provided by CN Rail [44], and is reproduced in Table 6.1. This information represents the total tonnage of freight and passenger trains that used the bridge in 1990. The total tonnage is subdivided between freight locomotives, freight cars, passenger locomotives, and passenger cars. (There is also an express train category given in the table but this type of train is not used on this line.) The freight cars are further subdivided into seven freight categories, where each category represents a range of freight car weights. For example, freight category 2 includes all the freight cars that weigh between 178 kN and 445 kN (40 and 100 tons).

CN Rail provided typical locomotive and passenger car weights and typical freight car weights for each freight category. These typical weights were used as the weights of the locomotive and railcars in the RFL program. The locomotive weight was set equal to 1 157 kN (130 tons), and seven freight cars were set equal to the typical weights of the seven freight categories. For example, freight car 1 weighed 267 kN (30 tons), freight car 2 weighed 534 kN (60 tons), and so on. One passenger car was defined as weighing 534 kN (60 tons).

Once the locomotive and railcar data had been entered into the program, the next step was to use that information to build typical trains. Because the makeup and arrangement of the trains that actually created the loads in the table is unknown, it was necessary to derive a typical train that represents all the traffic. This typical train was defined such that, in one year, the same total tonnage would cross the bridge as is indicated in Table 6.1. Use of a typical train should be satisfactory since the damage is calculated on a yearly basis and the sequence of trains within the year will not affect the amount of damage produced.

To construct the typical train, it was first assumed that there were always two locomotives per freight train. This assumption is based upon the train listings in Chapter 3, where the actual number of locomotives ranged from one to four, but averaged about 2.1. Using this assumption, the total number of trains that used the bridge in a year could be calculated. To do this, the total freight locomotive tonnage was divided by the weight of two locomotives, in the manner:

$$\frac{924\ 000\ \text{tons}}{\text{year}} \times \frac{\text{locomotive}}{130\ \text{tons}} \times \frac{\text{train}}{2\ \text{locomotives}} \cong \frac{3\ 554\ \text{trains}}{\text{year}}$$

Therefore, there will be 3 554 typical train passages per year. The objective now is to arrange the railcars in a typical train such that when it is applied 3 554 times a year, it will produce the same total tonnage as identified in Table 6.1. Since the total tonnage in each category is known, this can be easily calculated. For example, freight car Category 1 weighed 30 tons and the total tonnage in one year was 2 778 000 tons. Thus:

$$\frac{2\ 778\ 000\ \text{tons}}{\text{year}} \times \frac{\text{car}}{30\ \text{tons}} \times \frac{\text{year}}{3\ 554\ \text{trains}} \cong \frac{26\ \text{cars}}{\text{train}}$$

and therefore the typical train must have 26 freight cars of 30 tons each in order to produce the required tonnage.

These calculations were done for each freight category so as to build a typical freight train, and, in a similar fashion, to build a typical passenger train. The arrangement of these typical trains are shown in Table 6.2. The reason there are two typical freight trains is that freight car Category 7, which weighed 1 263 kN (142 tons), occurred only once every 6th train. Train No. 2 is identical to Train No. 1 except that it includes one freight car Category 7, and accounts for one sixth of the total trains.

CN Rail suggested using the traffic tonnage listed in Table 6.1 for the period 1982 to 1992, and double that tonnage for the period 1971 to 1981. The reasoning for this was that prior to 1981 only one bridge existed at this location and it therefore carried all the traffic. In 1981, the mainline was double-tracked at this location, so traffic was divided between two bridges after that date. Traffic prior to 1971 was considered to be negligible, and the bridge was removed from service in 1992. The traffic tonnage in Table 6.1 is for 1990.

6.4.2 Input Data: Variables

The variable input data consisted of the fatigue evaluation parameters that will be examined for sensitivity. These comprise the influence line, the method of damage accumulation, and the fatigue resistance curve. Three variations of the influence line will be examined, all of which were developed in Chapter 3. The basic influence line is that for the stress at the lateral bracing gusset plate detail on the stringer. The first variation on the influence line is derived from the Pinned model, and, although the entire bridge was modeled to develop this influence line, it is merely equivalent to the influence line for a simply-supported beam. This model was developed as a possible upper bound limit on the stresses at the critical detail and as a possible analysis that an engineer may do for a first estimate of the stresses. The results from Chapter 3 showed that the Pinned model did not always provide the most conservative stresses if the railcars had a certain critical wheelbase. In the fatigue evaluations in this section, the railcars used did have this critical wheelbase.

The second variation on the influence line was obtained from the Continuous model, which reflects continuity at the stringer to floorbeam connection. The results from Chapter 3 indicate a generally improved representation of the stringer behaviour over the Pinned model, mainly because negative strains are represented. For railcars with the critical wheelbase, this influence line produced the most conservative results. Thus, it is expected to produce the shortest remaining fatigue lives.

The third variation on the influence line was obtained from the Continuous-with-Springs model. This model was developed specifically to reproduce the strains in the stringer as they were measured in the field. The model is similar to the Continuous model except that rotational springs were used at the stringer to floorbeam connection to

increase the stiffness of the floor system. The amount of spring stiffness was adjusted until the ratio of measured-to-calculated effective strain range was unity for one of the trains for which strain measurements were taken, and the ratios for the rest of the measured trains were less than unity. This was done to ensure that the strains produced by the influence line would be conservative.

An impact factor is not included in the analysis for the Pinned and Continuous models, but the RFL program that subsequently uses the results does calculate impact, based on the speed of the trains. For the Continuous-with-Springs model, which is based on field measurements, the effect of impact could be considered to have already been included. However, the amount of impact cannot be explicitly identified, and it must be recognized that full impact does not always occur with every train. The strain measurements taken from eight trains are probably not sufficient to assume that the impact measured is necessarily representative of a larger sample. Also, the Continuous-with-Springs model is based on one train, which reduces the size of the sample even more. Therefore, to be conservative, it was decided that the program RFL should calculate impact for the Continuous-with-Springs model as well. The amount of impact generally calculated by the program, for all the models, is about 10 %, which agrees well with values reported in the literature.

Fatigue resistance curves and the methods of damage accumulation were taken from the AREA standard, the ECCS standard, and the Kunz evaluation method. Based upon the results reported in Chapter 5, Category D was selected for use with the AREA standard as the fatigue resistance of the lateral bracing gusset plate detail. As recommended in that standard for evaluation of remaining fatigue life, the constant amplitude fatigue limit was removed and the Category D line was extended downwards at the same slope (three) to 100 million cycles. One hundred million cycles was used as the cut-off limit. The damage accumulation method recommended by the AREA standard is the Miner summation. The modified AREA fatigue resistance curve for rivets with normal clamping force was not used because the results from the Experimental program did not support it.

The AREA standard also allows the use of a factor (α) to account for the beneficial effect on load resistance of the bracing, floor system, and other three-

dimensional response features of the structure. It is also intended to account for the fact that impact does not occur for every cycle. For the span length in the bridge under investigation, the AREA standard recommends using 0.85, although another value may be used if an appropriate analysis provides a more accurate estimate of α. Considering this permission, the ratio of measured-to-calculated effective strain range from Chapter 3 was used as a more accurate estimate. This ratio is, coincidentally, the same for both the Pinned and Continuous models, and was calculated as 0.86. For the Continuous-with-Springs model it will be equal to 1.00, because this model already accounts for unintended and secondary restraint.

In the ECCS standard, fatigue details are provided for new work only: hence, no detail category is recommended for riveted connections. The decision was made herein to use the equivalent of the AREA Category D, which is ECCS Detail Category 69. (This is simply the Category D stress range value at two million cycles, which is 68.9 MPa (10 ksi). The ECCS constant amplitude fatigue limit and change in slope are to be taken at five million cycles (51 MPa, 7.4 ksi), and the cut off limit is 100 million cycles (28 MPa, 4.0 ksi). Note that the ECCS constant amplitude fatigue limit is slightly higher than the AREA constant amplitude fatigue limit.

The third evaluation method was the Kunz method, which consisted of the fracture mechanics based method of damage accumulation and the modified fatigue resistance curve. The modified fatigue resistance curve is based on the AREA Category D detail, with the constant amplitude fatigue limit at 48 MPa (7 ksi). No cut-off limit was used for the Kunz evaluations.

Two runs of the Kunz evaluation method were done. Both runs included the decreasing fatigue limit, but only one used the transition region. This was done so that the effect of the transition region could be examined.

6.5 Results

The results from the remaining fatigue life calculations carried out according to the criteria given above are listed in Table 6.3. The computer runs are grouped according to the type of influence line. The remaining fatigue life is given in years and is calculated relative to the year the bridge was removed from service, 1992. A limitation of the program is that the longest remaining fatigue life that could be calculated was 1 500 years.

Therefore, calculated remaining fatigue lives that were greater than this were identified by the notation ">1 500." The notation "no damage" means that the stress ranges applied to the detail are below the constant amplitude fatigue limit; thus, no crack propagation occurred for these cases. The reader is reminded that the calculated remaining fatigue lives are for comparison purposes only. Fatigue considerations at other details and other limiting conditions such as corrosion would need to be explored for a complete evaluation of the bridge.

A comparison of the remaining fatigue lives from the different types of influence lines shows that the evaluation using the Continuous influence line gives the shortest remaining fatigue life, followed by the Pinned, and then the Continuous-with-Springs cases. The Continuous influence line produces high stress ranges because of the critical wheelbase, which was present in all the freight trains. The higher stress ranges cause the lower remaining fatigue life. The Pinned influence lines produce remaining fatigue lives approximately 10 years longer than the Continuous influence lines.

The longest fatigue lives are predicted by the Continuous-with-Springs influence line. The strains predicted by this model are the lowest, and they are the most accurate. This increase in calculated fatigue life shows the benefit of using field measurements to determine the actual strains in the members.

The value used for α according to the AREA standard had a significant effect on remaining fatigue life calculations. In the runs that used the Pinned and Continuous influence lines, the use of $\alpha = 0.85$ produced remaining fatigue lives substantially greater than when $\alpha = 1.0$ is used. This factor accounts for the same effects as contained within the Continuous-with-Springs model, and the remaining fatigue lives are long in all cases (no damage and 57 years for Pinned and Continuous, respectively, and 55 years for the Continuous-with-Springs model). This suggests that the α factor accounts for the secondary effects in a reasonable way. However, this conclusion may only be valid for members with spans similar to the one in this report because, in the AREA standard, the α factor varies with the length of the span.

If the AREA remaining fatigue life for the Continuous influence line, using α equal to 0.86, is compared to the AREA remaining fatigue life for the Continuous-with-Springs influence line, the values are nearly identical to one another. These two remaining fatigue

life calculations are essentially the same, except that the Continuous model reduces the stress ranges after the Miner summation is performed, and the Continuous-with-Springs model reduces the stress ranges before the Miner summation is performed. In other words, whether the stress ranges are modified for inaccurate analyses before or after the damage accumulation does not seem to make much difference, at least for the traffic used in these evaluations.

Examination of the ECCS remaining fatigue lives for the different influence lines shows a longer life with lower stress ranges, which would be expected. The exception is the Continuous-with-Springs influence line, where there was zero damage predicted because all stress ranges were below the constant amplitude fatigue limit. If, to be consistent, the AREA constant amplitude fatigue limit is substituted, the effect is quite significant, going from no damage incurred to 76 years of remaining fatigue life. Apparently, the peak stress ranges applied to the detail are in between these two limits. This result shows the importance of determining the true value of the constant amplitude fatigue limit for riveted members, rather than just selecting one on the basis of information obtained primarily from welded details.

Comparison of the results obtained using the two Kunz fatigue resistance curves with one another shows that the effect of including the transition region is to significantly increase the remaining fatigue life. For the Pinned and Continuous influence lines, the transition region more than doubles the remaining fatigue life. In the Continuous-with-Springs influence line the actual amount cannot be determined, but, considering that the fatigue resistance curve is represented on a log scale, the increase in fatigue life is likely to be much more than double. Use of this naturally-observed region in fatigue resistance curves, particularly in remaining fatigue life evaluations, would be beneficial in the evaluation of existing structures.

The effect of the different fatigue curves in the standards can also be examined. In order to make comparisons of the fatigue live predictions with one another, the AREA results with $\alpha = 1.0$, the ECCS result with the constant amplitude fatigue limit at 48 MPa (7 ksi), and both Kunz curves will be used. For each of these results, the stress ranges applied to the detail are the same; only the fatigue resistance curve is varied. This

comparison also shows the differences between the damage accumulation methods provided by the Miner summation and the Kunz decreasing fatigue limit.

When the AREA and ECCS results are compared with one another, ECCS gives longer remaining fatigue lives. This is due to the slope of the ECCS curve that is used for variable amplitude stress ranges (slope = 5). As the effective stress range gets smaller, i.e. with the Continuous-with-Springs influence line, the difference between the AREA and ECCS curves increases.

When the AREA and ECCS remaining fatigue lives calculated using the Pinned and Continuous influence lines are compared to the corresponding Kunz remaining fatigue lives, the Kunz method predicts lives significantly longer than those calculated by the AREA and ECCS standards. It can be seen that this is almost entirely due to the inclusion of the transition region. In the Pinned and Continuous models, the damage accumulation method is not significant because many stress cycles exceed the damage limit. Thus, the damage limit is reduced rapidly, and the curve is extended downwards early in the traffic model. Therefore, most of the subsequent cycles contribute to crack propagation. However, for the Continuous-with-Springs influence line, when only a few stress ranges exceed the constant amplitude fatigue limit, the Kunz evaluation method calculates much greater remaining fatigue lives. This result shows that a significant portion of the longer remaining fatigue life is due to the damage accumulation method, which increased the life by approximately 1 300 years over the similar AREA curve. These results show that the Kunz damage accumulation method is useful when only a few cycles exceed the constant amplitude fatigue limit.

Based on all of the results, it is clear that stress range is one of the most important parameters in the remaining fatigue life calculations, as would be expected. When many stress ranges exceed the constant amplitude fatigue limit, as with the Pinned and Continuous influence lines, both the AREA ($\alpha = 1.0$), ECCS (CAFL = 48 MPa), and the Kunz-without-Transition evaluation methods gave remaining fatigue lives comparable to one another. However, when the Continuous-with-Springs influence line, or the AREA curve with $\alpha = 0.86$ are used, the predicted remaining fatigue life is significantly increased. Use of field measurements to accurately determine the stress ranges is very beneficial in establishing remaining fatigue life evaluations.

Both components of the Kunz evaluation method, the damage accumulation technique and the transition region, have a significant effect on the prediction of remaining fatigue life. When these components are used with the Pinned and Continuous influence lines, the predicted remaining fatigue life is significantly increased, even when many stress cycles exceed the constant amplitude fatigue limit. When used with influence lines based upon field strains measurements (Continuous-with-Springs), its use has a dramatic effect on the remaining fatigue life calculations.

Considering that the Continuous-with-Springs model represents the actual stresses in the bridge and that the Kunz damage accumulation method and transition region represent the most accurate amount of fatigue resistance of the detail, it can be concluded that the amount of previous fatigue damage in the stringers of this bridge is negligible.

PLANT INVENTORY – TRACK & ROADWAY
TRAFFIC DETAIL ENQUIRY SYSTEM

SUBDIVISION 670 ALBREDA YEAR 1990
MILE-FROM 0.43 MILE-TO 43.85 TRACK 01

MILLION GROSS TONS

	FREIGHT	PASSENGER	EXPRESS	TOTAL
LOCOMOTIVES	0.924	0.047	0.000	0.971
CARS	14.822	0.089	0.000	14.911
TOTAL	15.746	0.136	0.000	15.882

	FREIGHT CATEGORY	CAR LOADING, M.G.T.
1	0-40 TONS	2.778
2	40-100 TONS	0.802
3	100-110 TONS	2.446
4	110-120 TONS	1.295
5	120-125 TONS	0.775
6	125-131 TONS	6.695
7	OVER 131 TONS	0.031
		14.822

CATEGORY	TYPICAL TONS PER CAR
1	30
2	60
3	108
4	115
5	124
6	130
7	142

LOCOMOTIVES APPROXIMATELY 130 TONS ON AVERAGE
PASSENGER CARS APPROXIMATELY 60 TONS PER CAR

Table 6.1 Traffic information provided by CN Rail

Freight Trains

Model Year	1971-1981		1982-1992	
Typical Train No.	1	2	3	4
No. of Trains per year	6671	437	3336	218
Locomotives	2	2	2	2
Freight Car No. 1	26	26	26	26
Freight Car No. 2	4	4	4	4
Freight Car No. 3	6	6	6	6
Freight Car No. 4	3	3	3	3
Freight Car No. 5	2	2	2	2
Freight Car No. 6	15	15	15	15
Freight Car No. 7	0	1	0	1

Passenger Trains

Model Year	1971-1981	1982-1992
Typical Train No.	5	6
No. of Trains per year	362	181
Locomotives	2	2
Passenger Car No. 1	7	7

Table 6.2 Arrangement of typical trains and traffic model

Influence Line	Evaluation Method	Remaining Fatigue Life, years
Pinned	AREA Cat. D, α=1.00	29
Pinned	AREA Cat. D, α=0.85	no damage
Pinned	AREA Cat. D, α=0.86	no damage
Pinned	ECCS Detail 69	39
Pinned	Kunz without Transition	31
Pinned	Kunz with Transition	81
Continuous	AREA Cat. D, α=1.00	21
Continuous	AREA Cat. D, α=0.85	57
Continuous	AREA Cat. D, α=0.86	54
Continuous	ECCS Detail 69	25
Continuous	Kunz without Transition	21
Continuous	Kunz with Transition	47
Cont. with Springs	AREA Cat. D, α=1.00	55
Cont. with Springs	ECCS Detail 69	no damage
Cont. with Springs	ECCS Detail 69, CAFL=48 MPa	76
Cont. with Springs	Kunz without Transition	1 350
Cont. with Springs	Kunz with Transition	>1 500

Table 6.3 Results of remaining fatigue life calculations

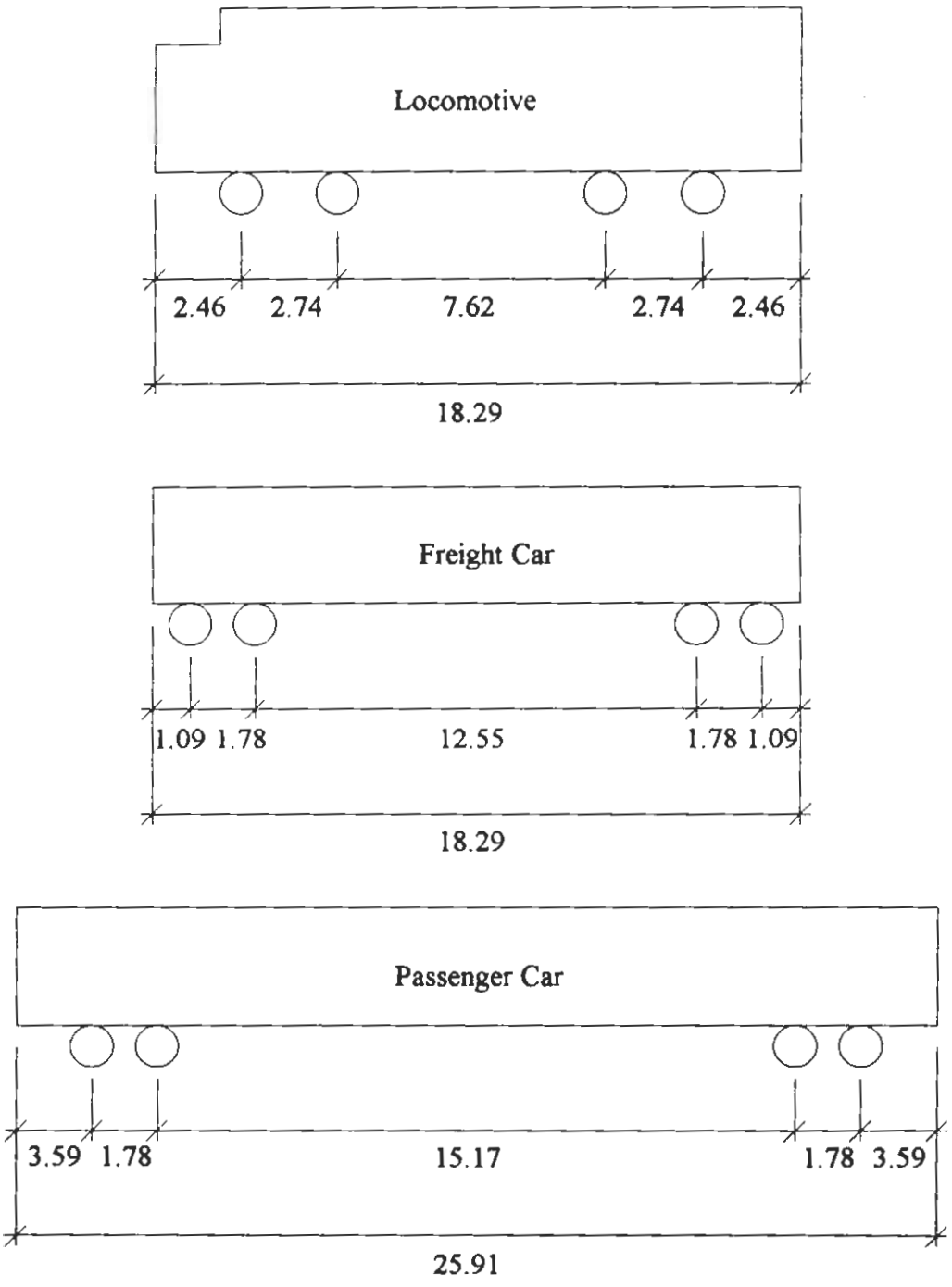

Figure 6.1 Typical locomotive and railcar geometry

7. DISCUSSION

7.1 Field Strain Measurements

7.1.1 General

Field strain measurements made under live loads enabled a comparison to be made between the theoretical behaviour of the bridge and its real behaviour. The measured strains were also used to develop an accurate influence line of the bridge so that a proper remaining fatigue life calculation could be made. The theoretical behaviour of the bridge was represented by three analytical models. The first two, a pinned space frame (referred to as Pinned) and a continuous space frame (Continuous), were models that could be used for any bridge if field measurements were not available. The third model, a continuous space frame that had the floor stiffened by the addition of springs (Continuous-with-Springs), was made specifically for the bridge treated in this report in order to be able to predict the measured strains as accurately as possible for use in the remaining fatigue life calculation.

The three models were evaluated on the basis of how well they predicted the effective strain range as compared to the measured effective strain range. To varying degrees, both the Pinned and Continuous models conservatively predicted the measured effective strain range to about the correct magnitude. Based on this observation, it would be safe to use either of these models to predict the effective strain range in the stringers of an existing railway bridge of the through truss type.

Between the two models, it was expected that the Pinned model would always predict the highest strain range, but this was not the case. For railcars of a certain wheelbase, it was found that the response of this bridge was such that the effective stress range predicted by the Continuous model could be the same or higher than that predicted by the Pinned model. The effect of this was reflected in the results of the remaining fatigue life calculations, where the Pinned model did not produce the most conservative results. Therefore, although both of these models predict conservative effective strain ranges, the

Pinned model may not always provide the most conservative result, as would have been expected.

As was anticipated, the Continuous-with-Springs model accurately predicted the measured effective strain range to almost exactly the correct magnitude. This model accounted for all the variation in floor stiffness of the bridge that the other two models could not. By taking this into account, the model showed a significant increase in the calculated remaining fatigue life of the bridge as compared to the others. However, the influence line from this model is specific to the bridge in this report, and so it may be unsafe to apply it to other bridges. Field measurements are needed to determine the amount of stiffness in the floor system of a given bridge, but the extra cost may be justified in some cases. Further investigation into the variations of floor stiffness of different bridge configurations is needed to produce general recommendations for this type of model.

Analysis of the strains in the diagonal member showed that the stiffness of the floor system did not have a significant effect upon the behaviour of the truss. Thus, the Continuous-with-Springs model is of no benefit in the analysis of such members. Considering the Pinned and Continuous models, neither were consistently conservative in predicting the effective strain range in the diagonal. However, it was observed that the most the Pinned model underestimated the measured strain range was 1%, compared with 11% for the Continuous model. Therefore, of the two models, the Pinned model is the best for a remaining fatigue life calculation.

The strains measured in the diagonal did indicate that some bending out of the plane of the truss was present. This is likely due to the connection between the floorbeam and the truss panel point, which was deep enough to transfer significant moment. This so-called secondary bending increases the stresses in some of the details associated with the web members of the truss and its effect should be considered in the analysis.

7.1.2 Comparison of Results with Standards and Literature

The α – factor provided in the AREA standard for the stringers studied in this report is 0.85. (The α – factor is intended to reflect that three-dimensional effects are present and that impact is not associated with all loads.) The standard does not specify to

what type of analysis this factor should be applied, but presumably it is either a pinned or continuous one. In any case, the AREA recommended value (0.85) and the ratio of measured-to-calculated strains determined for the models studied in this report, where the highest ratio was found to be 0.86, are reasonably close together. This will not necessarily be the case for other span lengths, however. In a general case, the value recommended by AREA could be considered as acceptable for an initial estimate of the stress range in a stringer, given the amount of effort required to produce a more accurate analysis.

For the diagonal, the α – factor recommended in the AREA standard is also to be taken as 0.85. Although, this is a reasonable value as compared with the ratios of measured-to-calculated strain ranges calculated by the Pinned and Continuous models, it must be recognized that there was considerable scatter in the calculated results.

Szeliski and Elkholy performed strain measurements on a bridge similar to the one in this report [6]. The four-span bridge consisted of two truss spans and two plate girder spans. Using a simple beam model, they calculated ratios of measured-to-calculated root mean square (RMS) strain ranges of about 1.0, and for a space frame model the ratios were about 1.2. This means that the measured strains were generally slightly higher than the strains measured in this report. It is not certain if the significant beneficial load distribution effect of the rail ties was included in the analysis.

In the same paper, the ratio of measured-to-calculated strains for the hangers ranged from about 0.913 to 1.013, which is close to the values observed in this report. In the study done by Fisher and Daniels [5], the ratio of measured-to-calculated axial stress in the hangers ranged from 0.96 to 1.02. This suggests that the web members in through truss type bridges generally behave the same from one bridge to another, and are relatively unaffected by the floor system stiffness.

7.2 Experimental Program

7.2.1 General

It was observed in the fatigue tests that the stringers could withstand from between 450 000 to 875 000 cycles after detection of the first crack. Similar observations are

reported in much of the literature. This effect is a reflection of the internal redundancy of riveted built-up members. The additional number of cycles may translate into a significant amount of fatigue life, and therefore it should be included in the fatigue resistance of these types of members. The failure criteria used in this report is intended to reflect the advantage of this cross-sectional redundancy.

Most of the data points obtained in this study support the idea that a transition region exists between the sloping straight line and the horizontal straight line representation of fatigue life used in the literature. The existence of this region also has been well documented in fracture mechanic testing. However, more testing and analysis should be done. If the transition region can be properly identified, its use will be very beneficial in remaining fatigue life calculations.

Based upon the results of the remaining fatigue life calculation, the previous damage in the critical detail of the stringers examined in this report can be considered to be negligible. The most accurate remaining fatigue life analysis, which used the Continuous-with-Springs influence line, the Kunz transition region, and the Kunz method of damage accumulation, produced a very large remaining fatigue life. Considering that the bridge was built approximately 80 years before it was removed from service, any crack growth that occurred would be a minute fraction of the growth required for failure.

7.2.2 Test Results

As mentioned in Chapter 5 (Results of Experimental Program), all of the fatigue tests exceeded the AASHTO Category D limit. This is consistent with most of the results of fatigue tests on riveted shear splices and full-scale fatigue tests reported in the literature. However, some of the results of the tests done in the normal orientation of the stringers are relatively lower than similar results from other full-scale fatigue tests. The test done in the inverted position, on the other hand, had a fatigue resistance comparable to the full-scale fatigue tests reported in the literature.

Most of the test results do not support the shift to Category C allowed in the AREA standard for rivets with normal clamping force. Using the allowance in fatigue evaluations may be unconservative for some riveted details.

In a general sense, the gusset plate detail (normal orientation tests) has a fatigue resistance comparable to that of shear splices, that is, closer to the Category D detail. On the other hand, the inverted stringer test, in which the critical detail is the continuous web-to-flange connection, seems to have a fatigue resistance closer to Category C. The inverted test is consistent with other fatigue tests on continuous web-to-flange connections (Fisher 1987, ATLSS 1993), as shown in Figure 7.1.

The main features relevant to fatigue in a riveted detail are the stress concentration caused by the presence of the rivet hole and bearing of the rivet on the edge of the hole (Section 2.2.1). The first factor, high stresses caused by the presence of the hole, is present in any riveted connection. The second factor, however, will be expected to occur only in connections that transfer some shear, such as shear splices, where the rivet bear against the side of the hole. Not all of the load in a shear splice is necessarily transferred by bearing of the rivet, though; some could be transferred by friction. The amount of load transferred by friction depends upon the level of clamping force in the rivet, and the degree to which the rivet fills the hole. The more a riveted connection transfers load by bearing, the greater will be the stress concentration at the hole and the lower the fatigue resistance.

In all tests done in this program, the critical detail was within the constant moment region. Thus, from elementary mechanics of materials analysis, there is no shear force in the rivets. However, in the tests on the gusset plate detail, recall that no slip was observed between the connected parts. This means that strain compatibility was being maintained. In order for this to happen, load must have been transferred into the gusset plate either by friction, by bearing of the rivets against the holes, or by a combination of both. For the rivets in the gusset plate connection, any bearing present would be oriented such as to reduce the fatigue life of the detail.

It is believed that the rivets in the gusset plate detail were likely to have been in bearing against the edges of the holes in at least some cases. The degree to which this may have affected the fatigue strength cannot be ascertained, however.

There were two tests on the stringer in the normal orientation where no cracking was observed. Possible reasons that these tests did not develop fatigue cracking could be that the clamping force in the critical detail rivets may have been high, or the rivets did not fill the holes as much as in the otherwise comparable tests that did develop fatigue cracking. Perhaps of more importance, it should be recognized that the stress ranges are approaching the fatigue limit, and the long life may simply reflect the normal scatter of fatigue test data.

7.2.3 Comparison of Test Results with the Work of Others

The specimens tested by Reemsnyder were truss connections that resembled lap splices, hence the load was transferred by friction and bearing [21]. The specimens were constructed in the laboratory using new materials, and the points plotted in Figure 7.1 represent the number of cycles when one component was partially fractured. The results plot in-between the Category C and D curves. If additional cycles were to be added to make the failure criteria consistent with the one used herein, the data points would move slightly to the right. However, since the stress range used in the Reemsnyder tests was high, the crack propagation would have been rapid.

The specimens tested by Baker et al. were tension hangers consisting of two pairs of back-to-back angles joined by lattice bars [22]. The hangers were loaded axially and therefore the rivets did not transfer any load. The failure criteria used was that corresponding to complete severing of one component. In Figure 7.1, the results generally straddle the Category C line.

The specimens tested by Out et al. and the ATLSS tests were riveted built-up girders [23,27]. The critical detail was the continuous web-to-flange connection, similar to the critical detail of the inverted stringer tested herein. The plotted points represent the number of cycles when the second crack was discovered. These data plot well right of the category D resistance curve.

Fisher et al. tested riveted built-up beams that had coverplates attached to the bottom flange [17]. Cracks initiated in both the rivet holes of the continuous web-to-flange connection and the rivet holes that connected the coverplate to the flange. The

results generally straddle the Category C resistance curve. The two data points that plot about half-way between the Category C and D resistance curves correspond to cracks that started in the shear span, where they would have been loaded in shear.

The specimens tested by Brühwiler et al. were rolled beams with coverplates riveted to the full length of the bottom flange [24]. The plotted points reflect an increase in girder deflection of 0.2 mm (0.008 inch) due to a crack, and the results generally plot on, or to the right of, the Category C curve.

Figure 7.2 shows the test results from girders with the type of detail where it is hypothesized that the rivets are loaded in shear. Figure 7.3 shows the results where it has been judged that the rivets are not being loaded in shear. By comparison, the shear-type riveted detail tends to have a lower fatigue resistance as compared with the case where the rivet is not in bearing. There are not sufficient full-scale riveted member fatigue test data to calculate the two standard deviation offset for either type of detail, however. As more fatigue life data from riveted connections becomes available, it is possible that the fatigue resistance of riveted details will best be described by two categories, say, Category D for bearing type cases and Category C otherwise.

7.3 Remaining Fatigue Life

7.3.1 General

The remaining fatigue life of the stringers was calculated in order to examine the effect of the information developed herein, and the effect of new methods of evaluation developed in the literature. Three basic variables were examined: stress range, fatigue resistance, and method of damage accumulation. Stress range was examined by using different influence lines to calculate the stress at the critical detail. The fatigue resistance was examined using various detail fatigue life curves from current standards and the new curve proposed by Kunz. The method of damage accumulation was examined by comparing the Miner summation with the new method developed by Kunz.

7.3.2 Effect of Stress Range

The calculated remaining fatigue life was significantly increased when the lower stress ranges predicted by the Continuous-with-Springs models was used. The small decrease in stress range had a significant effect on the number of cycles. Obviously this is expected, since the relationship between stress range and number of cycles is logarithmic. Stress range is a very important variable in remaining fatigue life evaluations.

The calculated fatigue lives were also increased when the AREA α – factor was used, which lowers the effective stress range. Whether the stress ranges were lowered before or after the damage accumulation did not change the remaining fatigue life significantly. This means the use of the AREA α – factor is very advantageous for remaining fatigue life calculations, considering the amount of work required to produce a more accurate representation of the applied stress ranges.

7.3.3 Effect of Fatigue Resistance

For variable amplitude stress ranges, use of the ECCS fatigue resistance curve produced longer remaining fatigue lives than did use of the AREA fatigue resistance curve. This is because of the change in slope allowed by this standard, which reflects the concept that not all stress ranges immediately contribute to fatigue crack propagation.

The location of the constant amplitude fatigue limit is very important in remaining fatigue life calculations since it established whether or not a crack has initiated. In one remaining fatigue life scenario, the stress ranges were such that the peak stress ranges were above the AREA constant amplitude fatigue limit, but below the ECCS limit, as these two standards are slightly different from one another in this regard. This produces unrealistic differences in the calculated remaining fatigue lives, even though the applied stress ranges are the same. Proper and consistent identification of the constant amplitude fatigue limit for riveted members is needed.

The use of a transition region superimposed upon the standard AREA fatigue resistance curve significantly increased the calculated remaining fatigue life. The amount of increase was strongly influenced by the stress range, since, as the stress range is reduced, the transition curve moves further from the standard slope of 3. The effect of

stress range was especially significant when the applied stress ranges were near the constant amplitude fatigue limit. Use of this experimentally observed region in fracture mechanics will significantly increase the calculated remaining fatigue life.

7.3.4 Effect of Method of Damage Accumulation

When many stress cycles exceed the constant amplitude fatigue limit, damage accumulation by either the Miner summation or by the Kunz method gave comparable results. However, when only a few cycles exceeded the constant amplitude fatigue limit, there was a very large difference between the two methods. This is because when many cycles exceed the damage limit, it is reduced faster and more cycles contribute to fatigue. When only a few stress cycles exceed the damage limit, it remains high and less stress cycles contribute to fatigue. For a fatigue evaluation where many of the stress ranges do not exceed the constant amplitude fatigue limit, the Kunz damage accumulation method could result in a significantly greater calculated remaining fatigue life.

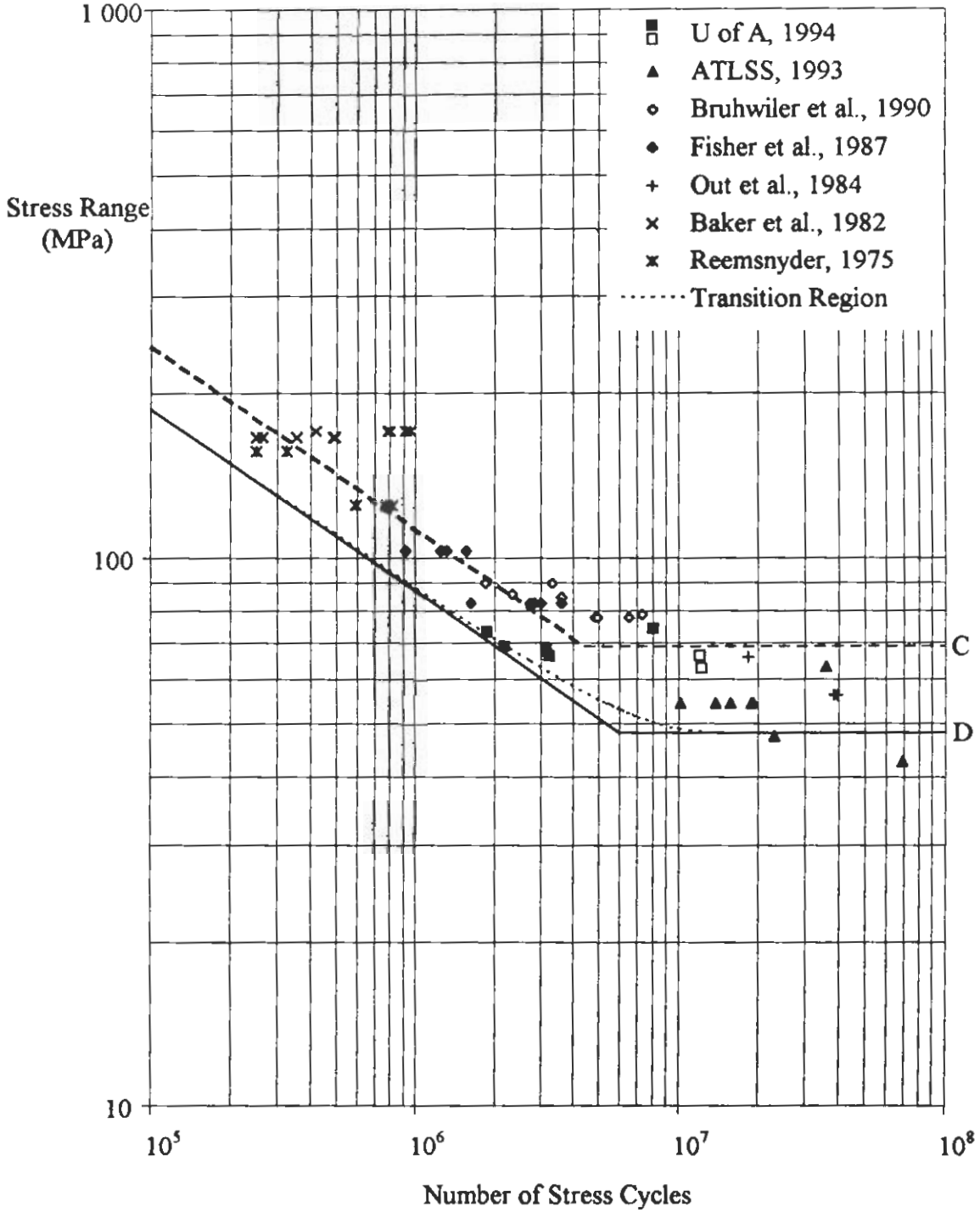

Figure 7.1 New and previously reported full-scale fatigue test results at failure

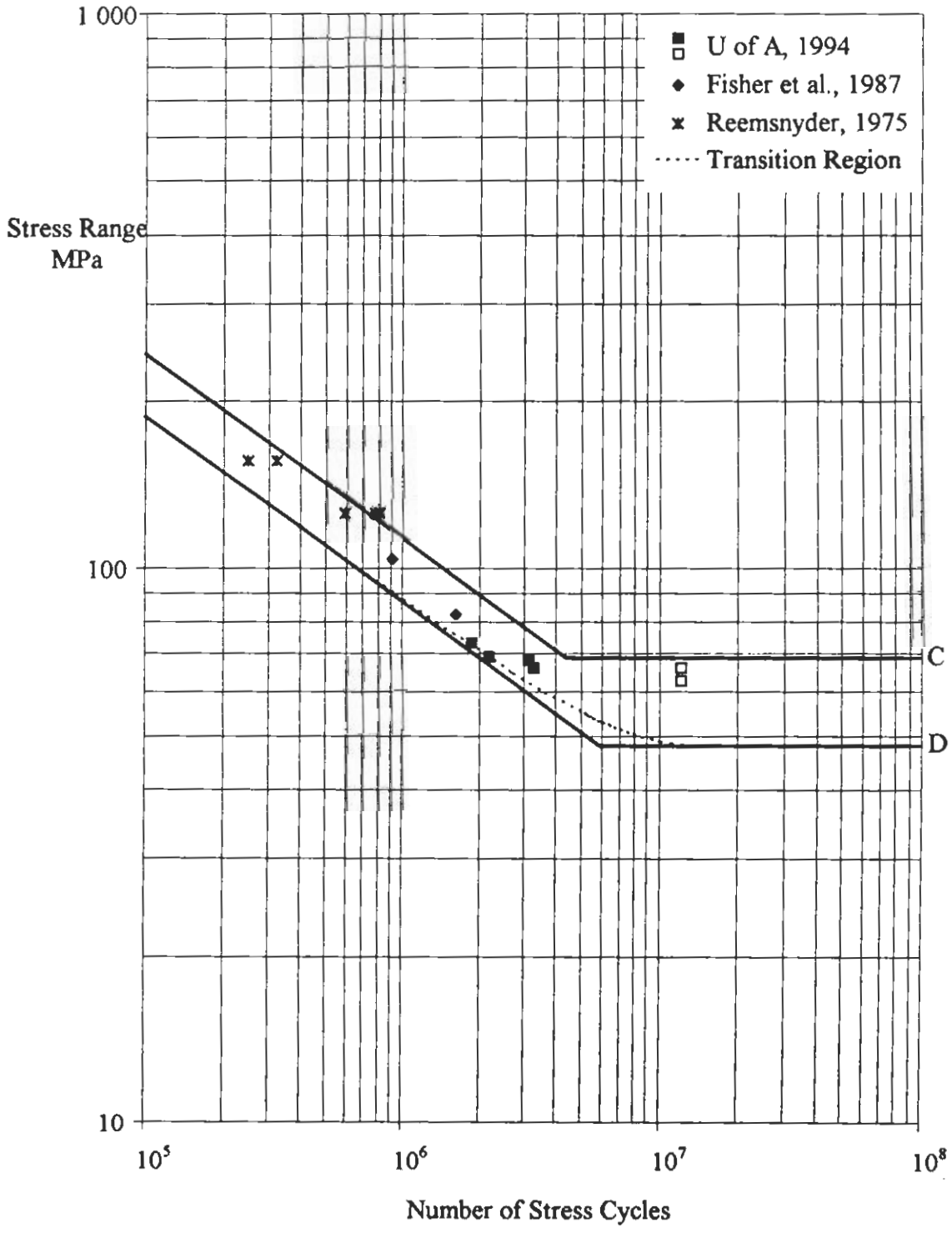

Figure 7.2 Fatigue resistance of members with rivets in bearing

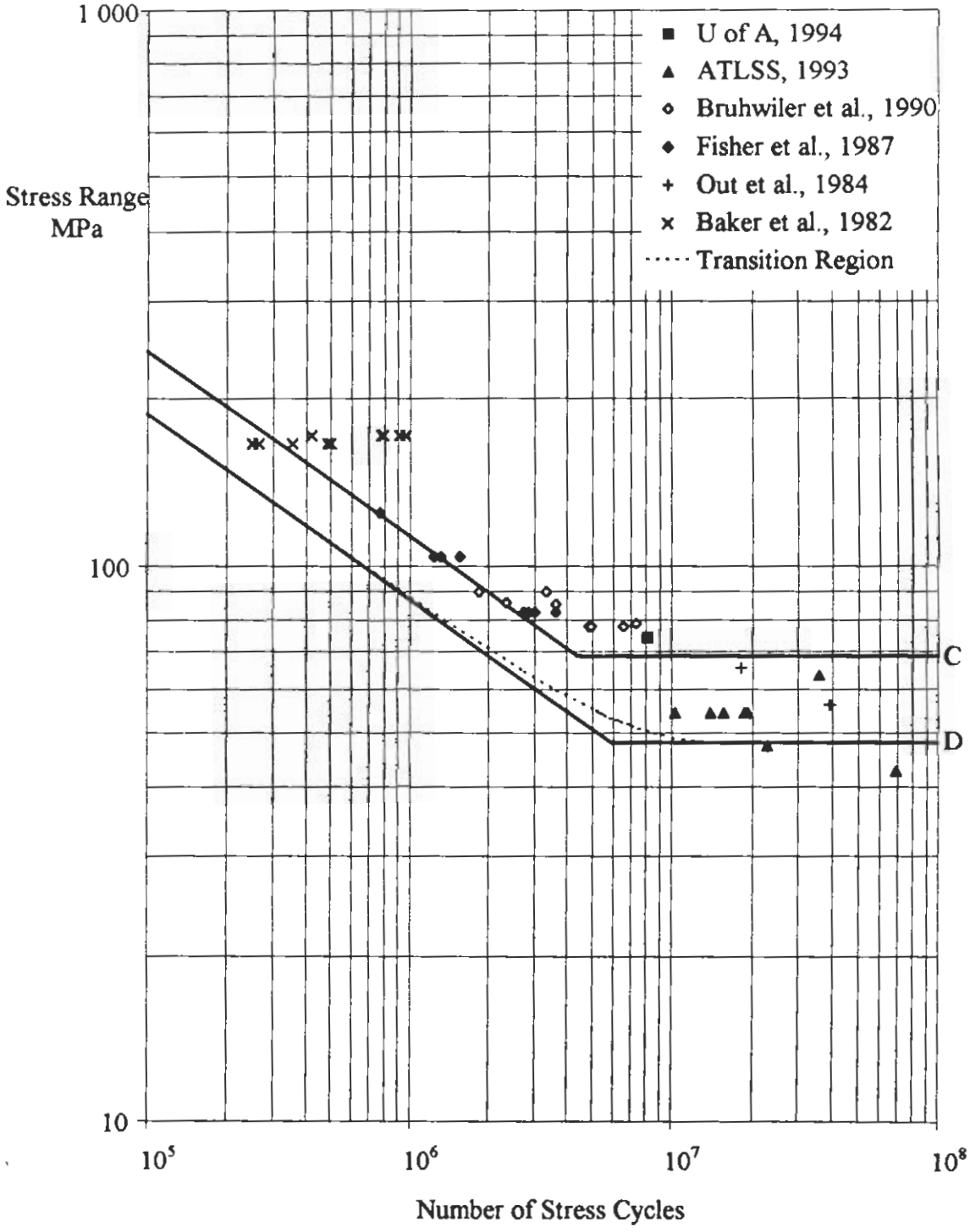

Figure 7.3 Fatigue resistance of members without rivets in bearing

8. SUMMARY, CONCLUSIONS, AND RECOMMENDATIONS

8.1 Summary and Conclusions

Field strain measurements were taken on a riveted railway bridge while it was still in service. After the measurements were taken, the bridge was removed from service and dismantled. Six stringers from the bridge were taken to a structural engineering laboratory and tested to determine their fatigue life. The data obtained from the field strain measurements was used to examine the structural behaviour of the bridge, and to develop influence lines that would accurately calculate the live load service strains. The information obtained from the full-scale fatigue tests was used to supplement the existing database of fatigue resistance of full scale riveted members.

The results from the field strain measurements and the full-scale fatigue tests were used in a remaining fatigue life calculation of the stringers. The fatigue calculation was done to examine the effect of different influence lines, fatigue resistance curves, and methods of damage accumulation. Included in the comparison of fatigue resistance curves was a modified form of the standard AREA fatigue resistance curve and a new method of damage accumulation, both developed by Kunz. The remaining fatigue life calculation was also carried out to determine the amount of previous fatigue damage at the critical detail of the stringers, if any.

The results of the work described above produced the following findings:

1. Modeling of a truss bridge with either pinned or continuous joints generally produces conservative results.
2. Modeling of a stringer with pinned connections does not always provide the upper bound on the stress range, since the influence length of a stringer modeled continuously can be longer than the stringer itself. For certain lengths of railcar, a continuous-type model may identify stress ranges equal to or greater than those predicted by a pinned-type model.

3. The stiffness of the floor system is influenced by secondary components such as the type of member connection, lateral bracing, and the presence of rails and rail-ties. The net effect of these stiffnesses can be satisfactorily represented by a rotational spring calibrated from live load strains measured in the field.
4. Fatigue resistance of riveted details exceeds the AASHTO Category D curve.
5. The fatigue resistance of a non-bearing type riveted detail may be higher than a bearing type riveted detail.
6. Both the test data developed in this report and in the literature justify further investigation of a transition region between the sloping straight line and horizontal straight line used for conventional fatigue resistance statements.
7. The internal redundancy of riveted built-up members adds significant additional fatigue resistance which should be considered in remaining fatigue life evaluations.
8. Stress range is very important in remaining fatigue life calculations. Use of extra effort to determine the actual service stress ranges can have a significant effect on the remaining fatigue life.
9. Use of the AREA α-factor appropriately and conservatively adjusts the effective stress range to account for secondary resistance effects.
10. Use of the Kunz method of damage accumulation can substantially increase the calculated remaining fatigue life when stress ranges are close to the constant amplitude fatigue limit.
11. Use of the transition region with the standard fatigue resistance curves increased the calculated remaining fatigue life for all stress ranges examined.

8.2 Recommendations

In order to accurately predict the remaining fatigue life of riveted members, field strain measurements should be used to determine the live load service stresses. When this is not possible, the use of a pinned or a continuous model to develop the influence lines

will generally produce conservative results, and the AREA α-factor should be applied to the resulting effective stress range to account for secondary load resistance effects.

The fatigue resistance of riveted details should be described by Category D. If it can be shown that the rivets in a detail are not subjected to significant bearing stresses, then the Category C can be used. When the appropriate fatigue resistance has been selected, the transition region should be incorporated into the fatigue resistance curve.

Fatigue damage should be accumulated using the Kunz damage accumulation method. Use of this method will identify a significant increase in the remaining fatigue life as compared with use of the Miner summation, especially when the applied stress ranges are near the constant amplitude fatigue limit.

LIST OF REFERENCES

1. Kulak, G.L. and Smith, I.F.C. (1993), "Analysis and Design of Fabricated Steel Structures for Fatigue: A Primer for Civil Engineers," *Structural Engineering Report No. 190*, Department of Civil Engineering, University of Alberta.
2. American Railway Engineering Association (AREA), (1994), "Steel Structures," *Manual for Railway Engineering*, Chapter 15.
3. Sweeney, R.A.P. (1990), "Update on Fatigue Issues at Canadian National Railways," *IABSE Reports*, IABSE Workshop, Lausanne, pp 111-116.
4. American Association of State and Highway Transportation Officials, (1990), *Guide Specifications for Fatigue Evaluation of Existing Steel Bridges*, Washington, D.C.
5. Fisher, J.W. and Daniels, J.H. (1976), "An Investigation of the Estimated Fatigue Damage in Members of the 380-ft Main Span, Fraser River Bridge," *Proceedings*, American Railway Engineering Association, Volume 77, Bulletin 658, pp 577-597.
6. Szeliski, Z.L. and Elkholy, I.A. (1984), "Fatigue Investigation of a Railway Truss Bridge," *Canadian Journal of Civil Engineering*, Volume 11, pp 625-631.
7. American Railway Engineering Association (AREA), (1980), "Steel Structures," *Manual for Railway Engineering*, Chapter 15.
8. Pietraszek, T.T. and Oommen, G. (1991), "Static and Dynamic Behaviors of an 85-year-old Railway Bridge," *Canadian Journal of Civil Engineering*, Volume 18, pp 201-213.
9. Wilson, W.M. and Thomas, F.P. (1938), "Fatigue Tests of Riveted Joints," *Bulletin 302*, Engineering Experiment Station, University of Illinois.
10. Munse, W.H. (1970), *Final Report on Riveted and Bolted Structural Joints Project IHR-5*, University of Illinois, pp 43.
11. Kulak, G.L., Fisher, J.W., and Struik, J.H.A. (1987), *Guide to Design Criteria for Bolted and Riveted Joints*, Second Edition, John Wiley & Sons, Toronto
12. Lenzen, K.H. (1950), "The Effect of Various Fasteners on the Fatigue Strength of a Structural Joint," *Proceedings*, AREA, Volume 51.
13. Parola, J. F., Chesson, E. Jr., and Munse, W. H. (1964), "Effect of Bearing Pressure on Fatigue Strength of Riveted Connections," *Bulletin 481*, Engineering Experiment Station, University of Illinois.
14. Munse, W.H., Wright, D.T., and Newmark, N.M. (1955), "Laboratory Tests of Bolted Joints," *Transactions*, ASCE, Volume 120, pp 1299-1318.

15. Baron F. and Larson, E.W. (1954), "The Effect of Grip on the Fatigue Strength of Riveted and Bolted Joints," *Proceedings*, AREA, Volume 55.
16. Carter, J.W., Lenzen, K.H., and Wyly, L.T. (1955), "Fatigue in Riveted and Bolted Single-Lap Joints," *Transactions*, ASCE, Volume 120, pp 1353-1380.
17. Fisher, J.W., Yen, B.T., Wang, D., and Mann, J.E. (1987), "Fatigue and Fracture Evaluation for Rating Riveted Bridges," *National Cooperative Highway Research Program Report 302*, Transportation Research Board, National Research Council, Washington, D.C.
18. Fisher, J.W. (1977) *Bridge Fatigue Guide*, American Institute of Steel Construction, New York.
19. American Association of State Highway and Transportation Officials (Interim 1991), *Standard Specifications for Highway Bridges*, Washington, D.C.
20. American *Association of State Highway and Transportation Officials (1983, Interim 1989), Manual for Maintenance Inspection of Bridges*, Washington, D.C.
21. Reemsnyder, H.S. (1975), "Fatigue life Extension of Riveted Connections," *Journal of the Structural Division*, ASCE, Volume 101, No ST12, pp 2591-2608.
22. Baker, K.A. and Kulak, G.L. (1985), "Fatigue of Riveted Connections," *Canadian Journal of Civil Engineering*, Volume 12, pp 184-191.
23. Out, J.M.M., Fisher, J.W., and Yen, B.T. (1984), "Fatigue Strength of Weathered and Deteriorated Riveted Members," *Transportation Research Record 950*, Transportation Research Board, National Research Council, Washington, D.C., pp 10-20.
24. Brühwiler, E., Smith, I.F.C., and Hirt, M.A. (1990), "Fatigue and Fracture of Riveted Bridge Members," *Journal of Structural Engineering*, ASCE, Volume 116, No. 11, pp 198-214.
25. Fisher, J.W., Yen, B.T., and Wang, D. (1990), "Fatigue Strength of Riveted Bridge Members," *Journal of Structural Engineering*, ASCE, Volume 116, No. 11, pp 2968-2981.
26. Kulak, G.L. (1992) Discussion of "Fatigue Strength of Riveted Bridge Members," *Journal of Structural Engineering*, ASCE, Volume 118, No. 8, pp 2280-2282.
27. Center for Advanced Technology for Large Structural Systems (ATLSS) (1993), "Assessment of Remaining Capacity and Life of Riveted Bridge Members," *Draft Project Report to Canadian National Railways*, Lehigh University, Bethlehem, Pennsylvania.

28. European Convention for Constructional Steelwork (1985), "Recommendations for the Fatigue Design of Steel Structures," ECCS Technical Committee 6, Brussels, Belgium.
29. Ontario Highway Bridge Design Code (1983) "Structural Fatigue and Fracture Control," Highway Engineering Division, Ontario Ministry of Transportation and Communications, Chapter 11.
30. Schilling, C.G., Klippstein, K.H., Barsom, J.M., and Blake, G.T. (1978), "Fatigue of Welded Steel Bridge Members under Variable-Amplitude Loadings," *National Cooperative Highway Research Program Report 188*, Transportation Research Board, National Research Council, Washington, D.C.
31. Moses, F., Schilling, C.G., and Raju, K.S. (1987), "Fatigue Evaluation Procedures for Steel Bridges," *National Cooperative Highway Research Program Report 299*, Transportation Research Board, National Research Council, Washington, D.C.
32. European Committee for Standardisation (1993), "Eurocode 3: Design of Steel Structures" *Part 1.1 : General Rules and Rules for Buildings*, European Prestandard, Brussels.
33. Kunz, P.M. (1992), "Probabilistic Method for the Evaluation of Fatigue Safety of Existing Steel Bridges," Doctoral Thesis No. 1023, Swiss Federal Institute of Technology, Lausanne, Switzerland. (in German)
34. Kunz, P.M., Bruhwiler, E., and Hirt, M.A. (1994), "Evaluation of The Remaining Fatigue Life of Steel Bridges," *Proceedings*, International Conference on Developments in Short and Medium Span Bridge Engineering '94, Canadian Society for Civil Engineering.
35. Canadian Engineering Standards Association (1922), "Specification for Structural Steel for Bridges," *Standard Specification for Steel Highway Bridges*, Appendix 5.
36. Computers and Structures, Inc. (1992), *SAP90, Student Edition, A Series of Computer Programs for the Finite Element Analysis of Structures*, Berkeley, California.
37. Wilson, E.L. and Habibullah, A. (1992), *SAP90. Structural Analysis Users Manual*, Computers and Structures, Inc., Berkeley, California.
38. Downing, S.D. and Socie, D.F. (1982), "Simple Rainflow Counting Algorithms," *International Journal of Fatigue*, Volume 4, No. 1, pp. 31-40.
39. Livesay, H.C. (1975), *Andrew Carnegie and the Rise of Big Business*, Little, Brown and Company, Boston, Toronto.
40. Boswell, J.S. (1983), *Business Policies in the Making, Three Steel Companies Compared*, George Allen & Unwin (Publishers) Ltd., pp 35-42.

41. Canadian Standards Association (1992), "General Requirements for Rolled or Welded Structural Quality Steel," *CAN/CSA-G40.20-M92*, Rexdale, Ontario, Canada.
42. American Society for Testing and Materials (1992), "Standard Test Methods and Definitions for Mechanical Testing of Steel Products," *ASTM Designation: A 370-92*, Philadelphia, Pennsylvania.
43. Kunz, P.M. (1994), "RFL – Remaining Fatigue Life (Computer Program)," University of Alberta, Edmonton, Alberta, Canada.
44. Private Communication from R.A.P. Sweeney, CN Rail, to G.L. Kulak (1991).

APPENDIX A

A.1 Metallurgical Report

Examination was carried out on samples cored from around the rivet holes where fatigue cracks initiated in test stringers ST7, ST8i, ST3, ST9, and on two cores from the uncracked stringer ST2E and ST2W, which were sawed open. The surfaces of the rivet holes were examined, both visually and using a stereobinocular microscope, before and after cleaning by ultrasonic vibration in an acetone bath. In the case of samples ST7 and ST8i, optical and scanning electron metallographic examinations were also carried out on polished and etched sections and on the fatigue fracture surfaces.

A.1.1 Examination of Rivet Hole Surfaces

The surfaces of the rivet holes, examined macroscopically, were found to be fairly heavily corroded. Corrosion products had formed in the gap between the rivet and the rivet hole. Cleaning in an ultrasonic bath permitted the observation of relevant features. The original holes had been punched and then reamed. The reaming had left circumferential marks around the rivet hole, more or less in the plane of the plates. The surface marks from the punching operation consisted of arrays of parallel grooves oriented in a direction normal to the plane of the plate. These would normally have been obliterated by the subsequent reaming, but in a few cases these punch rub marks were visible on the rivet hole surface, suggesting that the amount of reaming had not been sufficient. These punching marks were very often accompanied by a flaring on one surface of the plate, created during the punching operation.

As a result of the examination of the surfaces of the individual rivet holes, the following observations were made:

- ST7: (Flange Angle) Both reaming marks and punching rub marks were observed on this rivet hole. The punch marks were associated with flaring of

the surface of the plate. Careful examination was not able to find a link between the punching rub marks and the initiation of the fatigue cracks.

- ST8i: (Two Flange Angle Sections, stamped 2 and 4): These two rivet holes had identical features, wherein the surfaces of the holes were covered by circumferential reaming marks. A few diagonal marks were observed, possibly also associated with reaming. Slight flaring of the plate surface appeared to be remnant from the punching, but no punching rub marks were observed. Presumably these had been completely removed by the reaming.
- ST8i: (Web Section): Both reaming marks and punching rub marks were present on the surface, and it appeared that the center of the reaming tool had been slightly offset from the center of the punch. As a result, the hole was no longer circular. No association could be made between the presence of the punching rub marks and the initiation of the fatigue cracks.
- ST3: (Angle): The surfaces of this rivet hole included both reaming marks and punching rub marks. The punching marks occupied about 150 degrees around the circumference of the hole, and there was considerable flaring on the surface of the plate. Again, there was no obvious connection between the fatigue crack initiation location and the punching marks.
- ST9: (Flange Angle) Extensive areas of the surfaces of this rivet hole were covered in corrosion product, but reaming marks appeared to be present everywhere. (A type of rub marking was present on several areas of the surface but this is believed to be unrelated to the punching operation. These marks were not normal to the plane of the plate and were not associated with flaring of the plate surface. Furthermore the shiny appearance of these rub marks and the deformation of a fatigue fracture surface associated with some of them make it clear that this rubbing of the rivet hole surface occurred after the fatigue test.)

- ST2: (Flange Angle) The surfaces of the rivet holes in both ST2E and ST2W were covered with a layer of corrosion product. It was not removable by ultrasonic cleaning in acetone. The areas of surface exposed among the corrosion products show evidence of reaming marks everywhere with only a small amount of rubbing and little or no flaring of the plate surface.
- ST2: (Gusset Plate): The rivet hole surfaces on the thin component of this sample appear to have been punched and not reamed. There were punching rub marks on the surface and no sign of the circumferential reaming marks.

A.1.2 Microstructural Examination

Metallographic samples of the fatigued samples ST7 and ST8i were prepared and examined. Samples were sawed from the cores, mounted in Lucite, polished, etched with nital, and examined. Optical microscopy revealed that both steels had ferrite-pearlite microstructures, and the carbon content was estimated to be about 0.2%. This is as expected for this type of structural component, which is in the as-hot-rolled (or, conceivably, normalized) condition. The carbon content was somewhat heterogeneous, as evidenced by ferrite bands low in pearlite (hence, low in carbon). The steel was reasonably dirty by modern standards, containing significant amounts of manganese sulphide and manganese silicate inclusions, especially in the ferrite bands. These observations are consistent with what would be expected in a steel of the times, and no unusual features were observed. The microstructure in a layer at the surface of the rivet hole was observed to be distorted in a circumferential direction (parallel to the hole surface). This was undoubtedly caused by the reaming of the hole.

A.1.3 Fractographic Examination

Examination of two fatigue fracture surfaces from each of the samples ST7 and ST8i was carried out using a scanning electron microscope. All the fatigue fracture surfaces were found to be covered in highly typical fatigue striations, and it was possible to trace these back to the origin of the fatigue cracks. One of these origins was at the

corner of the fracture surface, where the surface of the rivet hole intersects the surface of the plate (angle). The initiation sites on the other three fracture surfaces were along the surface of the rivet hole and close to the center of the plate thickness. No microstructural defects were observed at the sites of initiation of the fatigue cracks. This is entirely normal and expected behaviour. The striation spacings on the fatigue fracture surfaces were used to give a crude estimate of local fatigue crack growth rates, which ranged from about 0.5 micrometer per cycle near the crack origins to roughly 2 micrometers per cycle after the fatigue crack was about 20 mm in length.

A.1.4 Summary

All the samples examined appeared to be normal in their metallurgical microstructure and their fatigue crack initiation and propagation behaviour. Some of the rivet holes in some stringers (e.g., the angle sections of stringers ST3 and ST7) appeared to have been inadequately reamed because some punching marks remained on the surface of the rivet holes. No evidence was found that would suggest that these rubbing marks influenced the fatigue behaviour of the stringer, however.